COORDINATED CONTROL OF DOUBLY FED INDUCTION GENERATOR WIND TURBINE AND STATIC VAR COMPENSATOR FOR ROBUST POWER SYSTEM STABILIZATION

SOTHY UONG

A THESIS SUBMITTED IN PARTIAL FULFILLMENT
OF THE REQUIREMENTS FOR THE DEGREE OF
MASTER OF ENGINEERING IN COMPUTING ENGINEERING
INTERNATIONAL COLLEGE
KING MONGKUT'S INSTITUTE OF TECHNOLOGY LADKRABANG
2015

KMITL-2014-IC-M-011-003

COORDINATED CONTROL OF DOUBLY FED INDUCTION GENERATOR WIND TURBINE AND STATIC VAR COMPENSATOR FOR ROBUST POWER SYSTEM STABILIZATION

SOTHY UONG

A THESIS SUBMITTED IN PARTIAL FULFILLMENT

OF THE REQUIREMENT FOR THE DEGREE OF

MASTER OF ENGINEERING IN COMPUTER ENGINEERING

INTERNATIONAL COLLEGE

KING MONGKUT'S INSTITUTE OF THECHNOLOGY LADKRABANG

2015

KMITL-2014-IC-M-011-003

Thesis Title	Coordinated Control of Doubly Fed Induction Generator Wind Turbine and Static Var Compensator for Robust Power System Stabilization
Student	Mr. Sothy Uong
Student I.D.	56610021
Degree	Master of Engineering
Program	Computing in Engineering Systems
Year	2015
Thesis Advisor	Associate Prof. Dr. Issarachai Ngamroo

ABSTRACT

The interconnection among power systems not only improves the system reliability, but also gets more economic efficiency. On the other hand, it may cause the problem of power system oscillations with frequency 0.2 to 2.0 Hz, i.e. local and inter-area oscillation modes. The poor damping of these oscillation modes may result in the loss of synchronism and wide area blackouts. The static var compensator (SVC) which is one of flexible AC transmission systems (FACTS) devices is installed with the power oscillation damper (POD), has been successfully applied to stabilize the inter-area oscillation. Recently, the wind farms also have been widely installed in power systems. The practical merits of DFIG wind turbines are low installation cost and controllability of active and reactive power outputs. However, because the output power of the wind power generation is intermittent in nature, it may cause the negative impact on the power oscillations. Under this condition, the stabilizing effect of SVC may be deteriorated. To enhance the stabilizing effect of SVC, the coordinated control of DFIG and SVC for robust power system stabilization is proposed in this thesis. The POD which is the 2^{nd}-order lead/lag compensator is equipped with the DFIG and SVC. To acquire both damping performance and robustness, the optimization of POD parameters is formulated based on a mixed H_2/H_∞ control. The backtracking search algorithm is automatically employed to solve the optimization problem. Simulation study confirms that the damping effect and robustness of the coordinated control of DFIG and SVC with the robust POD are higher than those of the conventional POD against various system faults, heavy power flow levels, and wind patterns.

ACKNOWLEDGEMENTS

First of all, I am really grateful to my family for their unconditional supports especially my parents, who are always so supportive in every step in my life.

I would like to express my sincere gratitude to my advisor, Associate Prof. Dr. Issarachai Ngamroo for his continuous supervision and guidance as well as advice during my Master's study. He brought me to the ophthalmology imaging field that I found to have great interest. I would not be able to work in this challenging and interesting topic without his suggestion and I could also not have come this far without his support.

I would also like to express my thoughtful gratitude to Prof. Dr. Shirai Yasuyuki (Kyoto University) and Assoc. Prof. Dr. Anantawat Kunakorn who are my co-advisors for their guidance, advice, and comments on my papers and my thesis.

My gratefully acknowledge goes also to all professors, lecturers and supporting staffs in both International College and Department of Electrical Engineering, who always help and give me a guideline during the whole period of my master's study here.

I wish to express my acknowledgement to ASEAN University Network/Southeast Asia Engineering Education Development Network (AUN/SEED-Net) for awarding me the scholarship with the financial support for master degree within 2 years. Furthermore, I also extend my sincere appreciation to KMITL for giving me the great opportunity to do research in a warmly and friendly environment.

Finally, I would like to recognize all friends, international students and Thai students for the enjoyable and stimulating atmosphere that they provide with their companion and friendship.

Bangkok, July 2015

Sothy Uong

TABLE OF CONTENTS

LIST OF TABLES

Table **Page**

LIST OF FIGURES

Figure **Page**

CHAPTER 1

INTRODUCTION

This chapter presents an overview of the research in this thesis, mainly, its introduction, motivation, literature review, objectives, data set and finally the structure of this thesis.

1.1 Motivation

Interconnection of neighboring utilities usually leads to improved system security and economy of operation. Improved security results from the mutual emergency assistance that the utilities can provide. Improved economy results from the need for less generating reserve capacity on each system. In addition, the interconnection permits the utilities to make economy transfers and thus take advantage of the most economical sources of power. These benefits have been recognized from the beginning and interconnections continue to grow. However, the design of such a system and its secure operation are indeed challenging problems. Among of those, power system instability commonly occurs on the interconnection system.

Instability in a power system may be manifested in many different ways depending on the system configuration and operation mode. Traditionally, the stability problem has been one of maintaining synchronous operation. Since power systems rely on synchronous machines for generation of electrical power, a necessary condition for satisfactory system operation is that all synchronous machines remain in synchronism or, colloquially. This aspect of stability is influenced by the dynamics of generator rotor angles and power-angle relationships. Instability may be also be encountered without loss of synchronism. For instant, a system consisting of a synchronous generator feeding an induction motor load through a transmission line can become unstable because of the collapse of load voltage.

Recently, the power system stability is still the interested research topic. A long time ago, this field research has been considered on the control devices such as the local controllers and the flexible AC transmission system devices. According to the increase of renewable energy, we should study the power system stability by considering on this type of energy. Doubly fed induction generator wind turbine (DFIG) which is a type of the renewable energies has been

installed, considerably. The DFIG wind turbine is very popular among other wind power generations due to low-installation cost, ability of active and reactive power control, and high energy transfer ability at various wind speeds [1], [2]. Especially, the use of a DFIG does not only improves the efficiency of energy transfer from the wind, but also provides wind farms with the capability of network support, voltage control, and power oscillation damping. Moreover, the effect of DFIG on power oscillation damping has been widely paid attentions [3-4]. The control of the DFIG wind turbine is achieved by controlling the RSC and GSC converters utilizing vector control techniques. As mentioned in [4], the control by rotor side converter provides better damping effect than that by grid side converter. Under this condition, the control at the rotor side converter will be proposed in this thesis. According to this method, DFIG can be designed as a close loop control by using with power oscillation damper (POD). Moreover, the DFIG wind turbine can be used as a coordinated controller with other FACTS devices to stabilize the power oscillation. The why of coordination control and its application are descripted in the section 1.2 and the chapter 4, respectively. Under the robust control design, the performance and robustness will be obtained when the mixed H_2/H_∞ robust method is carried out. The brief of the information of the mixed method is descripted in the chapter 2. Thus the stabilization technic using DFIG wind turbine should be an interested research topic.

1.2 Literature Review

In the evaluation of stability the concern is the behavior of the power system when subjected to a transient disturbance. After this negative action, with the poor damping of the oscillation modes with frequency between 0.2 to 2.0 Hz [5] such as local and inter-area modes, they may result in the loss of synchronism and wide area blackouts. To damp out the oscillation, there are some devices such as power system stabilizer (PSS) or auto voltage regulator (AVR) has been successfully used for a long time. The conventional PSS generally is installed with AVR of the synchronous generator. The input signal of the PSS is the local signal such as the generator speed, the output power. As a result, the local oscillation problem can be effectively solved. However, since the lack of observability of the inter-area oscillation mode, the PSS using the local signal may not be able to damp out the inter-area oscillations. To solve this problem, there are other flexible AC transmission system (FACTS) devices have been employed successfully such as the static var compensator (SVC), thyristor-Controlled Series Compensation (TCSC), high-voltage, direct current (HVDC) or Static Synchronous Series Compensator (SSSC)...etc.

The static var compensator (SVC) which is one of flexible AC transmission systems (FACTS) device can be commonly applied. The main application of an SVC [6] is to provide dynamic reactive power support to enable effective voltage regulation and to enhance transient stability; however, this device is also able to damp electromechanical oscillations provided a damping control loop made available [7], [8]–[9]. In [10, 11], the SVC which is installed with the power oscillation damper (POD), has been successfully applied to stabilize the inter-area oscillation.

Currently, the wind farms have been widely installed in power systems. Especially the doubly fed induction generator (DFIG) wind turbine which is a variable speed type wind turbine has been extensively paid attentions. The practical merits of DFIG wind turbines are low installation cost and controllability of active and reactive power outputs [2]. However, because the output power of the wind power generation is intermittent in nature, it may cause the negative impact on the power oscillations [12]. Under this condition, the stabilizing effect of SVC may be deteriorated. To enhance the control effect of SVC, the DFIG wind turbine which is equipped with a power oscillation damper (POD), can be employed [4]. For this purpose, the coordinated control between both devices DFIG and SVC FACTS device using POD controllers should be a good method employed to handle the both local and inter-area oscillation modes.

1.3 Objective

The objective of this thesis is the coordinated control design using the doubly fed induction generator wind turbine and static var compensator with the power oscillation dampers. The DFIG wind turbine will be used to stabilize the power system by individual control and coordination control. The robust controller using mixed control technic also is an objective in this thesis. Moreover, the optimization technic using backtracking search algorithm will show detail in this thesis. In conclusion, this thesis wants to show how to use the renewable energy wind turbine to coordinate with the FACTS devices in the stability application of the power system.

1.4 Data Set

For instant, three power systems such as single machine infinite bus, IEEE 9-bus system and four machines system are illustrated in this thesis. Two control methods, proposed mixed H_2/H_∞

and pole assignment method are compared. In optimization method, 25 populations with 100 to 200 iterations are set in the backtracking search optimization algorithm.

1.5 Thesis Structure

The thesis is organized in five chapters and is briefly summarized as follows.

Chapter 1 presents an overview of the research in this thesis, mainly, its motivation, literature review, objectives, data set and finally, the thesis structure.

Chapter 2 gives a brief introduction on the proposed control design method. In Section 2.1 shows some background of robust control and mixed H_2/H_∞ fixed structure control method. In Section 2.2, we discuss the backtracking search optimization algorithm. In here, the process of optimization will be descripted briefly. Finally, the conclusion is introduced in Section 2.3.

Chapter 3 illustrates the proposed control usage in the system. In section 3.1 and section 3.2, the application of proposed control design method will be applied into the single machine infinite bus, and the IEEE 9-bus system, respectively. In these sections, the study system and modeling, the proposed control and the discussion results also are described.

Chapter 4 descripts the application of proposed coordinated control method to stabilize the power oscillations of the four machine two area system. The study system and modeling, the proposed control, the discussion results and the conclusion of this section will be descripted and discussed in section 4.1, section 4.2, section 4.3 and section 4.4, respectively.

Chapter 5 offers the conclusion of the thesis by reviewing and highlighting its contributions which have been presented in this thesis. The recommendations for future works related to this research are given as well.

CHAPTER 2

PROPOSED CONTROL DESIGN METHOD

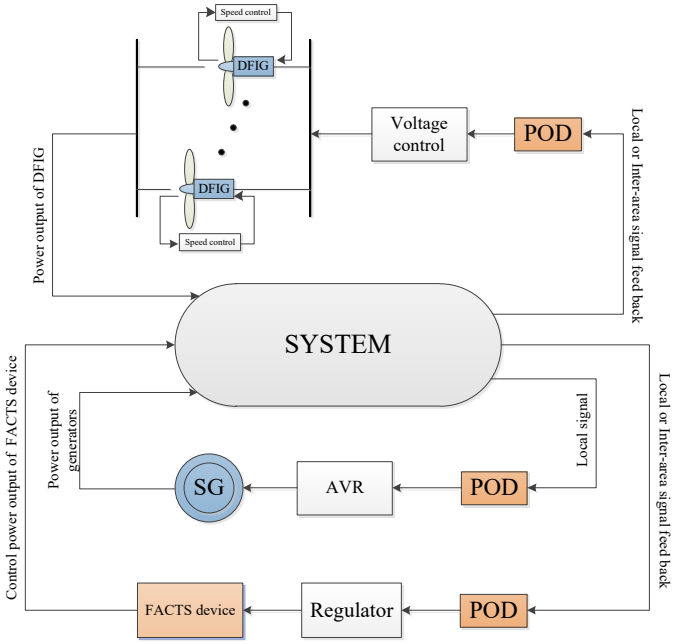

Figure 2.1 General proposed control structure.

This chapter gives a brief introduction of proposed control design method. Fig. 2.1 illustrates the general proposed control structure. In this structure, the doubly fed induction generator wind turbine (DFIG) is used to be a control device, and it can coordinate with the other control system of the synchronous generator (SG) or other FACTS devices to stabilize the system. This is called coordinated control method. The power oscillation dampers (PODs) can be employed with many types of devices. As shows in Fig. 2.1, PODs are used with DFIG wind turbine, synchronous generators and facts devices. Moreover, we will discuss the robust control in detail in section 2.1, and understand how to design a controller based on mixed H_2/H_∞ robust method in section 2.1.3. Backtracking search optimization algorithm will be employed to optimize the controller's parameters and will be described detail in section 2.2.

2.1 Robust Control

A control system is robust if it remains stable and achieves certain performance criteria in the presence of possible uncertainties. The robust design is to find a controller, for a given

system, such that the closed-loop system is robust. In this point, we will introduce the uncertainty system and the robust method using mixed H_2/H_∞.

2.1.1 Robust Control against System Uncertainties based on H∞-norm

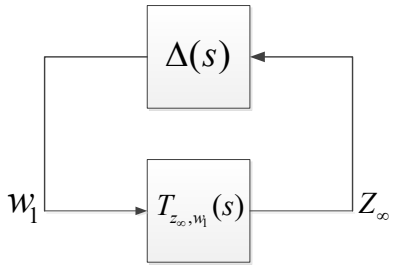

Figure 2.2 The system uncertainties presentation.

The Fig. 2.2 shows the system uncertainties presentation ($\Delta(s)$) in plant transfer function ($T_{z\infty;w1}(s)$) between the input signal w_1 and output signal z∞. Uncertainties are unavoidable in a real control system. The uncertainty can be classified into two categories: disturbance signals and dynamic perturbations. The former includes input and output disturbance, sensor noise and actuator noise, etc. Many dynamic perturbations that may occur in different parts of a system can, however, be lumped into one single perturbation block $\Delta(s)$, for instance, some unmodelled, high-frequency dynamics. In general speaking, the system uncertainty is the gap between the modulation equation of the system and the true physical characteristic of the system. For instance, the popular uncertainty presentations are the variation of power, the variation of size and fault location, the variation of wind speed (in case wind farm system) or variation of state variable of the system…etc. This uncertainty representation is referred to as "unstructured" uncertainty. In the case of linear, time-invariant systems, the block $\Delta(s)$ may be represented by an unknown transfer function matrix.

According to the small gain theorem, the term of plant transfer function of unstructured uncertainties $\Delta(s)$ and the nominal plant transfer function $T_{z\infty;w1}(s)$ are stable:

If $\Delta(s) \in H_\infty$, $T_{z\infty;w1}(s) \in H_\infty$, then the closed-loop system is internally stable if and only if

$$\left\|\Delta(s)T_{w_1,z_\infty}(s)\right\|_\infty < 1 \text{ and } \left\|T_{w_1,z_\infty}(s)\Delta(s)\right\|_\infty < 1 \tag{2.1}$$

We have $\left\|\Delta(s)T_{z_\infty,w_1}(s)\right\|_\infty \le \left\|\Delta(s)\right\|_\infty . \left\|T_{z_\infty,w_1}(s)\right\|_\infty$ replaces into (1)

$$\Rightarrow \qquad \left\|\Delta(s)\right\|_\infty . \left\|T_{w_1,z_\infty}(s)\right\|_\infty < 1$$

$$\Rightarrow \qquad \left\| T_{w_1, z_\infty}(s) \right\|_\infty < \frac{1}{\left\| \Delta(s) \right\|_\infty} \tag{2.2}$$

For the robustness against system uncertainties, the high term of $\left\| \Delta(s) \right\|_\infty$ is required. Because of unstructured uncertainties, it is useful to minimize the term of $\left\| T_{w_1, z_\infty}(s) \right\|_\infty$ in order to get the robust stability.

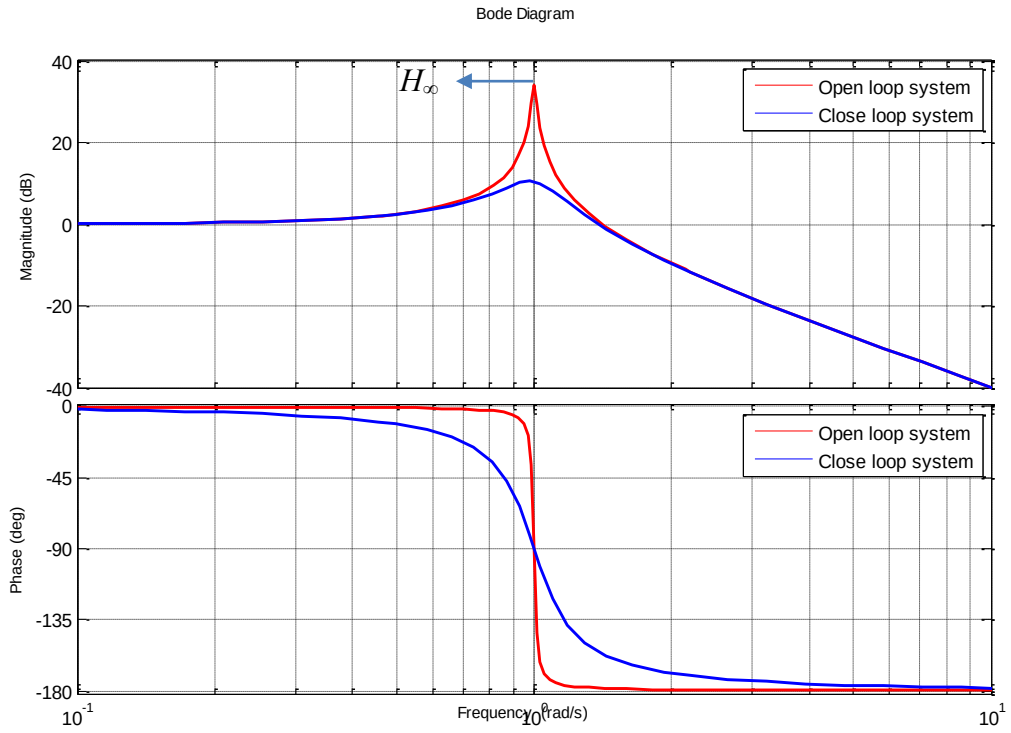

Figure 2.3 Bode plot of second order plant transfer function.

Consider a proper linear stable system $T_{z_\infty, w_1}(s)$. For the H_∞ norm we use the singular value (induced 2-norm) spatially (for the matrix) and pick out the peak value as a function of frequency

$$\left\| T_{z_\infty, w_1}(s) \right\|_\infty \triangleq \max_\omega \sigma(T_{z_\infty, w_1}(j\omega)) \tag{2.3}$$

In terms of performance we see from (2.3) that the H_∞ norm is the peak of the transfer function "magnitude", and by introducing weights, the H_∞ norm can be interpreted as the magnitude of some closed-loop transfer function relative to a specified upper bound. The Fig. 2.3 illustrates the example of bode plot of second order plant transfer function. The peak of red bode curve is the value of H_∞ norm at the dominant frequency of the open loop system. This point also descripts the robustness and damping ratio value of that dominant mode. After using the close loop control by H∞ controller K(s), the peak of blue bode curve of close loop transfer function is

reduced. From this we see that minimizing the H∞ norm corresponds to minimizing the peak of the largest singular value ("worst direction, worst frequency").

2.1.2 Performance Control Based on 2-norm

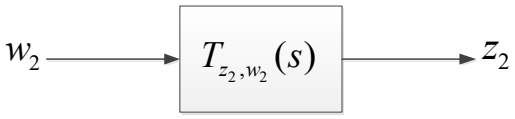

Figure 2.4 Nominal plant transfer function.

Consider the system in Figure 2.4, with a stable transfer function matrix $T_{z_2,w_2}(s)$ and impulse response matrix $g(t)$. To evaluate the performance we ask the question: given information about the allowed input signals w_2(t), how large can the outputs z_2(t) become? To answer this, we must evaluate the relevant system norm. The output signal in term of the usual 2-norm is evaluated by:

$$\|z_2(t)\|_2 = \sqrt{\sum_{ij}\int_{-\infty}^{\infty}|z_{2,i}(\tau)|^2\,d\tau} \tag{2.4}$$

Consider a strictly proper system $T_{z_2,w_2}(s)$. For the H_2 norm we use the Frobenius norm spatially (for the matrix) and integrate over frequency, we get:

$$\|T_{z_2;w_2}(s)\|_2 \triangleq \sqrt{\frac{1}{2\pi}\int_{-\infty}^{\infty} tr(T_{z_2;w_2}(j\omega)^H T_{z_2;w_2}(j\omega))d\omega} \tag{2.5}$$

We see that $T_{z_2,w_2}(s)$ must be strictly proper; otherwise the H_2 norm is infinite. The H_2 norm can also be given another interpretation. By Parseval's theorem, (2.5) is equal to the H_2 norm of the impulse response:

$$\|T_{z_2,w_2}(s)\|_2 = \|g(t)\|_2 \triangleq \sqrt{\int_0^{\infty} tr(g^T(\tau)g(\tau))d\omega} \tag{2.6}$$

We have $tr(g^T(\tau)g(\tau)) = \sum_{ij}|g_{ij}(\tau)|^2$ replaces in (2.6), we get:

$$\Rightarrow \left\| T_{z_2,w_2}(s) \right\|_2 = \left\| g(t) \right\|_2 = \sqrt{\sum_{ij} \int_0^\infty \left| g_{ij}(\tau) \right|^2 d\tau} \tag{2.7}$$

Following the meaning of (2.7), we have the following deterministic performance interpretation of the H2 norm:

$$\left\| T_{z_2,w_2}(s) \right\|_2 = \max \left\| z_2(t) \right\|_2 \tag{2.8}$$

When we minimize (2.8) the energy of output will be minimized. This claims the performance of the system when we minimize 2-norm of the plant transfer function.

In order to know the different between H_∞ and H_2, we can write the Frobenius norm in term of singular values as follow:

$$\left\| T_{z_2,w_2}(s) \right\|_2 = \sqrt{\frac{1}{2\pi} \int_{-\infty}^{\infty} \sum_i \sigma_i^2 (T_{z_2,w_2}(j\omega)) d\omega} \tag{2.9}$$

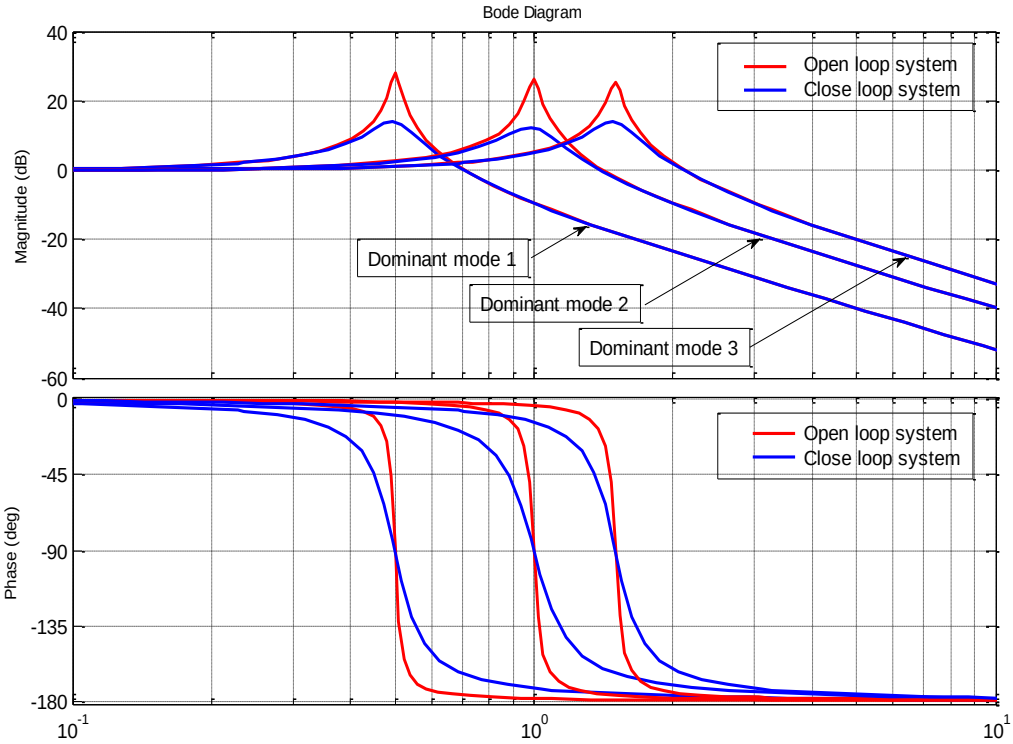

Figure 2.5 Bode plot of three dominant modes.

From (2.9) we see that minimizing the H_2 norm corresponds to minimizing the sum of the square of all the singular values over all frequencies (“average direction, average frequency”). For

example, the Fig. 2.5 illustrates the bode plots of plant transfer function which has three dominant modes. According to this graph, we find that the peak values at all the dominant mode frequencies of open loop plant transfer function are reduced after 2-norm of the close loop plant transfer function is minimized. It means that all the singular values (or damping ratios) of each dominant frequencies are considered by minimizing H_2 method.

2.1.3 Proposed Mixed H_2/H_∞ Fixed Structure Control Method

In this section, we will study the power oscillation damper design based on proposed mixed H_2/H_∞ robust method. The fixed structure of controller will be illustrated in section 2.1.3.1. The objective function of proposed control also shows detail in section 2.1.3.2.

2.1.3.1 Power Oscillation Damper

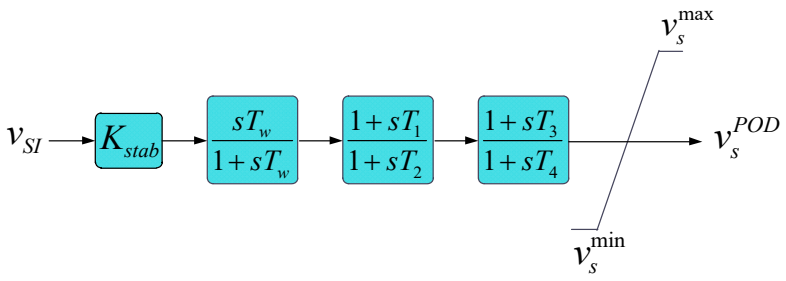

Figure 2.6 POD model.

Fig. 2.6 illustrates the block model of POD. The five important blocks of this control device are described as the transfer function in s-domain. The first block K_{stab} is the stability gain of POD, the second block is the reset block (washout filter) with time constant T_w, the third and fourth block are the phase lag/lead compensation block with parameters T_1, T_2, T_3, T_4, and the fifth block is the limit signal output of POD block, where v_s^{max} and v_s^{min} are the maximum and minimum value of signal output, respectively. The input signal of POD is defined by v_{SI}, and it has an output signal v_s^{POD} supplied to control vector device in order to stabilize power oscillation.

The stabilizer gain K_{stab} determines amount of damping introduced by the POD. Ideally, the gain should be set at a value corresponding to maximum damping; however, it is often limited by other considerations.

The signal washout block serves as a high-pass filter, with the time constant *Tw* high enough to allow signals associated with oscillations in ω_r to pass unchanged. Without it, steady changes

in speed would modify the terminal voltage. It allows the POD to respond only to changes in speed. From the view point of the washout function, the value of T_w is not critical and maybe in the range of 1 to 20 seconds. The main consideration is that it is long enough to pass stabilizing signals at the frequencies of interest unchanged, but not so long that it leads to undesirable generator voltage excursions during system-islanding condition.

The phase compensation blocks provide the appropriate phase-lead and lag characteristic to compensate for the phase-lead or lag of the control block connected by POD, i.e the exciter input of synchronous generator or the voltage control block of doubly fed induction generator…etc.

2.1.3.2 Proposed Objective Function based on Mixed H_2/H_∞ Method

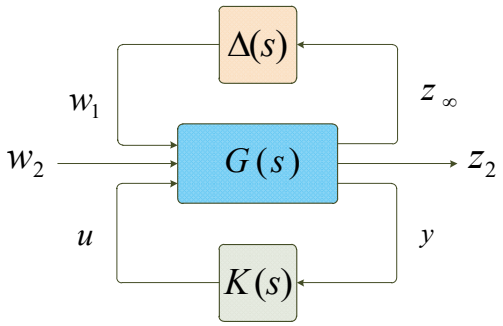

Figure 2.7 Closed loop system with mixed H_2/H_∞ control.

Generally, the robust control is used to capture a set of special specifications. For instance, the H_∞ control is more used to maintain the close loop stability in the presence of model uncertainties, but the H_2 tracking design is used to deal with the transient performance. To achieve both objectives, the mixed H_2/H_∞ control which is the powerful multi-objective control design, can be adopted. In Fig. 2.7 the closed loop system with a mixed H_2/H_∞ control is illustrated, where $G(s)$ is a nominal plant, $\Delta(s)$ is the model of system uncertainties, $K(s)$ is a controller, w_1 and w_2 are disturbance and external input vector, respectively, y is a measured output vector, u is an input vector from controller, z_2 is an output channel associated with the Linear Quadratic Gaussian (LQG) aspects (H_2 performance), and z_∞ is an output channel associated with the H_∞ performance. $T_{z\infty w1}(s)$ is defined as the closed-loop transfer function from w_1 to z_∞.

The system state equation of the close loop plant shown in Fig. 2.7 is modeled as follow:

$$G_{cl}:\begin{cases}\dot{x}=Ax+B_{11}w_1+B_{12}w_2+B_{13}u\\ z_\infty=C_{11}x+D_{11}w_1+D_{12}w_2+D_{13}u\\ z_2=C_{21}x+D_{21}w_1+D_{22}w_2+D_{23}u\\ y=C_{31}x+D_{31}w_1+D_{32}w_2\end{cases} \tag{2.10}$$

Where A is the state matrix of nominal plant; $B_{i,j}$ and $D_{i,j}$ are the matrix input of each input channel which effect with each state variable and each channel output; $C_{i,j}$ are the matrix output of each channel output.

From (2.10), we can find the plant transfer functions of each input and output channel as formula as follows:

$$P_{z_\infty,w_1}:\begin{cases}\dot{x}=Ax+B_{11}w_1+B_{13}u\\ z_\infty=C_{11}x+D_{11}w_1+D_{13}u\\ y=C_{31}x+D_{31}w_1\end{cases} \tag{2.11}$$

$$P_{z_2,w_2}:\begin{cases}\dot{x}=Ax+B_{12}w_2+B_{13}u\\ z_2=C_{21}x+D_{22}w_2+D_{23}u\\ y=C_{31}x+D_{32}w_2\end{cases} \tag{2.12}$$

Thus, according to (2.11) and (2.12), we can write P_{z_∞,w_2} and P_{z_2,w_2} in the plant matrix form as shown by:

$$\Rightarrow we\ \ get\ \ P_{z_\infty,w_1}=\begin{bmatrix}A & B_{11} & B_{13}\\ C_{11} & D_{11} & D_{13}\\ C_{31} & D_{31} & 0\end{bmatrix} \tag{2.13}$$

$$P_{z_2,w_2}=\begin{bmatrix}A & B_{12} & B_{13}\\ C_{21} & D_{22} & D_{23}\\ C_{31} & D_{32} & 0\end{bmatrix} \tag{2.14}$$

According to the fractional form, we can transform (2.13) and (2.14) to the fractional plant matrix by formula as bellow:

$$P_{z_\infty,w_1}(s)=\begin{bmatrix}P_{11} & P_{12}\\ P_{21} & P_{22}\end{bmatrix} \tag{2.15}$$

$$\Rightarrow we\ get\ \ \frac{z_\infty}{w_1} = T_{z_\infty, w_1} = P_{11} + P_{12}K(I - P_{22}K)^{-1}P_{21} \tag{2.16}$$

$$P_{z_2, w_2}(s) = \begin{bmatrix} P_{11}^{'} & P_{12}^{'} \\ P_{21}^{'} & P_{22}^{'} \end{bmatrix} \tag{2.17}$$

$$\Rightarrow we\ get\ \ \frac{z_2}{w_2} = T_{z_2, w_2} = P_{11}^{'} + P_{12}^{'}K(I - P_{22}^{'}K)^{-1}P_{21}^{'} \tag{2.18}$$

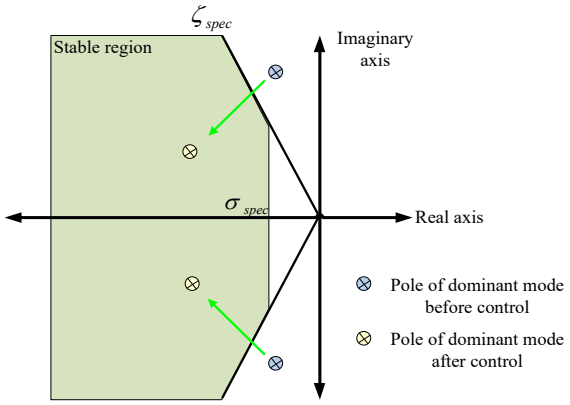

Figure 2.8 D-stability region.

Thus, by minimizing the infinite norm of $T_{z\infty w1}(s)$, i.e. $\|T_{z\infty w1}(s)\|_\infty$ and the two-norm of $T_{z2w2}(s)$, i.e. $\|T_{z2w2}(s)\|_2$, the robust stability of the system against uncertainties and the disturbance attenuation can be obtained as

$$\alpha \left\| T_{z\infty w1}(s) \right\|_\infty^2 + \beta \left\| T_{z2w2}(s) \right\|_2^2, \gamma \geq 0, \beta \geq 0 \tag{2.19}$$

In addition, by placing the dominant oscillation modes in the stability region with the specific damping ratio ζ_{spec} and specific real part σ_{spec} as shown in Fig. 2.8, the desired D-stability region can be guaranteed. Accordingly, the optimization problem can be formulated by

$$\text{Minimize} \quad \alpha \left\| T_{z\infty w1} \right\|_\infty^{\ 2} + \beta \left\| T_{z2w2} \right\|_2^{\ 2} \tag{2.20}$$

$$\text{Subject to} \begin{cases} \zeta_i \geq \zeta_{spec} \\ \sigma_i \leq \sigma_{spec} \end{cases}$$

where α and β are the weight of the term of $\left\| T_{z\infty w1}(s) \right\|_\infty^2$ and $\left\| T_{z2w2}(s) \right\|_2^2$ respectively. The weight is added into the function in order to make the balance or unbalance of each term depend on the

designer. If we minimize (2.20), the both robustness and performance will be obtained. Here, the performance is more required than robustness so that the unbalance between H_∞ and H_2 is proposed. Under this condition, we need to set α smaller than β. The specific damping ratio of oscillation modes are set as ζ_{spec}. Also the specific real part of the eigenvalue of oscillation modes are set as σ_{spec}. ζ_i and σ_i are defined as the damping ratio and real part of eigenvalue of oscillation modes, respectively.

2.2 Backtracking Search Optimization Algorithm

Optimization is a very important research area in applied mathematics. Optimization algorithms aim to find the best values for a system's parameters under various conditions. Optimization problems are usually designed in a way that defines the global optimum of an objective function as the global minimum. To be one of evolutionary optimization algorithms, backtracking search optimization algorithm (BSA) enables to solve numerical optimization problems successfully and rapidly [13]. BSA uses three basic genetic operations such as selection, mutation and crossover to generate trial individuals. BSA has a random mutation strategy that uses only one direction individual for each target individual and it is in contrast with many genetic algorithms such as DE and its derivatives JDE…etc. The direction individual from individuals of a randomly chosen previous generation is chosen randomly by BSA. Moreover, this algorithm uses a non-uniformly crossover strategy that is more complex than the crossover strategies used in many genetic algorithm.

To be a population-based interactive EA design, BSA can be explained by individual its functions into five processes as is done in other EAs: initialization, selection-I, mutation, crossover and selection-II. Fig. 2.9 shows the flow chat of BSA which can be described step by step as follows:

- Initialization: This part is described by step 1 and step 2.
  - Step 1: this is the initial step that generates the initial and old populations, and it is described by

$$\begin{aligned} p_{initial} &= rnd(up - low) + low \\ p_{old} &= rnd(up - low) + low \end{aligned} \tag{2.21}$$

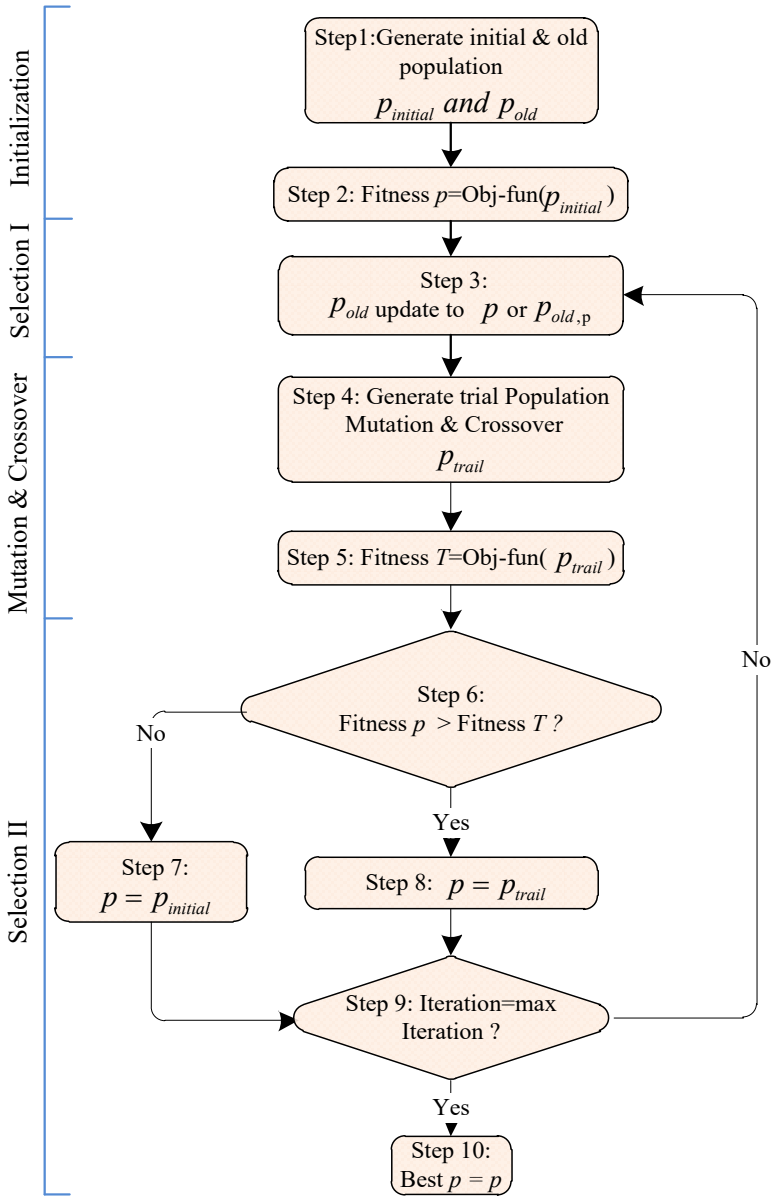

Figure 2.9 Flow chat of BSA.

where $p_{initial}$ and p_{old} are the initial and old populations, respectively, *up* and *low* are the limit range of dimensions of population, and *rnd* is the uniform distributed pseudo-random numbers.

- Step 2: The fitness value of initial population (Fitness p = Obj-fun ($p_{initial}$)) is calculated.

➢ Selection-I: this part is used to determine the historical population p_{old} and to be used for calculating the search direction. This part is described by step 3. BSA has the option of redefining p_{old} at the beginning of each iteration through the 'if-then' rule in (2.22):

If $i < j$ then p_{old} update to p

else $p_{old} = p_{old,p}$ = permuting(p_{old}) (2.22)

where p is population that obtains from selection randomly between old and initial population.

- Mutation and Crossover: BSA's mutation and crossover process generates the form of the trial population using (2.23).
  - Step 4: The new populations which are called as trail population, are generated by using mixed method between mutation and crossover and described by

$$p_{trail} = p + (map.F).(p_{old} - p) \quad (2.23)$$

where p_{trial} is the trail population , and *map* is a binary integer-valued matrix calculated for crossover term [13] . $F=3\times rndn$ is the get-scale-factor and *rndn* is the normally distributed pseudo-random numbers.

  - Step 5: the fitness of trial population (Fitness T = Obj-fun (p_{trial})) is calculated.
- Sellection-II : this part selects the best population by comparison method, and it is described in details by steps 6, 7, 8, 9 and 10.
  - Step 6: this is the selection step. The fitness population (Fitness p) and fitness of trial population (Fitness T) are compared.
  - Step 7: this is negative comment step "No". The best population (p) is equal to the initial population ($p_{initail}$), and then it continues to step 9.
  - Step 8: this is the positive comment step "Yes". The best population (p) is equal to the trial population (p_{trail}), and then it will continue to step 9.
  - Step 9: Check the maximum iteration. If "Yes", the process of minimization will stop and continue to step 10 "End", if No, it will return to step 3.
  - Step 10: The best population will be obtained.

2.3 Conclusion

Robust control design against system uncertainties is the considerably target method to get the robust controller. The structure of the proposed POD controller which is a practical 2nd-order

lead/lag compensator with single input, single output (SISO) is easily to simplify. Under using the mixed H_2/H_∞ method, the controller design is robustness and good performance. With optimization problem, the BSA is used to optimize the parameters of proposed controller.

CHAPTER 3

ROBUST POWER SYSTEM STABILIZATION BY DFIG WIND TURBINE

Recently, the power system has been developing considerably, but there are also some problems occur on the system. In condition that power system has the big power flow flows on the long transmission line, the power system oscillation with poor damping will occur in the system. This power oscillation with poor damping is a challenging problem in the power system stability and control [5]. The undammed power oscillation may cause the wide area blackouts and loss of system synchronism. To damp out the oscillation, the power system stabilizer (PSS) has been successfully used for a long time. Nevertheless, the PSS may cause the degradation in the quality of voltage control [3]. However, the PSS is not enough to stabilize the big power system with long transmission line.

The integration of wind power generation into power systems increases considerably. As the sharing of wind power generation increases, the contribution of wind power for power system control and stabilization is highly expected. As an example, in the new Spanish grid code for wind power, the ability of power oscillation damping is included [14]. Moreover, the wind energy system using doubly fed induction generator (DFIG) is widely accepted by wind energy industry today. The use of a DFIG does not only improve the efficiency of energy transfer from the wind, but also it provides wind farms with the capability of network support, voltage control, and power oscillation damping. Especially, the effect of DFIG on power oscillation damping has been widely paid attention [3-4]. The control of the DFIG wind turbine is achieved by controlling the RSC and GSC converters utilizing vector control techniques. The active and reactive power outputs of DFIG can be controlled independently by the power converters based on vector control [15], flux magnitude and angle control [16]. As a result, the DFIG-based wind turbine does not merely enhance the energy transfer efficiency but also provides the damping of power system oscillations. The vector control allows decoupled control of both real and reactive power. The idea is to use a rotating reference frame based on an AC flux or voltage and then to project the currents on this rotating frame. Such projections are usually referred to as the d and q components of their respective currents. For flux-based rotating frames, changes in the q component lead to

real power changes, while changes in the *d* component lead to reactive power changes. The cause of DFIG vector control, other control device also can supply its signal control stabilities in to the DFIG to make more controllability of the system. So that power oscillation damper (POD) control device is used with DFIG. In this chapter, the robust control design of POD used the mixed H_2/H_∞ method bases on DFIG wind turbines for stabilization of local-area oscillation in power system is focused on.

3.1 Stabilization of Single Machine Infinite Bus using DFIG Wind Turbine

The robust power oscillation damper (POD) design for doubly fed inducting generator (DFIG) based on a mixed H_2/H_∞ control method is proposed in this section. A practical 2^{nd}-order lead/lag compensator with local input signal is chosen as the POD structure. The POD is additionally installed with the voltage control loop of DFIG so that the modulation of reactive power output can be performed to damp out power oscillations. To acquire both damping performance and robustness, the optimization of POD parameters is formulated based on mixed H_2/H_∞ control. The backtracking search algorithm is automatically employed to solve the optimization problem. Simulation study indicates that the damping effect and robustness of the proposed robust POD are higher than those of the conventional POD against various system faults, heavy power flow levels, and wind patterns.

3.1.1 Study System and Modelling

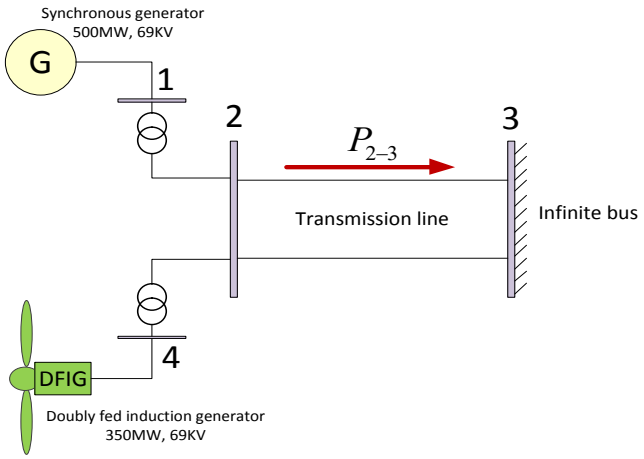

Figure 3.1 DFIG wind turbine and single synchronous generator connected to infinite bus.

Fig. 3.1 illustrates a DFIG wind turbine generator that grids with the single machine infinite bus system. This system has one synchronous generator and a wind turbine generator. The synchronous generator is presented by a six-order model. Also DFIG with back to back converter is used with wind turbine. Moreover, an automatic voltage regulator also is applied with synchronous generator to regulate voltage of terminal bus. The POD is applied to DFIG connected at bus 4 to supply power of wind farm to the main grid and to maintain power stability of this system. The total power flows from bus 2 to bus 3 ($P_{2\text{-}3}$) is chosen as the heavy power condition in this study.

3.1.1.1 Synchronous Generator

The synchronous generator is presented by a six-order model. This model is obtained assuming the presence of a field circuit and an additional circuit along the d-axis and two additional circuits along the q-axis. The system has six state variable (δ, ω, e'_q, e'_d, e''_q *and* e''_d) and the following equations:

$$
\begin{aligned}
\dot{\delta} &= \Omega_b(\omega - 1) \\
\dot{\omega} &= (p_m - p_e - D(\omega - 1))/M \\
e_q^{\bullet'} &= (-f_s(e'_q) - (x_d - x'_d - \frac{T''_{d0}}{T'_{d0}}\frac{x''_d}{x'_d}(x_d - x'_d))i_d + (1 - \frac{T_{AA}}{T'_{d0}})\upsilon_f^*/T'_{d0} \\
e_d^{\bullet'} &= (-e'_d + (x_q - x'_q - \frac{T''_{q0}}{T'_{q0}}\frac{x''_q}{x'_q}(x_q - x'_q))i_q)/T'_{q0} \\
e_q^{\bullet''} &= (-e''_q + e'_q - (x'_d - x''_d - \frac{T''_{d0}}{T'_{d0}}\frac{x''_d}{x'_d}(x_d - x'_d))i_d + \frac{T_{AA}}{T'_{d0}}\upsilon_f^*))/T''_{d0} \\
e_d^{\bullet''} &= (-e''_d + e'_d + (x'_q - x''_q - \frac{T''_{q0}}{T'_{q0}}\frac{x''_q}{x'_q}(x_q - x'_q))i_q)/T''_{q0}
\end{aligned}
\tag{3.1}
$$

where the electrical power $p_e = (\upsilon_q + r_a i_a)i_q + (\upsilon_d + r_a i_a)i_d$ and the algebraic constraints are as follows:

$$
\begin{aligned}
0 &= \upsilon_q + r_a i_q - e''_q + x''_d i_d \\
0 &= \upsilon_d + r_a i_d - e''_d + x''_q i_q
\end{aligned}
\tag{3.2}
$$

Table 3.1 Parameters of Synchronous Generator

Variable	Description	Unit
S_n	Power rating	500 MVA
V_n	Voltage rating	69 kV
f_n	Frequency rating	60 Hz
Type	Machine model	6 order
x_l	Leakage reactance	0.15 p.u.
r_a	Armature resistance	0.003 p.u.
x_d	d-axis synchronous reactance	1.81 p.u.
x'_d	d-axis transient reactance	0.3 p.u.
T'_{d0}	d-axis open circuit transient time constant	8 s
x_q	q-axis synchronous reactance	1.76 p.u.
x'_q	q-axis transient reactance	0.65 p.u.
T'_{q0}	q-axis open circuit transient time constant	0.25 s
$M=2H$	Mechanical starting time (2xinertia constant)	7kWs/kVA

3.1.1.2 Automatic Voltage Regulator

Automatic voltage regulators (AVRs) define the primary voltage regulation of synchronous machines. Several AVR models have been proposed and realized in practice. In this part, AVR type II which is the standard IEEE model will be described.

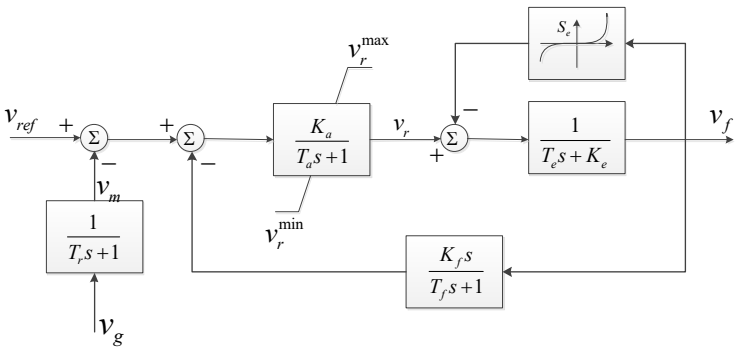

Figure 3.2 AVR type II model.

The reference voltages v_{ref} are initialized after the power flow computations. Limits are checked at the initialization step. AVR model has two algebraic equations, as follows:

$$\begin{aligned} 0 &= v_f - v_f^{sys} \\ 0 &= v_{ref}^0 - v_{ref} \end{aligned} \tag{3.3}$$

The AVR is depicted in Fig. 3.2 and described by the following equations:

$$\begin{aligned} v_m^{\bullet} &= (v_g - v_m)/T_r \\ v_{r1}^{\bullet} &= (K_a(v_{ref} - v_m - v_{r2} - \frac{K_f}{T_f}v_f) - v_{r1})/T_a \\ v_r &= \begin{cases} v_{r1} & if\ v_r^{\min} \le v_{r1} \le v_r^{\max}, \\ v_r^{\max} & if\ v_{r1} > v_r^{\max}, \\ v_r^{\min} & if\ v_{r1} < v_r^{\min}. \end{cases} \\ v_{r2}^{\bullet} &= -(\frac{K_f}{T_f}v_f + v_{r2})/T_f \\ v_f^{\bullet} &= -(v_f(K_e + S_e(v_f)) - v_r)/T_e \end{aligned} \tag{3.4}$$

v_r^{max} Maximum regulator voltage (p.u.)

v_r^{min} Minimum regulator voltage (p.u.)

K_a Amplifier gain (p.u./p.u.)

T_a Amplifier time constant (s)

K_f Stabilizer gain (p.u./p.u.)

T_f Stabilizer time constant (s)

K_e Field circuit integral deviation (p.u./p.u.)

T_e Field circuit time constant (s)

T_r Measurement time constant (s)

where v_g is the generator terminal voltage and the amplifier block is subjected to an anti-windup limit.

3.1.1.3 Doubly Fed Induction Generator Wind Turbine

Fig. 3.3 describes the DFIG control system. The DFIG control is performed by controlling the rotor side converter [4]. i_{qr}^* and i_{dr}^* are the quadrature and direct current of the rotor transformed from the system phase current of the rotor (i_a^*, i_b^*, i_c^*). The steady state electrical equations of the doubly fed induction generator are assumed, as the stator and rotor flux dynamics

are fast in comparison with grid dynamics and the converter controls basically decouple the generator from the grid. As a result of these assumptions, one has:

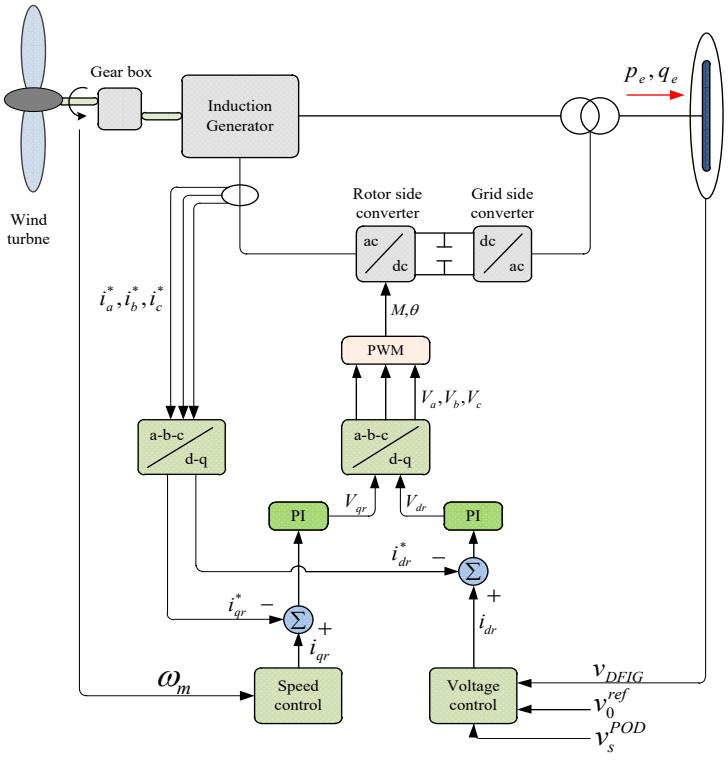

Figure 3.3 DFIG model.

$$
\begin{aligned}
v_{ds} &= -r_s i_{ds} + \left(\left(x_s + x_\mu\right) i_{qs} + x_\mu i_{qr}\right) \\
v_{qs} &= -r_s i_{qs} - \left(\left(x_s + x_\mu\right) i_{ds} + x_\mu i_{dr}\right) \\
v_{dr} &= -r_r i_{dr} - \left(1-\omega_m\right)\left(\left(x_s + x_\mu\right) i_{qr} + x_\mu i_{qs}\right) \\
v_{qr} &= -r_r i_{qr} - \left(1-\omega_m\right)\left(\left(x_s + x_\mu\right) i_{dr} + x_\mu i_{ds}\right)
\end{aligned}
\tag{3.5}
$$

where v_{ds}, v_{qs}, v_{dr}, v_{qr} are the voltage direct axis-(d) and quadrature axis-(q) of stator and rotor. The speed angle of wind turbine is defined as ω_m. The parameter r_s, r_r are the resistance stator and rotor of induction generator respectively. The parameters x_s and x_μ are the stator reactance and mutual reactance respectively of induction generator. And i_{ds}, i_{dr}, i_{qs}, i_{qr} are the stator and rotor current of direct and quadrature axis.

Since the converter dynamics are faster than the electromechanical transients [17], the converter is modeled as an ideal current source. Here, i_{qr} and i_{dr} are state variables used to control

the rotor speed and the terminal voltage, as depicted in Fig. 3.4(a) and 3.4(b), respectively. The differential and algebraic equations of the converter currents are given as follows:

$$i_{qr}^{\bullet} = \left(-\frac{x_s + x_\mu}{x_\mu v} p_\omega^* (\omega_m) / \omega_m - i_{qr} \right) \frac{1}{Te} \tag{3.6}$$

$$\begin{aligned} i_{dr}^{\bullet} &= K_V \left(v - v_{ref} \right) - v / x_\mu - i_{dr} \\ 0 &= v_{ref}^0 - v_{ref} + v_s^{POD} \end{aligned} \tag{3.7}$$

where $v_{ref}^{\ 0}$ is the initial reference voltage, v_s^{POD} is an additional signal of the POD, and the terminal magnitude voltage of wind turbine generator is presented as v. $p_w^*(\omega_m)$ is the power speed characteristic which roughly optimizes the wind energy capture ,and it is calculated by using the current rotor speed value. K_v and T_e are voltage control gain and power control time constant, respectively.

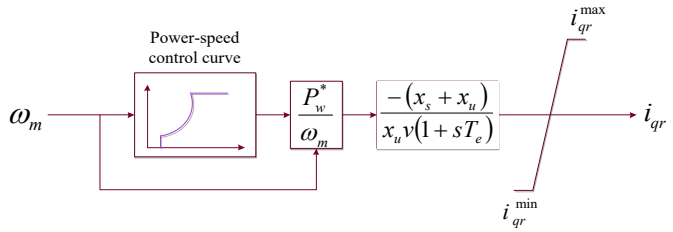

(a)

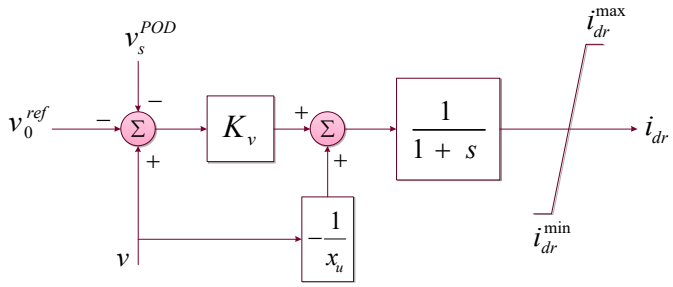

(b)

Figure 3.4 (a) Voltage control scheme of DFIG and (b) Rotor speed control scheme of DFIG.

The both speed and voltage controls undergo anti-windup limiters are considered in order to avoid the converter over-current. The rotor current limit is computed by basing on active and reactive power limits, and assuming bus voltage ≈ 1 as follows:

$$
\begin{aligned}
i_{qr}^{\max} &\approx -\frac{x_s + x_\mu}{x_\mu} p_e^{\min} \\
i_{qr}^{\min} &\approx -\frac{x_s + x_\mu}{x_\mu} p_e^{\max} \\
i_{dr}^{\max} &\approx -\frac{x_s + x_\mu}{x_\mu} q_e^{\min} - \frac{x_s + x_\mu}{x_\mu^2} \\
i_{dr}^{\min} &\approx -\frac{x_s + x_\mu}{x_\mu} q_e^{\max} - \frac{x_s + x_\mu}{x_\mu^2}
\end{aligned}
\tag{3.8}
$$

where i_{qr}^{max}, i_{qr}^{min}, i_{dr}^{max} and i_{dr}^{min} are the maximum and minimum rotor current of quadrature and direct axis, respectively. The maximum and minimum of the total active and reactive power output of DFIG are defined by p_e^{max} and q_e^{max}, respectively.

In Fig. 3.5, the pitch angle control can be described by the differential equation:

$$
\theta_p^{\bullet} = \left(K_p \phi \left(\omega_m - \omega_{ref} \right) - \theta_p \right) / T_p \tag{3.9}
$$

where ϕ is a function which allows varying the pitch angle set point only when the difference (ω_m-ω_{ref}) exceeds a predefined value $\pm\Delta\omega$. K_p and T_p are pitch control gain and pitch control time constant, respectively. The pitch control works only for super-synchronous speed. An anti-windup limiter locks the pitch angle to $\theta_p = 0$ for sub-synchronous speeds.

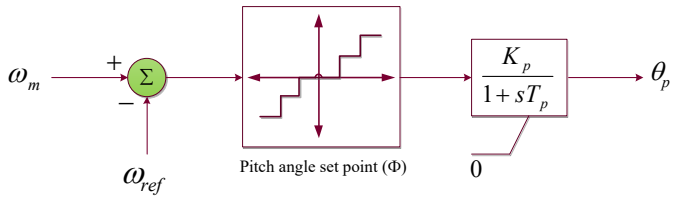

Figure 3.5 Pitch angle control.

The cause of vector control block, active power and reactive power can be controlled independently. To supply wind power to the main grid, active power and speed is controlled. In order to regulate voltage terminal, the reactive power control also is used. The current quadrature q-axis (i_{qr}) and the current direct d-axis (i_{dr}) at the rotor side is applied to the vector speed control device to control active power output and to the vector voltage control device to control reactive power output, respectively. The relative function between i_{qr}, i_{dr} and vector speed control, vector voltage control respectively are presented as follows:

$$p_e = \frac{x_s}{x_s + x_\mu} v i_{qr}$$
$$q_e = -\frac{x_\mu v i_{dr}}{x_s + x_\mu} - \frac{v^2}{x_\mu} \tag{3.10}$$

The active power (p_e) and reactive power (q_e) are the power total between stator power (p_s) and rotor power (p_r) output expressed by relative function as follows:

$$p_e = p_s + p_r$$
$$q_e = q_s + q_r \tag{3.11}$$

Table 3.2 Parameters of DFIG

Variable	Description	Unit
S_n	Power rating	350 MVA
V_n	Voltage rating	69 kV
f_n	Frequency rating	60 Hz
r_s	Stator resistance	0.01 p.u.
x_s	Stator reactance	0.1 p.u.
r_r	Rotor resistance	0.01 p.u.
x_r	Rotor reactance	0.08 p.u.
x_μ	Magnetizing reactance	3 p.u.
H_m	Rotor inertia	3 kWs/kVA
K_p	Pitch control gain	10 int
T_p	Pitch control time constant	3 s
K_v	Voltage control gain	10 int
T_ϵ	Power control time constant	0.01 s
p^{max}	Maximum active power	1 p.u.
p^{min}	Minimum active power	0 p.u.
q^{max}	Maximum reactive power	0.7 p.u.
q^{min}	Minimum reactive power	-0.7 p.u.

3.1.1.4 Power Oscillation Damper Model

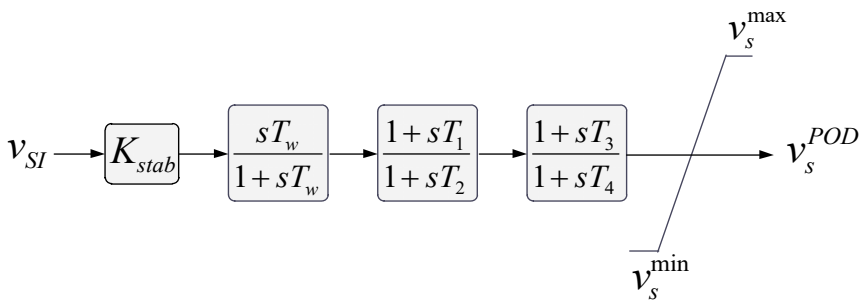

Figure 3.6 POD model.

Power oscillation damper (POD) is typically used for damping power system oscillations. The input signal of it can be the speed angle of synchronous generator ω_r , the currents or voltages of the system bus and line active or reactive power. This control device has three state variables v_1, v_2, v_3 described by the differential equations as follows:

$$\begin{aligned} v_1^{\bullet} &= -(K_w v_{SI} + v_1)/T_w \\ v_2^{\bullet} &= ((1-\frac{T_1}{T_2})(K_w v_{SI} + v_1) - v_2)/T_2 \\ v_3^{\bullet} &= ((1-\frac{T_3}{T_4})(v_2 + \frac{T_1}{T_2}(K_w v_{SI} + v_1)))/T_2 \\ v_s^{POD} &= v_3 + \frac{T_3}{T_4}(v_2 + \frac{T_1}{T_2}(K_w v_{SI} + v_1)) \end{aligned} \tag{3.12}$$

The POD structure, which is a 2nd-order lead-lag compensator, is delineated in Fig. 3.6. The POD consists of a stabilizer gain K_{stab}, a washout filter with time constant T_w=10 s, and two phase compensator blocks with time constants T_1, T_2, T_3 and T_4. The washout signal guarantees that the POD output is zero in steady state. An anti-windup limiter is equipped at the output of POD so that the output signal v_s^{POD} is between the minimum value (v_s^{min}) and the maximum value (v_s^{max}). To produce the satisfactory damping and the phase lead compensator, K_{stab} and T_1, T_2, T_3 and T_4 are optimally tuned. Here, the proposed design is used to optimize five parameters of POD.

3.1.2 Proposed Control

In this section, the control structure will be proposed. The doubly fed induction generator wind turbine with the power oscillation damper is used in this close loop control structure. Also

this section illustrates how to apply the mixed control method studied in chapter 2 to design the robust controller.

3.1.2.1 Propose Control Structure

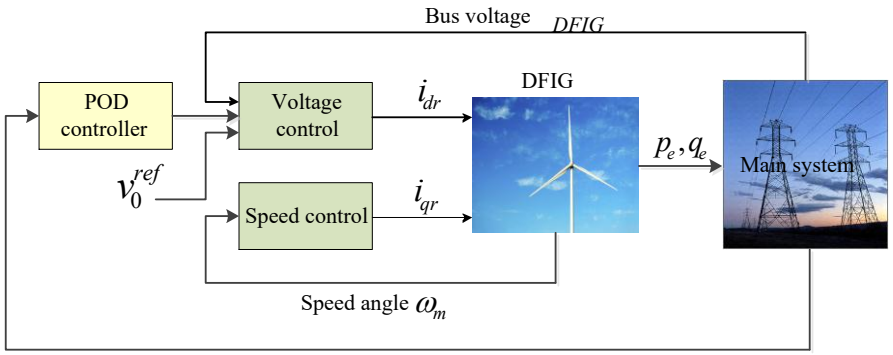

Figure 3.7 Control loop using DFIG with POD.

Control loop is commonly used for the stabilization work because it can observe and apply the control signal to the system well. As shown in Fig. 3.7, DFIG wind turbine with POD is employed to control the main system. The input signal of POD gets from the main system, and the signal output of controller send to the voltage control of DFIG. This allows the DFIG can control its reactive power in order to compensate with the reactive power of the main system. The results of this can eliminate the power oscillation of the whole system.

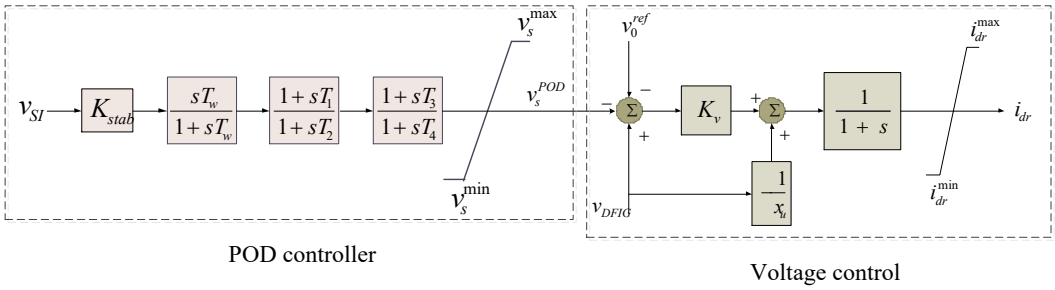

Figure 3.8 Connection between POD and voltage control.

The POD is additionally equipped with the controller of rotor side converter. By vector control technique in the rotor side converter, the independent control of active and reactive power outputs can be acquired. The converter is modeled by an ideal current source. As depicted in Fig. 3.4 (b) , i_{dr} is the output signal of voltage control block. The reactive power outputs of DFIG can be expressed in terms of i_{dr} as:

$$q_e = -\frac{x_u v i_{dr}}{x_s + x_u} - \frac{v^2}{x_u} \tag{3.13}$$

3.1.2.2 Optimized Objective Function based on Mixed H_2/H_∞ Method

By using the mixed control method which mentioned in chapter 2, we will get the robustness and good performance. Besides, by placing the dominant oscillation modes in the stability region with the specified damping ratio ζ_{spec} and specified real part σ_{spec} as shown in Fig. 2.8, the desired stability region can be guaranteed.

Accordingly, the optimization problem can be formulated by

$$\text{Minimize } \alpha \left\| T_{z\infty w1} \right\|_\infty^2 + \beta \left\| T_{z2w2} \right\|_2^2 \tag{3.14}$$

$$\text{Subject to } \begin{cases} \zeta \geq \zeta_{spec} \\ \sigma \leq \sigma_{spec} \end{cases}$$

$$\zeta_{spec} = 10\%, \sigma_{spec} = -0.5,\ \alpha = 0.1,\ \beta = 1$$
$$0.01 \leq K_{stab} \leq 5$$
$$0.01 \leq T_1, T_2, T_3, T_4 \leq 20$$

The stabilized control design of robust power oscillation damper (RPOD) is compared with the conventional POD (CPOD) which is designed by the pole replacement method. To obtain the same damping ratio as RPOD, the optimization problem of CPOD is given as follows:

$$\text{Minimize } \left(\left| \zeta - \zeta_{spec} \right| + \left| \sigma - \sigma_{spec} \right| \right) \tag{3.15}$$

$$\text{Subject to } \begin{cases} \zeta \geq \zeta_{spec} \\ \sigma \leq \sigma_{spec} \end{cases}$$

$$0.01 \leq K_{stab} \leq 5$$
$$0.01 \leq T_1, T_2, T_3, T_4 \leq 20$$
$$\zeta_{spec} = 10\%, \sigma_{spec} = -0.5$$

3.1.3 Discussion Results

Four cases were proposed to study in order to show the controllability between the proposed and conventional control under presenting the uncertainties system such as fault location, wind speed pattern and power flow…etc. The Table 3.3 illustrates all of the four cases studies.

Table 3.3 Case studies (Base=100 MVA, 60 Hz)

Case	Condition study	$P_{2\text{-}3}$ (p.u.)	Wind pattern (m/s)
1.	The 3 phase fault occurs at a transmission line between bus 2 and bus 3 at time = 5s, and cleared by circuit breaker (not reclose) at time = 5.05s.	4.33	Fig. 3.10 (a)
2.	The 3 phase fault occurs at a transmission line between bus 2 and bus 3 at time = 5s, and cleared by circuit breaker (not reclose) at time = 5.1s.	5.15	Fig. 3.10 (b)
3.	The 3 phase fault occurs at bus 2 at time = 5s, and cleared naturally at time = 5.1s.	5.74	Fig. 3.10 (c)
4.	The 3 phase fault occurs at bus 2 at time = 5s, and cleared naturally at time = 5.1s.	6.02	Fig. 3.10 (d)

3.1.3.1 Optimization Results

The parameters of POD were tuned automatically using the backtracking search algorithm. The equation (3.14) and (3.15) were used to be the optimized objective function of proposed controller and conventional controller. The BSA parameters were set as the population 25 and maximum iteration 100. The POD is designed under case 1 as shown in Table 3.3. After the optimization, Fig. 3.9 demonstrates the convergence curve of objective function of the proposed

control method. The optimized parameters of RPOD and CPOD are provided in Table 3.4. The eigenvalue analysis results in case 1 are shown in Table 3.5. Without POD, the damping ratio of the oscillation mode is very poor. On the other hand, the damping ratio of the oscillation mode is improved as expected by both CPOD and RPOD.

Eigenvalue analysis results and nonlinear simulation clearly confirm the superior robustness and damping performance of the proposed POD over the conventional POD.

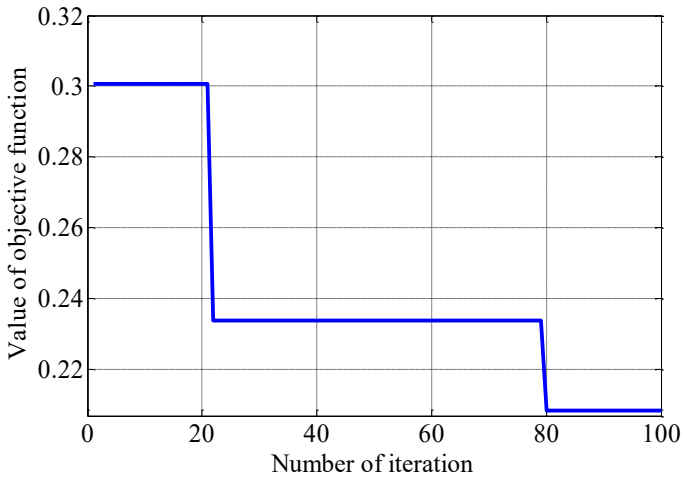

Figure 3.9 Convergence curve of Objective function.

Table 3.4 Opimal parameters of PODs

POD	K	Tw	T_1	T_2	T_3	T_4
RPOD	2.0154	10	3.2892	0.5765	1.2550	16.8830
CPOD	3.3543	10	0.2146	9.4152	11.7140	1.3701

Table 3.5 Eigenvalue analysis results

Control device	Eigenvalue	Damping ratio	Frequency (Hz)
No POD	$-0.232 \pm j7.62$	3.04%	1.21
RPOD	$-1.070 \pm j7.42$	14.25%	1.18
CPOD	$-0.847 \pm j6.90$	12.19%	1.10

3.1.3.2 Simulation Results

The Simulink tests are developed by MATLAB, Simulink and PSAT tool box [18]. The Figs. 3.10 demonstrates the wind speed pattern of all cases studies. Next, nonlinear simulations of case studies 1 to 4 in Table 3.3 are carried out. Figs. 3.11 (a)-(d) show the power flow from bus 2 to bus 3 of cases 1-4, respectively. In cases 1 and 2, the DFIG without POD cannot damp out the power oscillation. On the contrary, both CPOD and RPOD are able to suppress the power oscillation. In cases 3 and 4, the CPOD completely loses damping effect and fail to stabilize the oscillation. On the other hand, the RPOD is very robust against various uncertainties. It is able to get rid of the oscillation robustly.

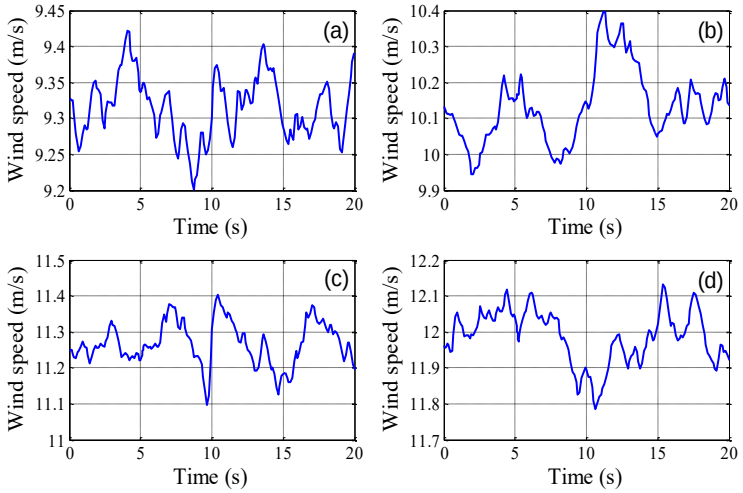

Figure 3.10 Wind speed patterns of (a) case 1, (b) case 2, (c) case 3, and (d) case 4.

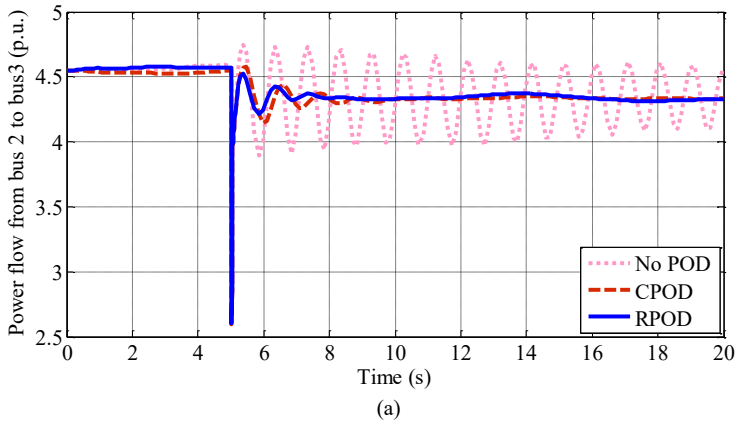

(a)

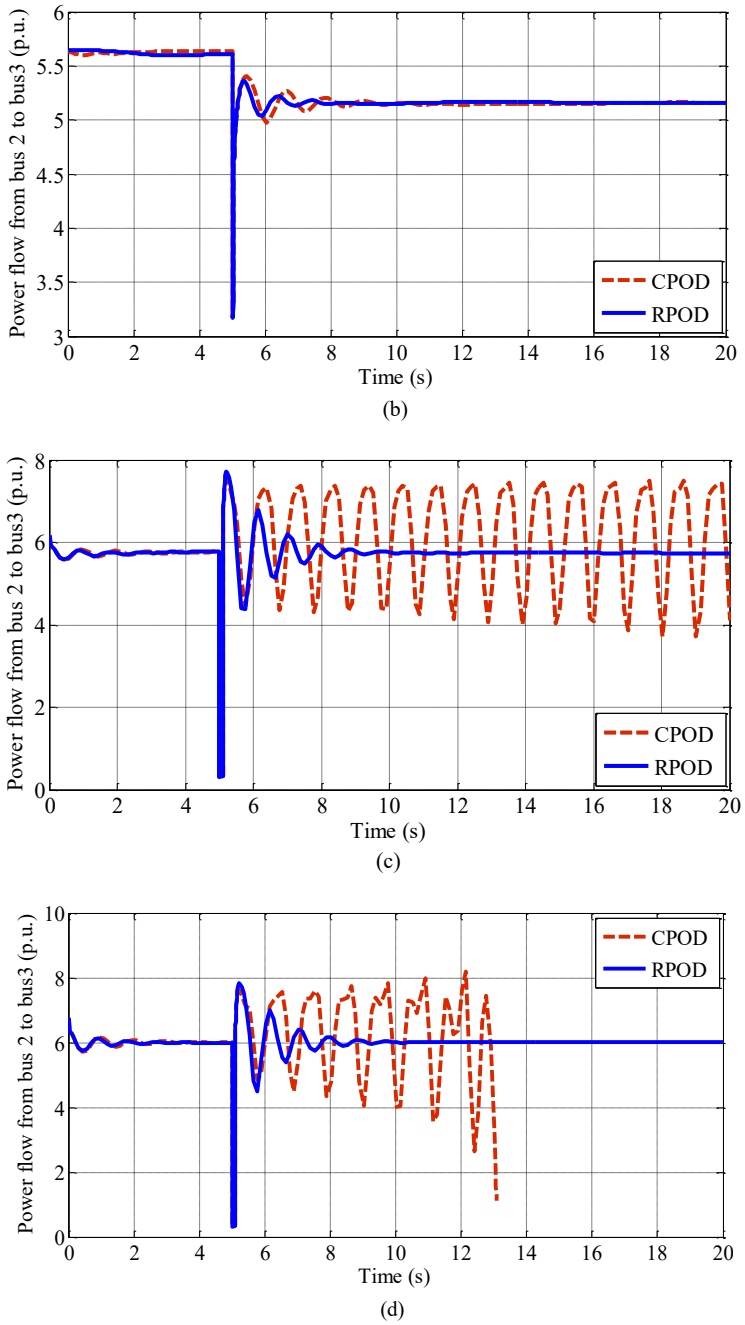

Figure 3.11 Power flow from bus 2 to 3 of (a) case 1, (b) case 2, (c) case 3, (d) case 4.

Fig. 3.12 shows the comparison between $||T_{z\infty_{w1}}||_\infty$ of CPOD and $||T_{z\infty_{w1}}||_\infty$ of RPOD when $P_{2\text{-}3}$ is varied from 3.2 to 5.45p.u. Note that $||T_{z\infty_{w1}}||_\infty$ implies the robustness of POD against system uncertainties. Obviously, when the power flow increases, $||T_{z\infty_{w1}}||_\infty$ in case of CPOD largely changes. The CPOD is very sensitive to the heavy power flow from bus 2 to infinite bus. This signifies that the damping effect of CPOD is deteriorated at the high level power flow. On the other hand, the change in $||T_{z\infty_{w1}}||_\infty$ in case of RPOD is lesser. The RPOD is not much sensitive to the variation of the power flow. This shows the high robustness of RPOD.

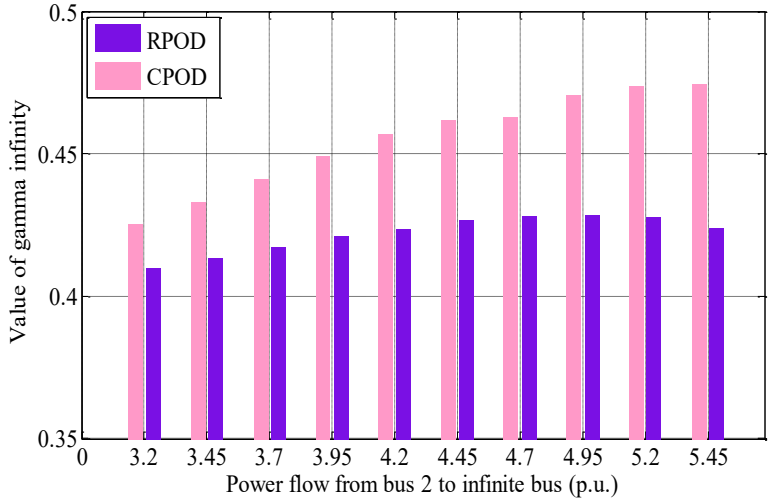

Figure 3.12 Value of gamma infinity ($\|T_{Z\infty w1}\|_\infty$).

3.1.4 Conclusion

The POD parameters tuning technique based on a mixed H_2/H_∞ method has been done. Since the POD structure is the 2nd-order lead/lag compensator with local input signal, it is easy to realize in real power system. The optimization of POD is conducted so that the desired system damping and robustness can be guaranteed. The POD parameters are automatically tuned by backtracking search algorithm. Eigenvalue analysis results and nonlinear simulation clearly confirm the superior robustness and damping performance of the proposed POD over the conventional POD under various power flow levels and severe faults.

3.2 Stabilization of the IEEE 9 Bus System Using DFIGs Wind Turbine

Two Doubly Fed Induction Generators grid with IEEE-9 bus system will be studied for this section. The H_2/H_∞ mix method is used for design RPOD to get robustness and good performance of system's dynamic. Backtracking Search optimization Algorithm (BSA) also applied with H_2/H_∞ to optimize the parameters of POD. The POD parameters are optimized so that the performance and robustness of the POD against system disturbances and uncertainties are maximal. The POD structure is a practical 2nd-order lead/lag compensator with single input, single output (SISO). As a result, the mixed H_2/H_∞ control gives a powerful multi-objective control design so that both closed-loop stability and performance of designed controller can be guaranteed.

3.2.1 Study System and Modeling

Two wind turbine generators which are gridded with IEEE-9 bus system are illustrated in Fig. 3.13. This system has three synchronous generator and two doubly fed induction generator wind turbines. The synchronous generator is presented by fourth-order model. Moreover, auto-voltage regulators (AVR) also are applied with synchronous generators to regulate the terminal voltage. The POD-1 and POD-2 are applied to DFIG-1 and DFIG-2 connected at bus 2 and 3 respectively to supply power of wind farm to the main grid. In this system, power flow from bus 9 to bus7 ($P_{9\text{-}7}$) and from bus 11 to bus 8 ($P_{11\text{-}8}$) are the heavy power flow condition.

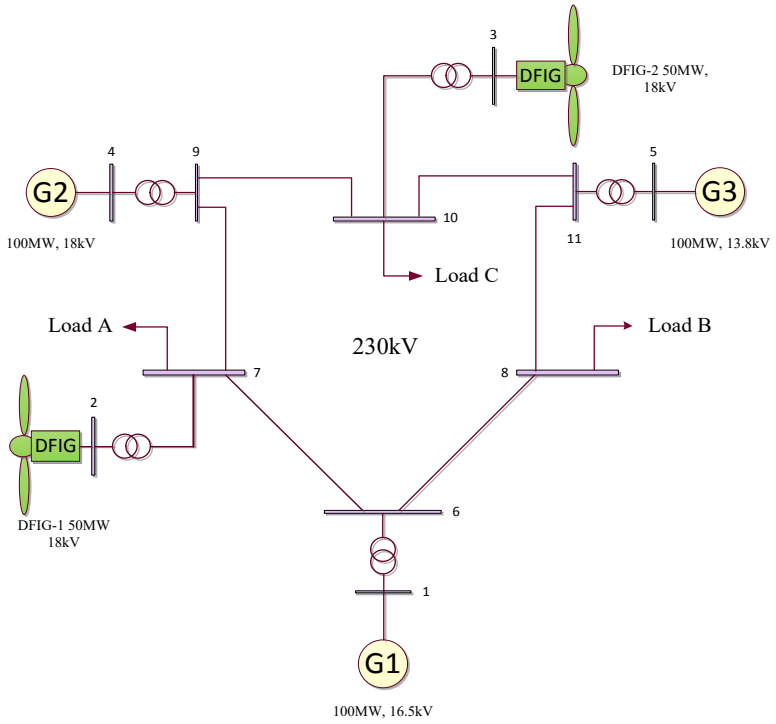

Figure 3.13 Two DFIGs grid with IEEE-9 bus system.

Table 3.6 Parameters of the synchronous machine

Generator	S_n	V_n	f_n	*Type*	x_d	x'_d	T'_{d0}	x_q	x'_q	T'_{q0}	$M=2H$
SG 1	100	16.5	60	4	0.14	0.06	8.96	0.09	0.09	0.31	47.28
SG 2	100	18	60	4	0.89	0.11	6	0.86	0.19	0.53	12.80
SG 3	100	13.8	60	4	1.31	0.18	5.89	1.25	0.25	0.60	6.02

S_n *Power rating (*MVA)

V_n	Voltage rating (kV)
f_n	Frequency rating (Hz)
Type	Machine model (int)
x_d	d-axis synchronous reactance (p.u.)
x'_d	d-axis transient reactance (p.u.)
T'_{d0}	d-axis open circuit transient time constant (s)
x_q	q-axis synchronous reactance (p.u.)
$\boldsymbol{x}'_q$	q-axis transient reactance (p.u.)
T'_{q0}	q-axis open circuit transient time constant (s)
$M=2H$	Mechanical starting time (2xinertia constant) (kWs/kVA)

Table 3.7 Parameters of DFIG

Variable	**Description**	**Unit**
S_n	Power rating	50 MVA
V_n	Voltage rating	18 kV
f_n	Frequency rating	60 Hz
r_s	Stator resistance	0.023 p.u.
x_s	Stator reactance	0.18 p.u.
r_r	Rotor resistance	0.016 p.u.
x_r	Rotor reactance	0.16 p.u.
x_μ	Magnetizing reactance	2.9 p.u.
H_m	Rotor inertia	3 kWs/kVA
K_p	Pitch control gain	10 int
T_p	Pitch control time constant	3 s
K_v	Voltage control gain	25 int
T_ϵ	Power control time constant	0.01 s
p^{max}	Maximum active power	1 p.u.
p^{min}	Minimum active power	0 p.u.
q^{max}	Maximum reactive power	0.5 p.u.
q^{min}	Minimum reactive power	-0.5 p.u.

Table 3.8 Parameters of AVR third order

Variable	Description	Unit
v_r^{max}	Maximum regulator voltage	5.00 p.u.
v_r^{min}	Minimum regulator voltage	-5.00 p.u.
K_0	Regulator gain	20 p.u./p.u.
T_2	Regulator pole	0.20 s
T_1	Regulator zero	0.063 s
Te	Field circuit time constant	0.31 s
T_r	Measurement time constant	0.001 s

3.2.2 Proposed Control

In this section, the control structure will be proposed. The two doubly fed induction generators wind turbine with the power oscillation damper are used in this close loop control structure. Also this section illustrates how to apply the mixed control method studied in chapter 2 to design the robust controller.

3.2.2.1 Proposed Control Structure

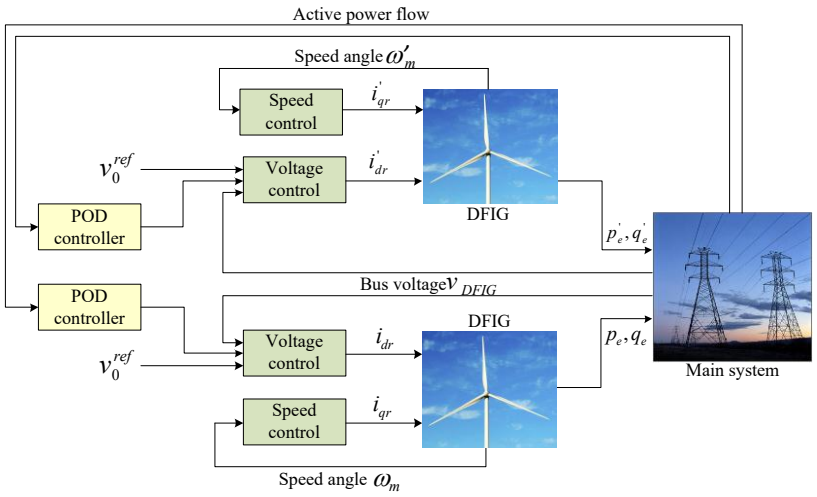

Figure 3.14 Coordinate control using DFIGs with PODs.

Two PODs are designed simultaneously by getting the input signal from the main system and sending their output signal into the DFIGs wind turbines, respectively. Because of control

loop, DFIGs wind turbines provide their active and reactive output power back into the system. This called the coordinated control loop between two or more of control devices.

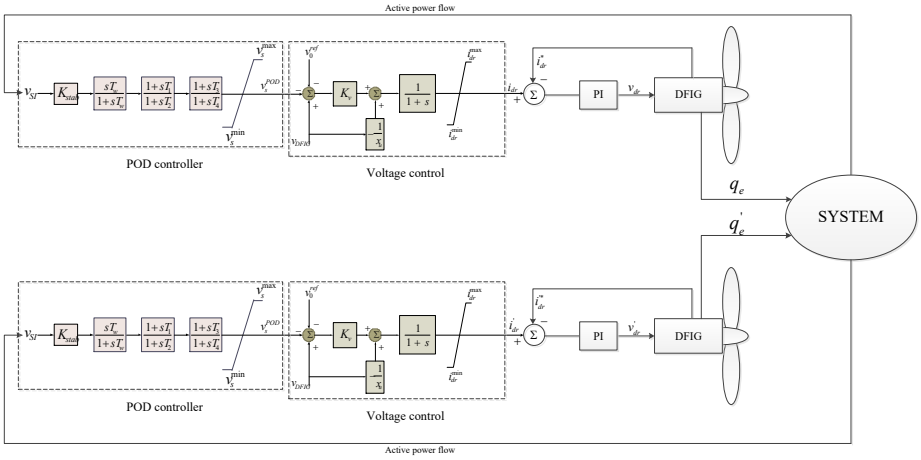

Figure 3.15 Model connection specifies on the reactive power generation.

The PODs are additionally equipped with the voltage control block of rotor side converter. By vector control technique in the rotor side converter, the independent control of the reactive power outputs can be acquired. The converter is modeled by an ideal current source. i_{dr} is the output signal of voltage control block. The reactive power outputs of both DFIGs can be expressed in equation (3.12).

3.2.2.2 Optimized Objective Function based on Mixed H_2/H_∞ Method

Following the mixed method which was discussed in chapter 2, the objective function is defined by:

$$\text{Minimize } \alpha \left\| T_{z\infty w2} \right\|_\infty^2 + \beta \left\| T_{z2w1} \right\|_2^2 \tag{3.16}$$

$$\text{Subject to } \begin{cases} \zeta_{1,2} \geq \zeta_{spec} \\ \sigma_{1,2} \leq \sigma_{spec} \\ 0.001 \leq K_{stab} \leq 2 \\ 0.001 \leq T_{1,2,3,4} \leq 0.1 \end{cases}$$

$$\zeta_{spec} = 5\%, \sigma_{spec} = -0.5, \ \alpha = 0.1, \ \beta = 1$$

where α=0.1 and β=1, are the weights. The specific damping ratio of oscillation modes are defined as ζ_{spec}. Also the specific real part of the eigenvalue of oscillation mode is defined as σ_{spec}. ζ_i, and σ_i are defined as the damping ratio and real part of eigenvalue of oscillation modes, respectively.

This method is compared with pole assignment method which considers only on the ideal modeling system to replace the pole location of oscillation modes, not consider on uncertainties part of the real modeling system. The objective function of this method is shown as follows:

$$\text{Minimize} \sum_{i=1}^{mn}\left(\left|\zeta_i-\zeta_{spec}\right|+\left|\sigma_i-\sigma_{spec}\right|\right) \tag{3.17}$$

$$\text{Subject to} \begin{cases} \zeta_{1,2} \geq \zeta_{spec} \\ \sigma_{1,2} \leq \sigma_{spec} \\ 0.001 \leq K_{stab} \leq 2 \\ 0.001 \leq T_{1,2,3,4} \leq 0.1 \end{cases}$$

$$\zeta_{spec} = 5\%, \sigma_{spec} = -0.5$$

3.2.3 Discussion Results

For cases studies which are under the variation of system uncertainties such as variation of the total power flow between power from bus 9 to 7 and power from bus 11 to 8, variation of fault location and wind speed pattern is used to do the experiment.

3.2.3.1 Optimization Results

The parameters of POD were tuned automatically using the backtracking search algorithm. The equation (3.16) and (3.17) were used to be the optimized objective function of proposed controller and conventional controller. The BSA parameters were set as follows; population = 25, maximum iteration = 200. The POD is designed under case 1 as shown in Table 3.9. After the optimization, Fig. 3.16 demonstrates the convergence curve of the objective function value of (3.16). The optimized parameters of POD are provided in Table 3.10. The eigenvalue analysis results in case 1 are shown in Table 3.11. Without POD, the damping ratio of the inter-area mode is very poor. On the other hand, the damping ratio of the inter-area mode is improved by both robust and conventional coordinated control.

Eigenvalue analysis results and nonlinear simulation clearly confirm the superior robustness and damping performance of the proposed coordinated control over the conventional control.

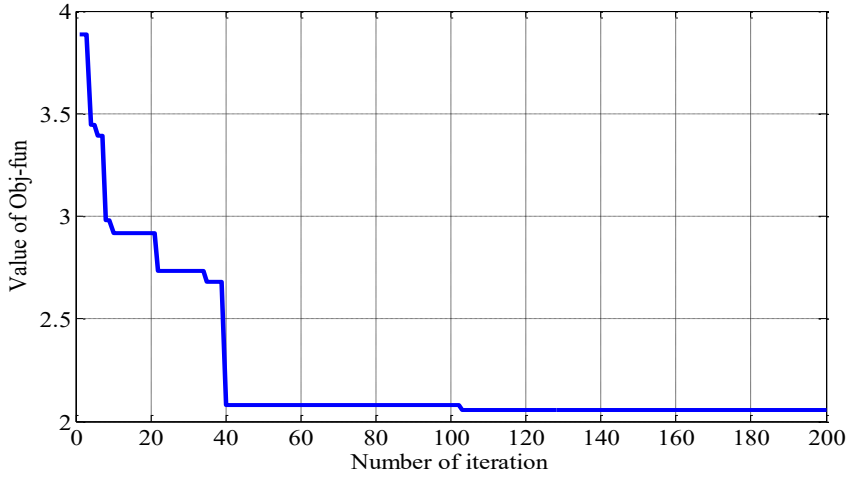

Figure 3.16 Convergence curve of Objective function.

Table 3.9 Case studies (Base=100 MVA, 60 Hz)

Case	Condition study	P_{total} (MW)	Wind speed pattern (m/s)
1.	The 3 phase fault occurs on bus 9 at time 1s cleared by nature of system at time 1.05s.	169.98	Fig. 3.17 (a)
2.	The 3 phase fault occurs on bus 9 at time 1s cleared by nature of system at time 1.066s.	202.40	Fig. 3.17 (b)
3.	The 3 phase fault occurs on bus 7 at time 1s cleared by nature of system at time 1.083s.	261.56	Fig. 3.17 (c)
4.	The 3 phase fault occurs on bus 7 at time 1s cleared by nature of system at time 1.1s.	261.56	Fig. 3.17 (d)

Table 3.10 Parameters of controllers

Control device	K	Tw	T1	T2	T3	T4
RPOD-1	1.1135	20	0.0471	0.0678	0.0500	0.0919
RPOD-2	1.9545	20	0.0087	0.0719	0.0199	0.0321
CPOD-1	1.7170	20	0.0583	0.0992	0.0887	0.0558
CPOD-2	1.6555	20	0.0143	0.0556	0.0208	0.0630

Table 3.11 Eigenvalue analysis

Control device		eigenvalue	Damping radio	Frequency (Hz)
No POD	Mode 1	-0.671 ± j12.6	5.31%	2.00
	Mode 2	-0.154 ± j8.44	1.82%	1.34
RPOD-1	Mode 1	-0.899 ± j12.6	7.12%	2.00
RPOD-2	Mode 2	-1.05 ± j7.74	13.44%	1.23
CPOD-1	Mode 1	-0.997 ± j12.6	7.89%	2.00
CPOD-2	Mode 2	-0.882 ± j7.33	11.95%	1.16

3.2.3.2 Simulation Results

The Simulink tests are developed by MATLAB, Simulink and PSAT tool box [18]. In case studies, the wind speed, fault position and fault time duration is changed. The Fig. 3.17 illustrates about the wind speed pattern changed in all case. Also power flow on transmission line from bus 9-7 and 11-8 are increased.

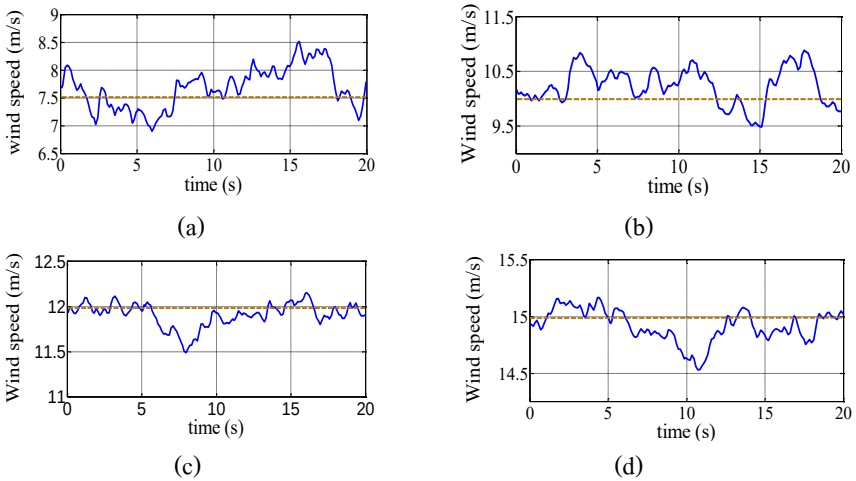

Figure 3.17 Wind speed of (a)-case 1, (b)-case 2, (c)-case 3, (d)-case 4.

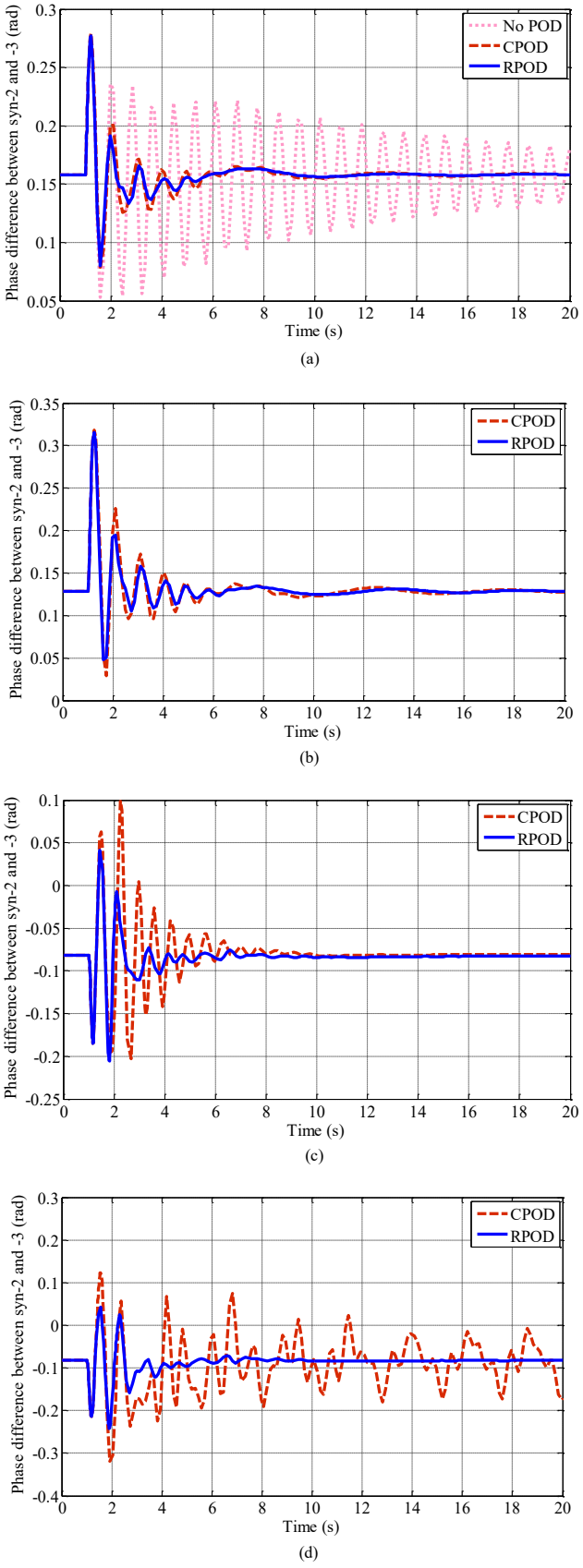

Figure 3.18 Phase difference between syn-2 and 3 of (a)-case 1, (b)-case 2, (c)-case 3, (d)-case 4.

The Fig. 3.18-(a) demonstrates the phase difference between the synchronous machine 2 and 3 of the design case 1. The damping effect of both DFIG-RPODs and DFIG-CPODs is much more than of No-POD. The Figs. 3.18-(b), (c), (d) illustrate the result of phase difference between the synchronous machine 2 and 3 of case 2, 3 and 4, respectively. In case 2 and 3, DFIG-RPOD and DFIG-CPOD still can damp power oscillation, but the damping effect of robust control device is better than conventional control device. On the other hand, DFIG-CPOD still cannot damp out the phase oscillation while DFIG-RPOD absolutely can damp out the oscillation.

The Fig. 3.19 shows the comparison of $||T_{z\infty_{w2}}||_\infty$ between DFIG-CPODs and DFIG-RPODs when the total power of $P_{9\text{-}7}$ and $P_{8\text{-}11}$ was varied from 1.85 to 2.74 p.u. Obviously, $||T_{z\infty_{w2}}||_\infty$ in case of DFIG-CPODs largely changes. The DFIG-CPODs is very sensitive to the uncertainty due to the total power flow from bus 9 to 7 and 8 to 11. On the other hand, the change in $||T_{z\infty_{w2}}||_\infty$ in case of DFIG-RPODs is lesser. The DFIG-RPODs is not much sensitive to the variation of the power flow on infinite transmission line.

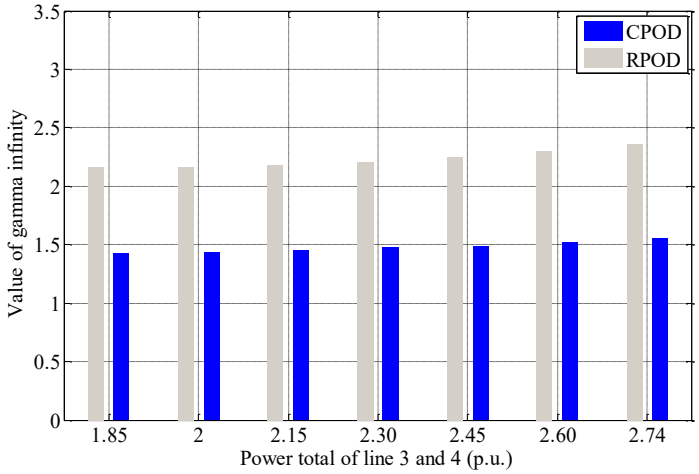

Figure 3.19 Value of gamma infinity ($||T_{z\infty_{w1}}||_\infty$).

3.2.4 Conclusion

In conclusion, as all the results that shows about the comparison between robust proposed control and conventional power oscillation damper really express that damping effect of robust control method considers on the uncertainty system is much superior than conventional method. The structure of POD is easy to linearize, and its parameters are optimized automatically by Backtracking Search optimization Algorithm. The inverse output multiplicative perturbation is used to model unstructured uncertainty. The parameters of RPOD are optimized base on mixed

H_2/H_∞ method. This optimization condition makes the robustness against system uncertainties and stabilization performance of the system be augmented.

CHAPTER 4

COORDINATED CONTROL OF DFIG WIND TURBINE AND SVC FOR STABILIZATION

This chapter will describe the coordinated work of multiple control devices. A coordinated control of doubly fed induction generator (DFIG) and static var compensator (SVC) facts device using power oscillation damper (POD) will discuss in the chapter. To understand well the objective of this part, the question "Why coordination?" should have the present here.

The power oscillation with low frequency between 0.2-2.0 Hz is still the challenging problem for interconnection power system. Some of local control devices such as power system stabilizer (PSS) and auto voltage regulator (AVR) have been used successfully for local oscillation mode. However, since the lack of observability of the inter-area oscillation mode, the PSS using the local signal may not be able to damp out the inter-area oscillations. On the other hand, the static var compensator (SVC) which is one of flexible AC transmission systems (FACTS) device can be applied. In [10, 11], the SVC which is installed with the power oscillation damper (POD), has been successfully applied to stabilize the inter-area oscillation.

Currently, the wind farms have been widely installed in power systems. Especially the doubly fed induction generator (DFIG) wind turbine which is a variable speed type wind turbine has been extensively paid attentions. The practical merits of DFIG wind turbines are low installation cost and controllability of active and reactive power outputs [2]. However, because the output power of the wind power generation is intermittent in nature, it may cause the negative impact on the power oscillations [12]. Under this condition, the stabilizing effect of SVC may be deteriorated. To enhance the control effect of SVC, the DFIG wind turbine which is equipped with a power oscillation damper (POD), can be employed [4]. For this purpose, the coordinated control between both devices DFIG and SVC facts using POD controllers should be a good method employed to handle the both local and inter-area oscillation modes.

4.1 Study System and Modeling

The two area four machine system [5] which is used to discuss in here, is illustrated in Fig. 4.1. The rated power and voltage of each synchronous generator are 900 MVA and 20 kV,

respectively. The DFIG wind farm with 50 MVA, 20 kV is installed at bus 6. To regulate the voltage at bus 8, the SVC with 100 MVA, 230 kV is connected. To stabilize the power oscillation in this system, the POD is added to the voltage control loops of both DFIG and SVC.

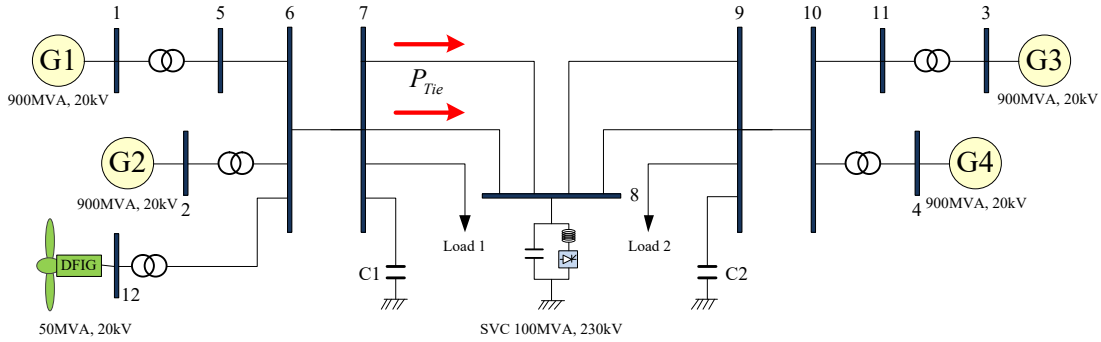

Figure 4.1 Two-area four machine system.

The static var compensator (SVC) is one of the flexible AC transmission system (FACTS). It is used to control the inter-area low frequency oscillation of the system. The reactive power output of SVC is used to compensate with the reactive power of the system while the system is unstable.

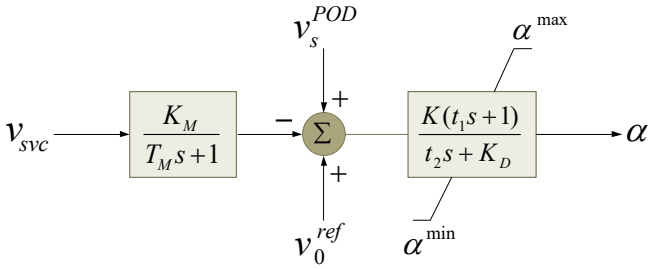

Figure 4.2 SVC regulator.

The differential and algebraic equations are as follows:

$$
\begin{aligned}
v_M^{\bullet} &= (K_M v - v_M)/T_M \\
\alpha^{\bullet} &= (-K_D\alpha + K\frac{T_1}{T_2 T_M}(v_M - K_M v) + K(v_{ref} + v_s^{POD} - v_M))/T_2 \\
q &= \frac{2\alpha - \sin 2\alpha - \pi(2 - x_L/x_C)}{\pi x_L} v^2 = b_{SVC}(\alpha)v^2
\end{aligned}
\tag{4.1}
$$

where the state variable α undergoes an anti-windup limiter. V is the terminal voltage of SVC, and q is the reactive output power of SVC (MVar).

Table 4.1 Parameters of the synchronous machine

Variable	Description	Unit
S_n	Power rating	900 MVA
V_n	Voltage rating	20 kV
f_n	Frequency rating	60 Hz
Type	Machine model	6 order
x_l	Leakage reactance	0.2 p.u.
r_a	Armature resistance	0.0025 p.u.
x_d	d-axis synchronous reactance	1.80 p.u.
x'_d	d-axis transient reactance	0.30 p.u.
x''_d	d-axis sub-transient reactance	0.25 p.u.
T'_{d0}	d-axis open circuit transient time constant	8 s
T''_{d0}	d-axis open circuit sub-transient time constant	0.03 p.u.
x_q	q-axis synchronous reactance	1.7 p.u.
x'_q	q-axis transient reactance	0.55 p.u.
x''_q	q-axis sub-transient reactance	0.25 p.u.
T'_{q0}	q-axis open circuit transient time constant	0.4 s
T''_{q0}	q-axis open circuit sub-transient time constant	0.05 p.u.
$M=2H$	Mechanical starting time (2xinertia constant)	13 kWs/kVA

Table 4.2 Parameters of SVC second type

Variable	Description	Unit
S_n	Power rating	100 MVA
V_n	Voltage rating	230 kV
f_n	Frequency rating	60 Hz
T_2	Regulator time constant	10 s
K	Regulator gain	10 p.u./p.u.
v_{ref}	Reference Voltage	1 p.u.
α^{max}	Maximum firing angle	2 p.u.
α^{min}	Minium firing angle	-0.2 p.u.
K_D	Intergral deviation	0.001p.u.
T_1	Transient regulator time constant	0 s
K_M	Measure gain	1 p.u./p.u.
T_M	Measure time delay	0.01 s
x_L	Reactance (inductive)	0.2 p.u.
x_C	Reactance (capacitive)	0.1 p.u.

Table 4.3 Parameters of AVR second order

Variable	Description	Unit
v_r^{max}	Maximum regulator voltage	5.00 p.u.
v_r^{min}	Minimum regulator voltage	-5.00 p.u.
K_a	Amplifier gain	20 p.u./p.u.
T_a	Amplifier time constant	0.055 s
K_f	Stabilizer gain	0.125 p.u./p.u.
T_f	Stabilizer time constant	1.8 s
K_e	Field circuit integral deviation	1 p.u./p.u.
Te	Field circuit time constant	0.36 s
T_r	Measurement time constant	0.05 s

Table 4.4 Parameters of DFIG

Variable	Description	Unit
S_n	Power rating	50 MVA
V_n	Voltage rating	20 kV
f_n	Frequency rating	60 Hz
r_s	Stator resistance	0.023 p.u.
x_s	Stator reactance	0.18 p.u.
r_r	Rotor resistance	0.016 p.u.
x_r	Rotor reactance	0.16 p.u.
x_μ	Magnetizing reactance	2.9 p.u.
H_m	Rotor inertia	4.32 kWs/kVA
K_p	Pitch control gain	10 int
T_p	Pitch control time constant	3 s
K_v	Voltage control gain	50 int
T_ϵ	Power control time constant	0.01 s
p^{max}	Maximum active power	1 p.u.
p^{min}	Minimum active power	0 p.u.
q^{max}	Maximum reactive power	0.5 p.u.
q^{min}	Minimum reactive power	-0.5 p.u.

4.2 Proposed Control

In this section, the coordinated control structure will be illustrated. The doubly fed induction generator wind turbine with POD and the Static var compensator FACTS device with POD are used in this close loop control structure. Also in this section illustrates how to apply the proposed control method studied in chapter 2 to design the robust controller.

4.2.1 Proposed Coordinated Control Structure

Fig. 4.3 illustrates the coordinated control loop structure using DFIG and SVC. The PODs are adapted with the DFIG and SVC, respectively. Two PODs are designed simultaneously by

getting the input signal from the main system and sending their output signal into the DFIG wind turbine and SVC FACTS device, respectively. Because of control loop, DFIG wind turbines and SVC provide their reactive output power back into the system. This called the coordinated control loop between two or more of difference types of control devices. In Fig. 4.4, the reactive power generation of the both DFIG and SVC are demonstrated.

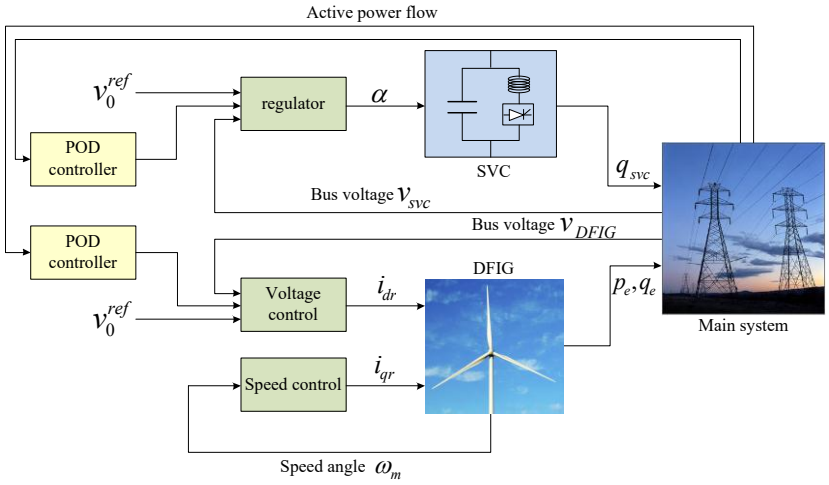

Figure 4.3 Coordinated control loop using DFGI and SVC facts.

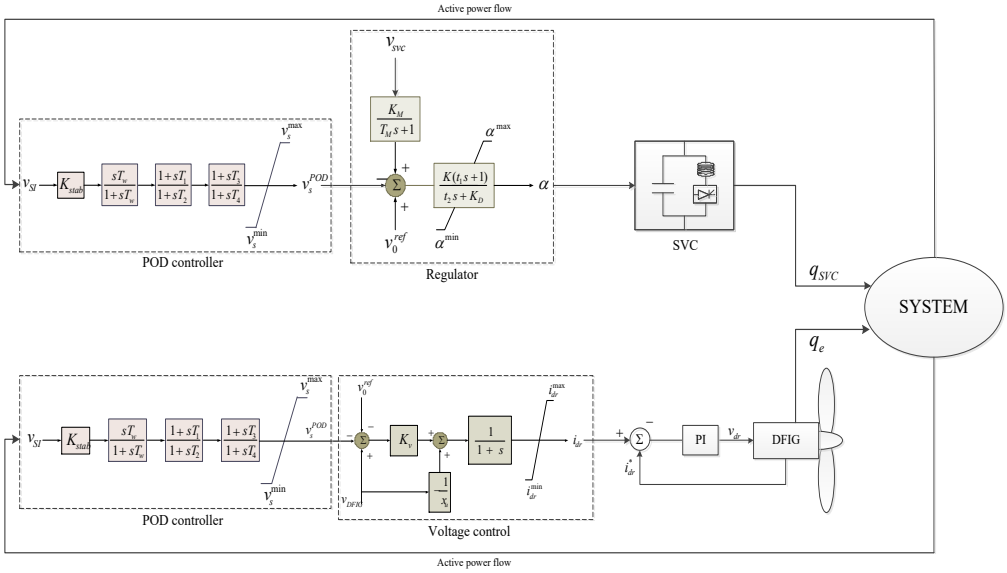

Figure 4.4 Connection model of controller specified on the reactive power generation.

4.2.2 Optimized Objective Function based on Mixed H_2/H_∞ Method

As defined in Chapter 2, by minimizing the infinite norm of $T_{z\infty w1}(s)$, i.e. $\|T_{z\infty w1}(s)\|_\infty$ and the two-norm of $T_{z2w2}(s)$, i.e. $\|T_{z2w2}(s)\|_2$, the robust stability of the system against uncertainties and the disturbance attenuation can be obtained.

In addition, by placing the dominant oscillation modes in the stability region with the specific damping ratio ζ_{spec} and specific real part σ_{spec}, the desired D-stability region can be guaranteed. Accordingly, the optimization problem can be formulated by

$$\text{Minimize} \quad \gamma \left\| T_{z\infty w1} \right\|_\infty^{\ 2} + \beta \left\| T_{z2w2} \right\|_2^{\ 2} \tag{4.2}$$

$$\text{Subject to} \begin{cases} \zeta_i \geq \zeta_{spec} \\ \sigma_i \leq \sigma_{spec} \\ 0.001 \leq K_{stab} \leq 5 \\ 0.001 \leq T_1, T_2, T_3, T_4 \leq 5 \end{cases}$$

where γ=0.1 and β=1, are the weights. The specific damping ratio of oscillation modes are set as ζ_{spec}=5%. Also the specific real part of the eigenvalue of oscillation modes are set as σ_{spec} = -0.1. ζ_i and σ_i are defined as the damping ratio and real part of eigenvalue of oscillation modes, respectively.

The pole assignment method is applied to compare with the proposed objective function. This method is used to formulate the optimization problem of conventional POD (CPOD). The objective function is defined as follows:

$$\text{Minimize} \sum_{i=1}^{nm} \left(\left| \zeta_i - \zeta_{spec} \right| + \left| \sigma_i - \sigma_{spec} \right| \right) \tag{4.3}$$

$$\text{Subject to} \begin{cases} \zeta_i \geq \zeta_{spec} \\ \sigma_i \leq \sigma_{spec} \\ 0.001 \leq K_{stab} \leq 5 \\ 0.001 \leq T_1, T_2, T_3, T_4 \leq 5 \end{cases}$$

where *nm* is the number of the oscillation modes of the system. Here, we have tree dominance modes (one inter-area mode and two local modes).

4.3 Discussion Results

Three cases were proposed to study in order to show the controllability between the proposed and conventional control under presenting the uncertainties system such as fault location, wind speed pattern and power flow…etc. The Table 4.5 illustrates all of the three cases studies.

Table 4.5 Case studies (Base=100 MVA, 60 Hz)

Case	Condition study	P_{Tie} (p.u.)	Wind pattern (m/s)
1.	The 3 phase fault occurs on bus 9 at time 1 s, naturally cleared at time 1.05 s.	4.0	Fig. 4.7 (a)
2.	The 3 phase fault occurs on bus 8 at time 1 s, naturally cleared at time 1.06 s.	5.5	Fig. 4.7 (b)
3.	The 3 phase fault occurs on bus 8 at time 1 s, naturally cleared at time 1.08 s.	6.0	Fig. 4.7 (c)

4.3.1 Optimization Results

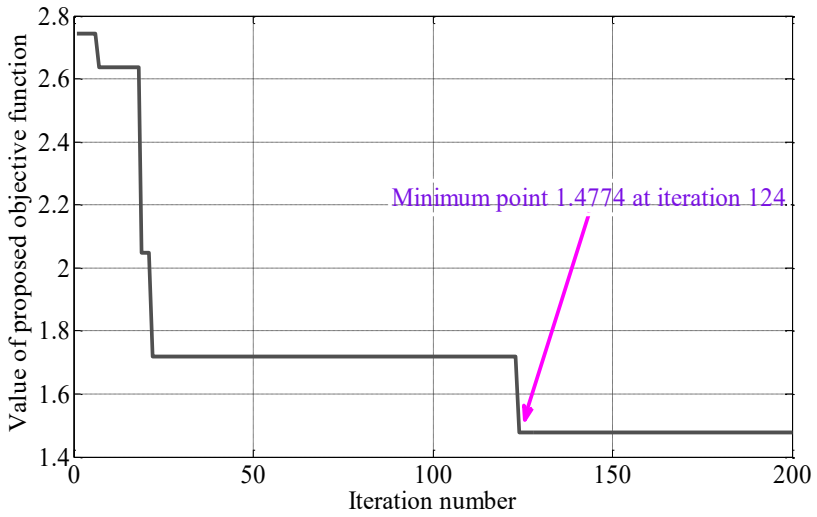

Figure 4.5 Convergence curve of objective function.

The parameters of POD were tuned automatically using the backtracking search algorithm. The equation (4.2) and (4.3) were used to be the optimized objective function of proposed controller and conventional controller. The BSA parameters were set as follows; population = 25,

maximum iteration = 200. The POD is designed under case 1 as shown in Table 4.5. After the optimization, Fig. 4.5 demonstrates the convergence curve of the objective function value of (4.2). The optimized parameters of POD are provided in Table 4.6. The eigenvalue analysis results in case 1 are shown in Table 4.7. Without POD, the damping ratio of the inter-area mode is very poor. On the other hand, the damping ratio of the inter-area mode is improved by both robust and conventional coordinated control.

Eigenvalue analysis results and nonlinear simulation clearly confirm the superior robustness and damping performance of the proposed coordinated control over the conventional control.

Table 4.6 Optimal parameters of PODs

Devices	K_{stab}	T_1	T_2	T_3	T_4
Robust coordinated control					
RPOD-DFIG	3.8820	0.8982	4.5501	0.0171	0.5068
RPOD-SVC	4.7952	4.6985	4.6487	0.0577	1.4426
Conventional coordinated control					
CPOD-DFIG	3.3754	0.0048	1.6353	0.1806	1.6139
CPOD-SVC	2.9063	1.0043	3.2355	4.5274	1.9796

Table 4.7 Eigenvalue analysis results

Control device		**Eigenvalue**	**Damping ratio**	**Frequency (Hz)**
Without POD	Local 1	-0.534 ± *j*6.84	7.78%	1.08
	Local 2	-0.524 ± *j*6.64	7.86%	1.05
	Inter-area	**-0.045 ± *j*3.56**	**1.28%**	**0.56**
Robust coordinated control	Local 1	-0.528 ± *j*6.84	7.69%	1.08
	Local 2	-0.529 ± *j*6.67	7.90%	1.06
	Inter-area	**-0.354 ± *j*3.49**	**10.10%**	**0.55**
Conventional coordinated control	Local 1	-0.538 ± *j*6.84	7.83%	1.08
	Local 2	-0.524 ± *j*6.64	7.86%	1.05
	Inter-area	**-0.397 ± *j*3.42**	**11.50%**	**0.54**

The locus of the eigenvalue corresponding to the inter-area mode under the variation of P_{Tie} from 4.0 to 6.0 p.u. is delineated in Fig. 4.6. At heavy P_{Tie}, the locus of the inter-area mode in case of without POD and CPOD coordinated control moves to the unstable region. On the other hand, the locus in case of RPOD coordinated control is still in the D-stability region. This result indicates that the robustness of RPOD coordinated control against heavy power flow is superior to that of CPOD coordinated control.

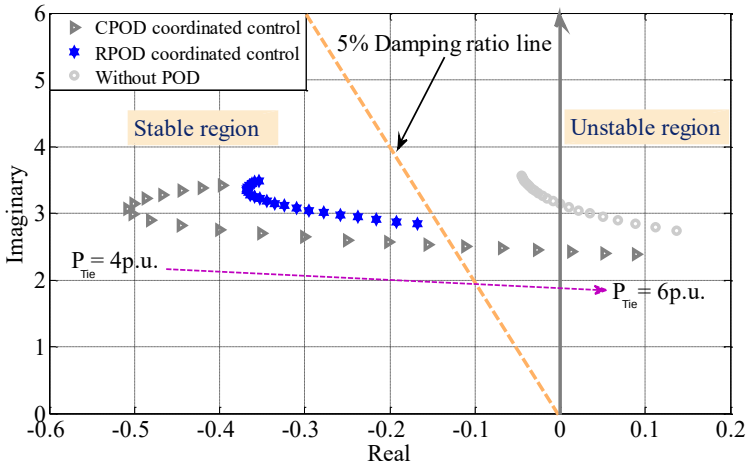

Figure 4.6 Locus of inter-area mode.

4.3.2 Simulation Results

The Simulink tests are developed by MATLAB, Simulink and PSAT tool box [18]. The nonlinear simulations of case studies 1 to 3 in Table 4.5 are conducted. Figs. 4.8, 4.9 and 4.10 show the comparison of the voltage at the faulted bus between CPOD and RPOD coordinated controls of case 1 to case3, respectively. Figs. 4.11, 4.12 and 4.13 demonstrate P_{Tie} of case 1 to case 3, respectively. In the first case, both RPOD coordinated control and CPOD coordinated control are able to damp out the oscillation. In case 2, the damping effect of the RPOD coordinated control is more than that of the CPOD coordinated control. Absolutely, the last case shows that the RPOD coordinated control can damp out the oscillation while the CPOD coordinated control fails to eliminate the oscillation. According to the simulation results, the superior robustness and stabilizing effect of the proposed RPOD coordinated control is obviously superior to the CPOD coordinated control.

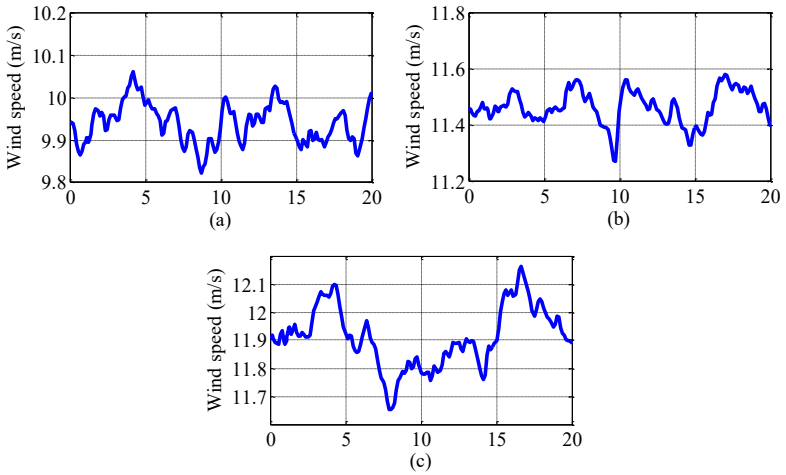

Figure 4.7 Wind speed patterns of (a) case 1, (b) case 2, (c) case 3.

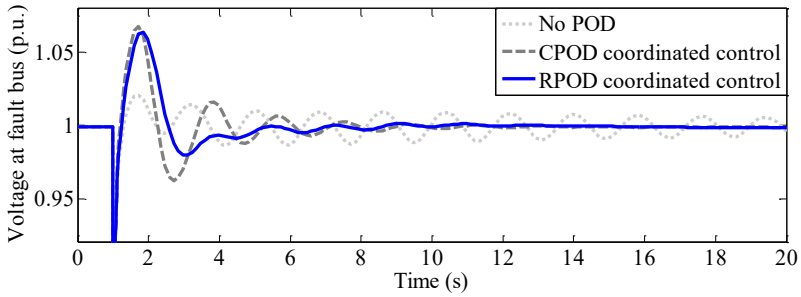

Figure 4.8 Voltage at fault bus of case 1.

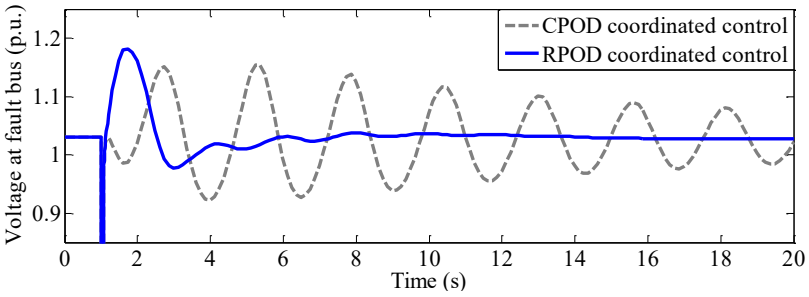

Figure 4.9 Voltage at fault bus of case 2.

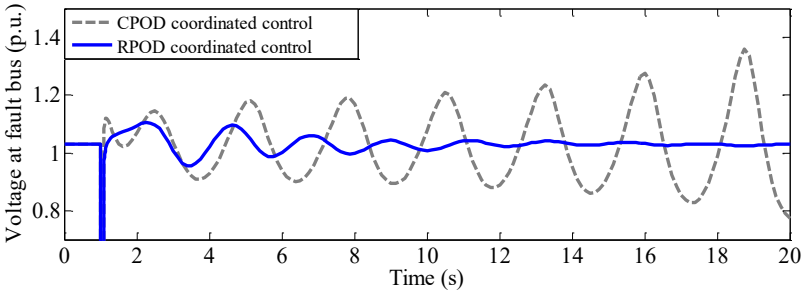

Figure 4.10 Voltage at fault bus of case 3.

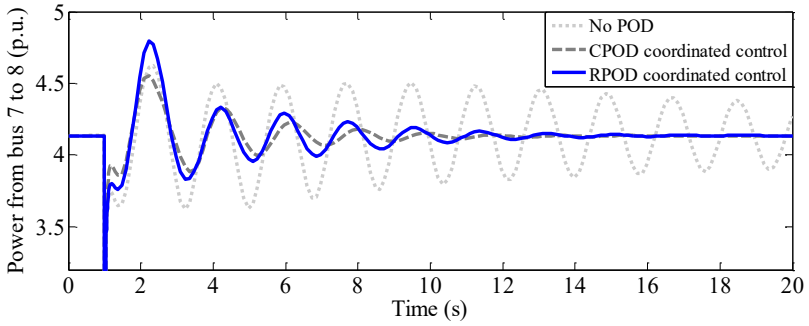

Figure 4.11 P_{Tie} of case 1.

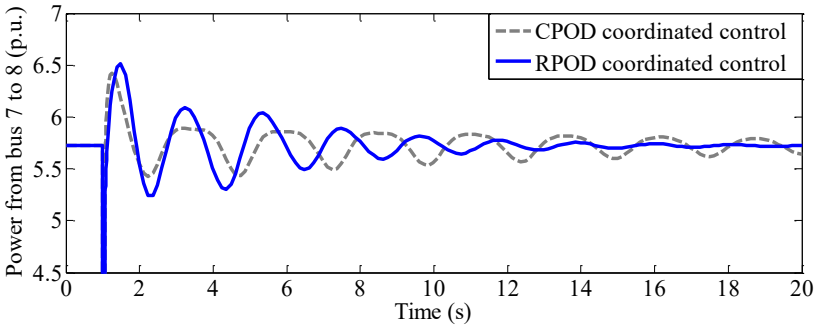

Figure 4.12 P_{Tie} of case 2.

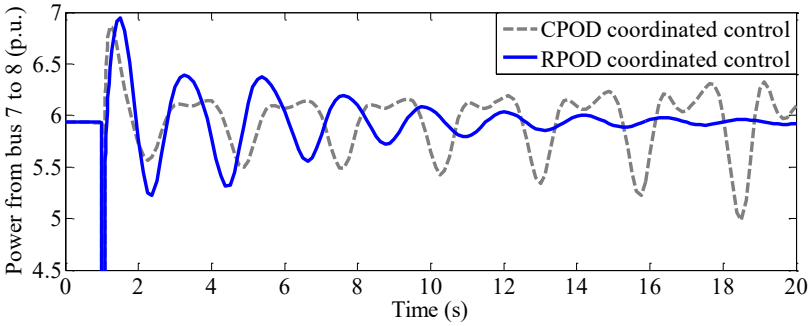

Figure 4.13 P_{Tie} of case 3.

4.4 Conclusion

The POD with the practical 2nd-order lead/lag structure with local input signal is installed with the DFIG and SVC. The mixed H_2/H_∞ control method was employed to set the optimization problem of the POD parameters. The optimal parameters of PODs are automatically tuned by the backtracking search algorithm. Eigenvalue analysis results and nonlinear simulation show the higher robustness and damping effect of the proposed robust coordinated control under heavy power flow levels and various fault locations.

CHAPTER 5

CONCLUSION

This thesis gives the brief information of the power system stabilization problems and the new proposed control method to solve these problems. Here we focus on the control technic using renewable energy wind turbine. Robust power oscillation damper is adapted with DFIG and FACTS devices. To give the detail information, there were four main chapters that were addressed in this thesis:

Chapter 1 provided the brief introduction of some information as follows:

1) Problem : Power system oscillation between 0.2 to 2.0 Hz is still the challenging problem. The undammed power oscillation may cause the wide area blackouts and loss of system synchronism.
2) Motivation : The power stability is still interested field research. Using DFIG wind turbine to coordinate with SVC FACTS device to stabilize the power system oscillation is a new control technic that we should propose. POD is proposed to support DFIG and SVC.
3) Objective : Designing the robust coordinated control using DFIG wind turbine and SVC supporting by POD.
4) Data set : Two control methods (proposed control and conventional control) was compared. Three power systems were studied in this thesis. 25 populations with 100 to 200 iterations were set for BSA.

Chapter 2 provided the brief proposed control design technic and is concluded as follows:

1) In order to get the robustness and good performance, mixed H_2/H_∞ method is proposed.
2) To be one of evolutionary optimization algorithms, backtracking search optimization algorithm (BSA) enables to solve numerical optimization problems successfully and rapidly.

Chapter 3 gave the practice examples. Stabilization the system by using DFIG wind turbine with POD is described. This chapter can be concluded as follows:

1) One DFIG and Two DFIG were used to stabilize the system.
2) The POD structure which is a 2^{nd}-order lead-lag compensator was designed based on mixed H_2/H_∞ method. The parameters of POD were tuned automatically by BSA. The

optimization of POD is conducted so that the desired system damping and robustness can be guaranteed.

3) The both optimization and simulation results confirm the superior robustness and damping performance of the proposed POD over the conventional POD under various power flow levels and severe faults.

Chapter 4 demonstrated the coordinate control technic using DFIG and SVC facts device. Here the four machine system was be an example and be concluded as follows:

1) DFIG and SVC coordinated to control the inter-area oscillation mode.
2) PODs were adapted with DFIG and SVC, respectively. The POD structure which is a 2^{nd}-order lead-lag compensator was designed based on mixed H_2/H_∞ method. The mixed H_2/H_∞ control method was employed to set the optimization problem of the POD parameters. The optimal parameters of PODs are automatically tuned by the backtracking search algorithm. The optimization of POD is conducted so that the desired system damping and robustness can be guaranteed.
3) Eigenvalue analysis results and nonlinear simulation show the higher robustness and damping effect of the proposed robust coordinated control under heavy power flow levels and various fault locations.

All the optimization and simulation results were developed by MATLAB program and PSAT control tool box.

For the future work, the observability and controllability should be considered on. The uncertainty system with time delay will be applied into the interconnection system stability. The simulation results should be tested by using Hard ware simulator with real time simulator.

References

[1] G. Abad, J. Lopez, M. Rodriguez, L. Marroyo, and G. Iwanski, Doubly Fed Induction Machine. Hoboken, NJ, USA: Wiley, 2011.

[2] L. Fan, H. Yin, and Z. Miao, "On active/reactive power modulation of DFIG-based wind generation for interarea oscillation damping," IEEE Trans. Energy Convers., vol. 26, no. 2, pp. 513–521, Jun. 2011.

[3] F. M. Hughes, O. A-Lara, N. Jenkins, and G. Strbac, "A power system stabilizes for DFIG-based wind generation", IEEE Trans. Power Systems, vol. 21, no.8, pp. 763-772, May 2006.

[4] A.H.M.A. Rahim, and I.O. Habiballah, "DFIG rotor voltage control for system dynamic performance enhancement", Electric Power System Research, vol.81, pp. 503-509, 2011.

[5] P. Kundur, Power System Stability and Control, New York, McGraw Hill, 1994.

[6] P. Aree and E. Acha, "Block diagram model for fundamental studies of a synchronous generator—Static VAR compensator system," *Proc. Inst. Elect. Eng., Gen., Transm. Distrib.*, vol. 146, no. 3, pp. 507–514, 1999.

[7] N. Mithulananthan, C. A. Canizares, J. Reeve, and G. J. Rogers, "Comparison of PSS, SVC, and STATCOM controllers for damping power system oscillations," *IEEE Trans. Power Syst.*, vol. 18, no. 2, pp. 786–792, May 2003.

[8] S. C. Kapoor, "Dynamic stability of static compensator—Synchronous generator combination," *IEEE Trans. Power App. Syst.*, vol. PAS-100, no. 4, pp. 1694–1702, Apr. 1981.

[9] J. Chen, J. V. Milanovic, and F. M. Hughes, "Selection of auxiliary input signal and location of a SVC for damping electromechanical oscillations," in *Proc. IEEE Power Eng. Soc. Winter Meeting*, 2001, vol. 2, pp. 623–627.

[10] M.W. Mustafa, N. Magaji, "Design of power oscillation damping controller for SVC device," IEEE Power Eng. Conf., pp. 1329-1332, 2008.

[11] N.N. Islam, M.A. Hannan, H. Shareef, A. Mohamed, "SVC damping controller design based on firefly optimization algorithm in multi machine power system," IEEE Conf. Clean Eng. Tech., pp. 66-70, 2013.

[12] H. Yu, C. Y. Chung, K. P. Wong, and J. H. Zhang, "A chance constrained transmission network expansion planning method with consideration of load and wind farm uncertainties," IEEE Trans. Power Syst., vol. 24, no. 3, pp. 1568–1576, Aug. 2009.

[13] P. Civicioglu, "Backtracking search optimization algorithm," Appl. Math. Comput., vol. 219, no. 15, pp. 8121-8144, Apr. 2013.

[14] M. de Industria Turismo y Comercio, " Secretaria de Estado de Energia. Instalaciones conectadas a la Red de Transporte y equipo generador: requisites minimos de diseno, equipaminento, funcionamiento, puesta en servicio y seguridad," Technical Report, Red Electrica., 2008.

[15] Dominguez-Garcia JL, Gomis-Bellmunt O, Trilla-Romero L, Junyent-Ferre A. Vector control of squirrel cage induction generator for wind power. In: Proceedings of the international conference on electrical machines 2010.

[16] Jauch C, Cronin T, Sorensen P, Jensen B. A fuzzy logic pitch angle controller for power system stabilization. Wind Energy 2007;10:19e30.

[17] Bin Wu, T. Lang, N. Zargari, and S.Kouro, Power conversion and control of wind energy systems, John Wiley & Sons, Inc., Hoboken, New Jersey 2011.

[18] F. Milano, Power system analysis toolbox (PSAT), Documentation for PSAT version 2.1.6, Oct. 2011.

Appendix A

Appendix B

List of Publications

1. Sothy Uong, Issarachai Ngamroo, "*Robust Power Oscillation Damping by DFIG Wind Turbine using Mixed H_2/H_∞ Control*," The 2nd AUN/SEED-Net regional conference on energy Engineering, November 13-14, 2014, Bangkok, Thailand.
2. Sothy Uong, Issarachai Ngamroo, "*Coordinated Control of DFIG Wind Turbine and SVC for Stabilization of Power System Oscillation*," The 2nd AUN/SEED-Net regional conference on energy Engineering, November 13-14, 2014, Bangkok, Thailand.
3. Sothy Uong, Issarachai Ngamroo, "*Coordinated Control of DFIG Wind Turbine and SVC for Robust Power System Stabilization*," The 12th International Conference on Electrical Engineering/Electronics, Computer, Telecommunications and Information Technology, June 24-27, 2015, Hua Hin, Thailand.

RCEneE 2014

Bangkok, Thailand

13.-14.11.2014

2nd AUN/SEED-Net Regional Conference on ENERGY ENGINEERING

Advancement in Technology and Management for Tomorrow

PROCEEDINGS

Japan 60 years

60 years
Japan's Official Development Assistance

KMITL
พระจอมเกล้าลาดกระบัง

AUN/SEED-Net

JICA

SEACUS
Southeast Asian Center for Urban Sustainability

Robust Power Oscillation Damping by DFIG Wind Turbine using Mixed H_2/H_∞ Control

Sothy Uong
International College
King Mongkut's Institute of Technology Ladkrabang
Bangkok 10520, Thailand
uongsothy.itc@gmail.com

Issarachai Ngamroo
Electrical Engineering Department, Faculty of Engineering
King Mongkut's Institute of Technology Ladkrabang
Bangkok 10520, Thailand
knissara@kmitl.ac.th

***Abstract* —The robust power oscillation damper (POD) design for doubly fed inducting generator (DFIG) based on a mixed H_2/H_∞ control method is proposed in this paper. A practical 2nd-order lead/lag compensator with local input signal is chosen as the POD structure. The POD is additionally installed with the voltage control loop of DFIG so that the modulation of reactive power output can be performed to damp out power oscillations. To acquire both damping performance and robustness, the optimization of POD parameters is formulated based on a mixed H_2/H_∞ control. The backtracking search algorithm is automatically employed to solve the optimization problem. Simulation study indicates that the damping effect and robustness of the proposed robust POD are higher than those of the conventional POD against various system faults, heavy power flow levels, and wind patterns.**

***Keywords* —Power Oscillation Damping, Doubly Fed Induction Generator Wind Turbine, Mixed H_2/H_∞ Control, Backtracking Search Optimization Algorithm.**

I. INTRODUCTION

The interconnection among power systems not merely enhances the system reliability, but also augments the system economics. However, the longitudinal structure of system interconnection may suffer from the power oscillation with poor damping [1]. In the scenario of heavy power flow and severe faults, the undamped power oscillation may invoke the loss of system synchronism and the wide area blackouts. To handle the power oscillation, the power system stabilizer (PSS) has been successfully used. Nevertheless, the control of PSS may cause an adverse impact on the quality of voltage control of automatic voltage regulator (AVR) [2].

Currently, the integration of wind power generation into power systems highly increases. With the large participation of wind generators, the contribution of wind generators for stabilization of power oscillation is significantly anticipated. For instance, in the new Spanish grid code for wind power, the power oscillation damping function is included [3]. To realize this function, the doubly fed induction generator (DFIG) wind turbine has been paid attentions since the active and reactive power outputs of DFIG can be controlled. By equipping the power oscillation damper (POD), the power output can be modulated to eliminate the power oscillation [4]. Generally, the POD structure is the same as the PSS, which is the second-order lead/lag compensator. To achieve the satisfactory stabilizing effect of POD, an optimal tuning technique of POD parameters is required.

In the past researches, the parameters tuning methods based on bacterial foraging [5], differential evolution [6] and particle swarm optimization [7] have been proposed. The PODs in these works are optimized at one operating condition so that the damping effect of POD can be obtained. Nevertheless, PODs in these works may fail to handle the power oscillation in the face of system uncertainties such as various power flow levels, severe short circuits, and network structures etc. The new POD tuning technique which considers both damping performance and robustness, is essentially required.

In this paper, the robust control design of POD using a mixed H_2/H_∞ control method is presented. The optimization of POD parameters is carried out so that both damping performance and robust stability margin against system uncertainties are acquired. The backtracking search algorithm is applied to solve the optimization problem. Simulation study confirms the superior damping effect of the proposed robust POD over the conventional POD.

II. STUDY SYSTEM AND MODELING

A. Study System

Fig. 1 illustrates the DFIG wind generator and synchronous generator which are connected to the infinite bus. The synchronous generator (G) is presented by the six-order Park's model. The DFIG wind turbine which is connected at bus 4, is used to supply electric power to the main grid. The electromechanical oscillation with poor damping causes the stability problem in this system.

B. DFIG and POD Modeling

Fig. 2 delineates the structure of DFIG wind turbine and control system [8], where v_a, v_b, v_c are voltages of phases *a, b, c*, respectively, i^*_a, i^*_b, i^*_c are reference currents of phases *a, b, c*, respectively, v_{dr} and v_{qr} are direct (*d*) and quadrature (*q*) axis voltages of the rotor side converter, respectively, i^*_{dr} and i^*_{qr} are reference *d* and *q* axis currents of the rotor side converter, respectively, i_{dr} and i_{qr} are *d* and *q* axis currents of the rotor side converter.

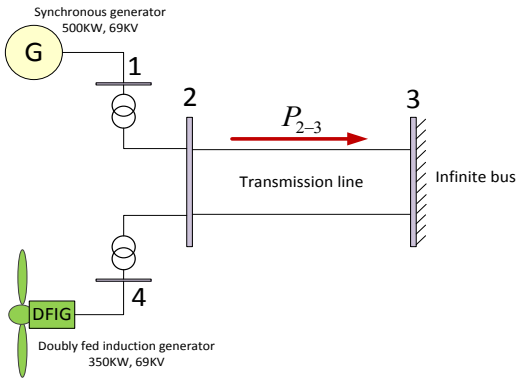

Fig. 1. DFIG wind turbine and single synchronous generator connected to infinite bus.

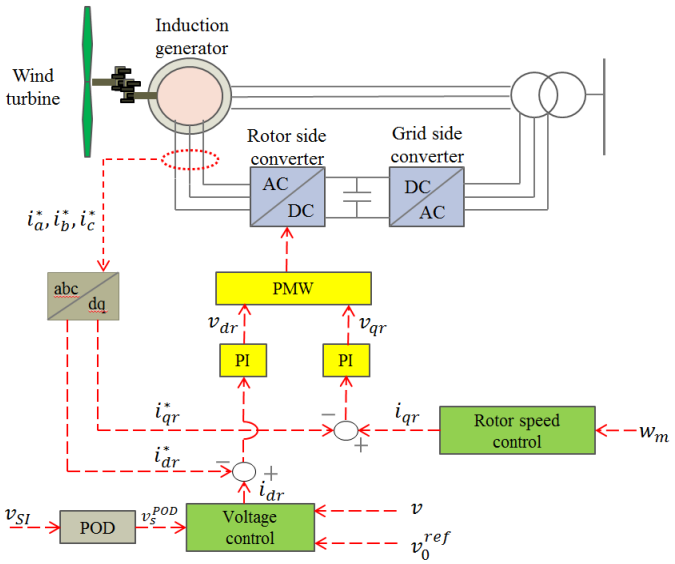

Fig. 2. DFIG model.

As mentioned in [4], the control by rotor side converter provides better damping effect than that by grid side converter. In this study, the POD is additionally equipped with the controller of rotor side converter. By vector control technique in the rotor side converter, the independent control of active and reactive power outputs can be acquired. The converter is modeled by an ideal current source. As depicted in Figs. 3 (a) and 3 (b), i_{qr} and i_{dr} are used for rotor speed control and voltage control, respectively. The active and reactive power outputs of DFIG can be expressed in terms of i_{qr} and i_{dr} as:

$$P = \frac{x_s}{x_s + x_u} v i_{qr} \tag{1}$$

$$Q = -\frac{x_u v i_{dr}}{x_s + x_u} - \frac{v^2}{x_u} \tag{2}$$

where P and Q are active and reactive power outputs, respectively, ω_m is a rotor speed of DFIG, p^*_w is the power speed characteristic which roughly optimizes the wind energy

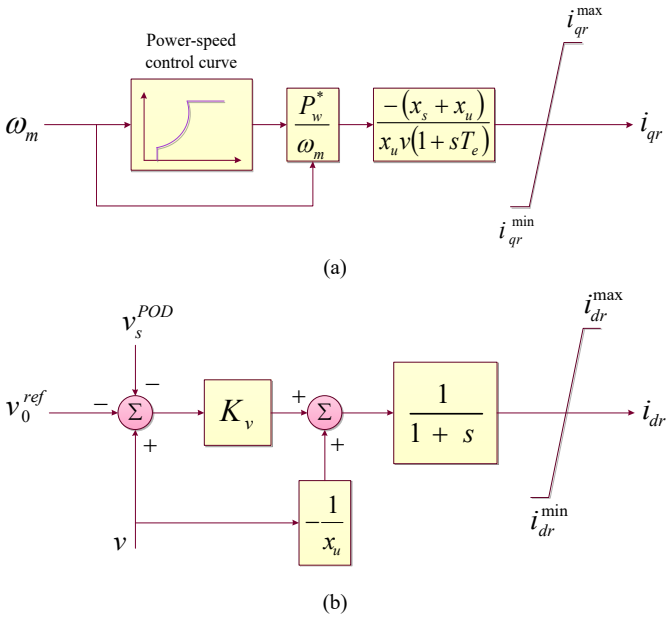

Fig. 3. (a) Voltage control scheme of DFIG. (b) Rotor speed control scheme of DFIG.

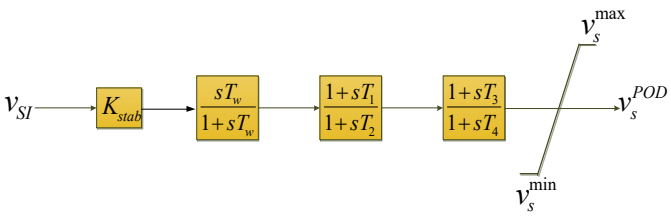

Fig. 4. POD model.

capture, x_s is a stator self-reactance, x_u is a magnetizing reactance, T_e is the time constant of power control, v is a magnitude of DFIG terminal voltage, v_0^{ref} is the initial reference voltage, v_{ref} is the actual reference voltage, v_{SI} is input signal of POD, v_s^{POD} is an additional signal of POD, K_v is the voltage controller gain, and i_{dr}^{min}, i_{dr}^{max}, i_{qr}^{min}, i_{qr}^{max} are d and q axis minimum and maximum rotor currents, respectively. Here, reactive power output which can be controlled by i_{dr}, is used to damp out the power oscillation by the stabilizing signal v_s^{POD} from POD.

The POD structure which is a 2nd-order lead-lag compensator, is delineated in Fig.4. The POD consists of a stabilizer gain K_{stab}, a washout filter with time constant T_w=10 s, and two phase compensator blocks with time constants T_1, T_2, T_3 and T_4. The washout signal guarantees that the POD output is zero in steady state. An anti-windup limiter is equipped at the output of POD so that the output signal v_s^{POD} is between the minimum value (v_s^{min}) and the maximum value (v_s^{max}). To produce the satisfactory damping and the phase lead compensator, K_{stab} and T_1, T_2, T_3 and T_4 are optimally tuned. Here, the proposed design is used to optimize five parameters of POD.

III. PROPOSED CONTROL METHOD

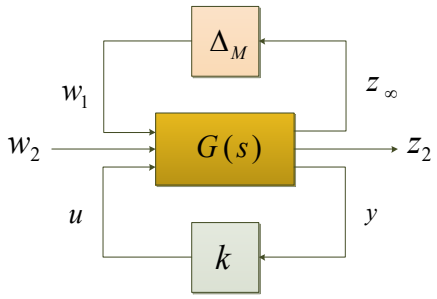

Fig. 5. Closed loop system with mixed H2/H∞ control.

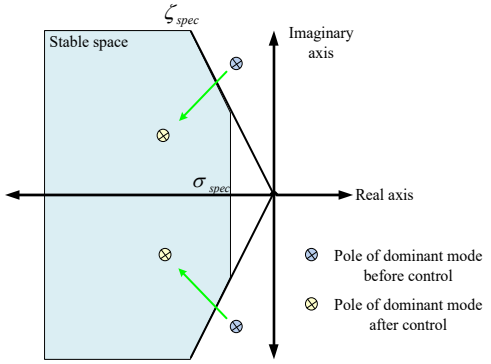

Fig. 6. Pole assignment in a specific damping region.

A. Mixed H_2/H_∞ Control

In the controller design problems, it is desirable to simultaneously attain multiple objectives such as robust stability against system uncertainties, disturbance attenuation and reference tracking performance. To achieve these objectives, the mixed H_2/H_∞ control which is the powerful multi-objective control design [9], can be applied. Here, the closed loop system with a mixed H_2/H_∞ control can be illustrated in Fig. 5, where $G(s)$ is a nominal plant, Δ_M is the model of system uncertainties, $K(s)$ is a controller, w_1 and w_2 are disturbance and external input vector, respectively, y is a measured output vector, u is an input vector from controller, z_2 is an output channel associated with the Linear Quadratic Gaussian (LQG) aspects (H_2 performance), and z_∞ is an output channel associated with the H_∞ performance. $T_{z\infty w1}(s)$ is defined as the closed-loop transfer function from w_1 to z_∞.

By minimizing the infinite norm of $T_{z\infty w1}(s)$, i.e. $\|T_{z\infty w1}(s)\|_\infty$, the robust stability of the system against uncertainties can be obtained. On the other hand, $T_{z2w2}(s)$ is defined as the closed-loop transfer function from w_2 to z_2. By minimizing the two-norm of $T_{z2w2}(s)$, i.e. $\|T_{z2w2}(s)\|_2$, the disturbance attenuation and reference tracking can be acquired. Accordingly, by minimizing a trade-off criterion

$$\alpha \left\| T_{z\infty w1}(s) \right\|_\infty^2 + \beta \left\| T_{z2w2}(s) \right\|_2^2, \alpha \geq 0, \beta \geq 0 \tag{3}$$

Both objectives mentioned above can be obtained [9]. Besides, by placing the dominant oscillation modes in the stability region with the specified damping ratio ζ_{spec} and specified real part σ_{spec} as shown in Fig. 6, the desired stability region can be guaranteed.

Accordingly, the optimization problem can be formulated by

$$\text{Minimize } \alpha \left\| T_{z\infty w1} \right\|_\infty^2 + \beta \left\| T_{z2w2} \right\|_2^2 \tag{4}$$

$$\text{Subject to } \begin{cases} \zeta \geq \zeta_{spec} \\ \sigma \leq \sigma_{spec} \end{cases}$$

$$\zeta_{spec} = 10\%, \sigma_{spec} = -0.5, \alpha = 0.1, \beta = 1$$

$$0.01 \leq K_{stab} \leq 5$$

$$0.01 \leq T_1, T_2, T_3, T_4 \leq 20$$

B. Backtracking Search Algorithm

The backtracking search algorithm (BSA) is a new evolutionary algorithm for solving real-valued numerical optimization problems. The BSA's unique mechanism for generating a trial individual enables it to solve numerical optimization problems successfully and rapidly. The BSA uses three basic genetic operators such as selection, mutation and crossover to generate trial individuals [10]. BSA has a random mutation strategy that uses only one direction individual for each target individual, in contrast with many genetic algorithms. Fig. 7 shows the flow chat of BSA which can be described step by step as follows:

- Step 1: this is the initial step that generates the initial and old population, and it is described by formula bellow:

$$\begin{aligned} P_{initial} &= rnd(up - low) + low \\ P_{old} &= rnd(up - low) + low \end{aligned} \tag{5}$$

  where $P_{initial}$ and P_{old} are the initial and old population respectively. *Up* and *low* are the limit range of dimensions of population, and *rnd* is the uniformly distributed pseudorandom numbers.

- Step 2: The objective function of initial population (Obj-fun ($P_{initial}$)) is calculated.

- Step 3: The new populations which are called as trail population, are generated by using mixed method between mutation and crossover described by

$$P_{trail} = P + (map.F).(P_{old} - P) \tag{6}$$

  where P_{trial} is the trail population, and P is population that obtains from selection randomly between old and initial population. *map* is a binary integer-valued matrix calculated for crossover term [10] . $F=3\times rndn$

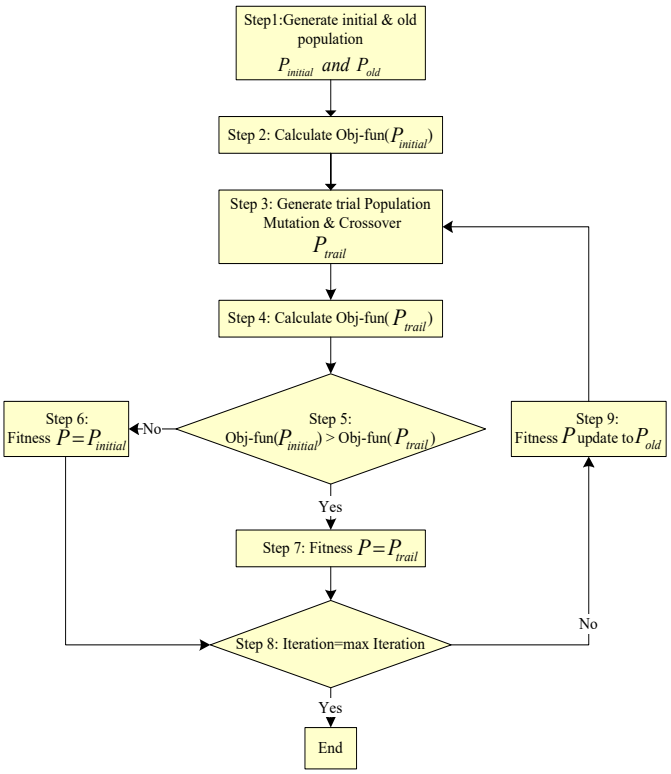

Fig. 7. Flow chat of BSA.

is the get-scale-factor, and *rndn* is the normally distributed pseudorandom numbers.

- Step 4: the objective function of trial population (Obj-fun (P_{trial})) is calculated.
- Step 5: this is the selection step. The objective function between initial and trial population are compared.
- Step 6: this is negative comment step "No". The fitness population (fitness P) is equal to the initial population ($P_{initail}$), and then it continues to step 8.
- Step 7: this is the positive comment step "Yes". The fitness population (fitness P) is equal to the trial population (P_{trail}), and then it will continue to step 8.
- Step 8: Check the maximum iteration. If "Yes", the process of minimization will stop and continue to step "End", if No, it will continue to step 9.
- Step 9: In this step, the fitness population will update to old population, and the process of minimization will do again.

IV. Simulation Results

The POD design is developed by MATLAB, Simulink and PSAT tool box [8]. The BSA parameters are set as follows; population = 25, maximum iteration = 100. The POD is designed under case 1 as shown in TABLE I. After the optimization, Fig. 8 demonstrates the convergence curve of

TABLE I. Case Studies (Base=100 MVA, 60 Hz)

Case	Condition study	$P_{2\text{-}3}$ (p.u.)	Wind pattern
1.	The 3 phase fault occurs at a transmission line between bus 2 and bus 3 at time = 5s, and cleared by circuit breaker (not reclose) at time = 5.05s.	4.33	Fig. 9 (a)
2.	The 3 phase fault occurs at a transmission line between bus 2 and bus 3 at time = 5s, and cleared by circuit breaker (not reclose) at time = 5.1s.	5.15	Fig. 9 (b)
3.	The 3 phase fault occurs at bus 2 at time = 5s, and cleared naturally at time = 5.1s.	5.74	Fig. 9 (c)
4.	The 3 phase fault occurs at bus 2 at time = 5s, and cleared naturally at time = 5.1s.	6.02	Fig. 9 (d)

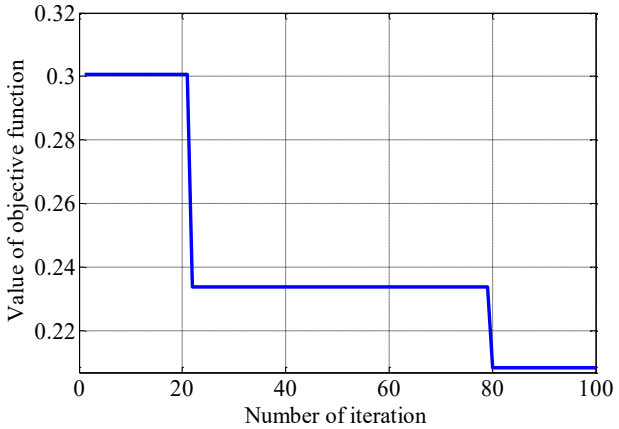

Fig. 8. Convergence curve of Objective function.

objective function of the proposed control method. The optimized parameters of POD which is referred to as RPOD are provided in TABLE II.

The stabilizing effect of RPOD is compared with the conventional POD (CPOD) which is designed by the pole replacement method. To obtain the same damping ratio as RPOD, the optimization problem of CPOD is given as follows:

$$\text{Minimize } \left(\left|\zeta-\zeta_{spec}\right|+\left|\sigma-\sigma_{spec}\right|\right) \tag{7}$$

$$\text{Subject to } \begin{cases}\zeta \geq \zeta_{spec}\\ \sigma \leq \sigma_{spec}\end{cases}$$

$$0.01 \leq K_{stab} \leq 5$$

$$0.01 \leq T_1, T_2, T_3, T_4 \leq 20$$

$$\zeta_{spec}=10\%, \sigma_{spec}=-0.5$$

TABLE II. OPTIMAL PARAMTERS OF PODS

POD	*K*	*Tw*	T_1	T_2	T_3	T_4
RPOD	2.0154	10	3.2892	0.5765	1.2550	16.8830
CPOD	3.3543	10	0.2146	9.4152	11.7140	1.3701

TABLE III. EIGENVALUE ANALYSIS RESULTS

Control device	Eigenvalue	Damping ratio	Frequency (Hz)
No POD	$-0.232 \pm j7.62$	3.04%	1.21
RPOD	$-1.070 \pm j7.42$	14.25%	1.18
CPOD	$-0.847 \pm j6.90$	12.19%	1.10

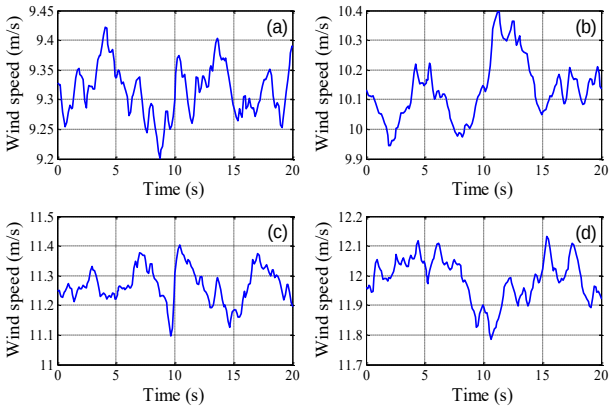

Fig. 9. Wind speed patterns of (a) case 1, (b) case 2, (c) case 3, (d) case 4.

The optimized parameters of CPOD are provided in TABLE II. The eigenvalue analysis results in case 1 are shown in TABLE III. Without POD, the damping ratio of the oscillation mode is very poor. On the other hand, the damping ratio of the oscillation mode is improved as expected by both CPOD and RPOD.

Next, nonlinear simulations of case studies 1 to 4 in TABLE I are carried out. Figs. 10 (a)-(d) show the power flow from bus 2 to bus 3 of cases 1-4, respectively. In cases 1 and 2, the DFIG without POD cannot damp out the power oscillation. On the contrary, both CPOD and RPOD are able to suppress the power oscillation. In cases 3 and 4, the CPOD completely loses damping effect and fail to stabilize the oscillation. On the other hand, the RPOD is very robust against various uncertainties. It is able to get rid of the oscillation robustly.

Fig. 11 shows the comparison of $||T_{z\infty wI}||_\infty$ between CPOD and RPOD when $P_{2\text{-}3}$ is varied from 3.2 to 5.45p.u. Note that $||T_{z\infty wI}||_\infty$ implies the robustness of POD against system uncertainties. Obviously, when the power flow increases, $||T_{z\infty wI}||_\infty$ in case of CPOD largely changes. The CPOD is very sensitive to the heavy power flow from bus 2 to infinite bus. This signifies that the damping effect of CPOD is deteriorated at the high level power flow. On the other hand, the change in $||T_{z\infty wI}||_\infty$ in case of RPOD is lesser. The RPOD is not much sensitive to the variation of the power flow. This shows the high robustness of RPOD.

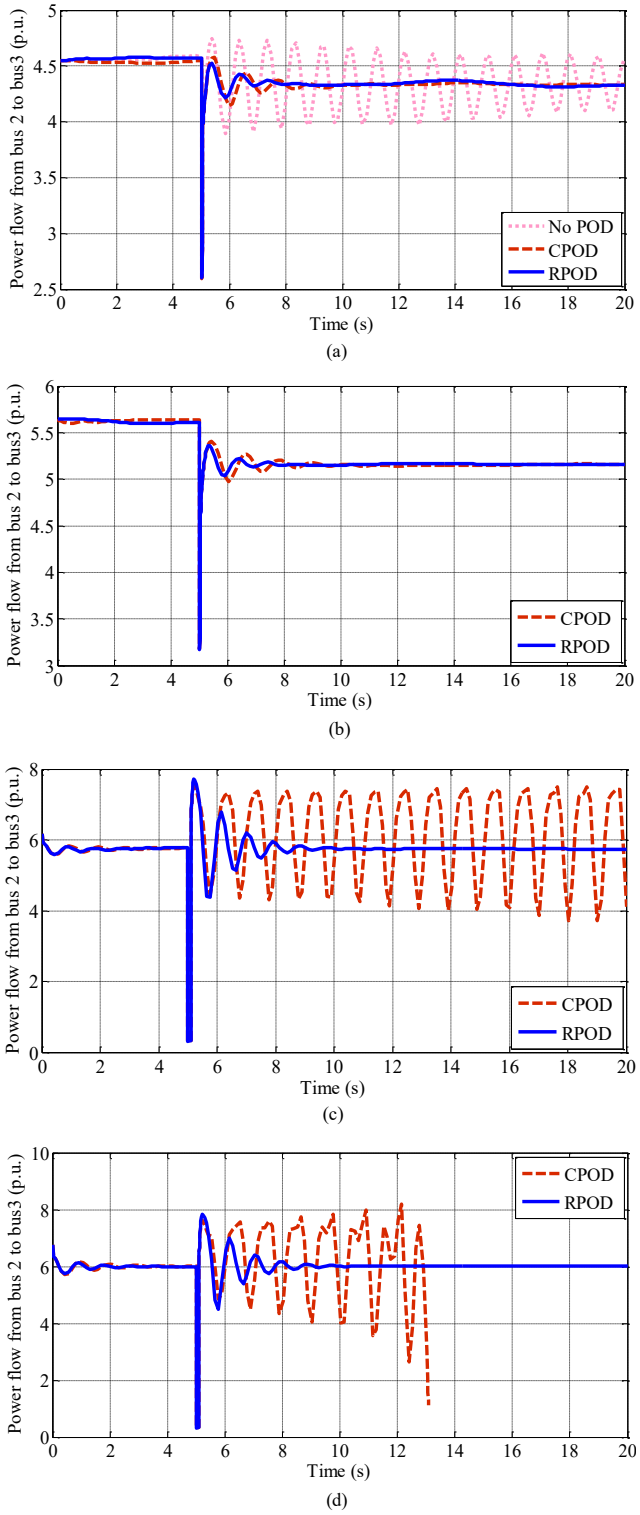

Fig. 10. Power flow from bus 2 to 3 of (a) case 1, (b) case 2, (c) case 3, (d) case 4.

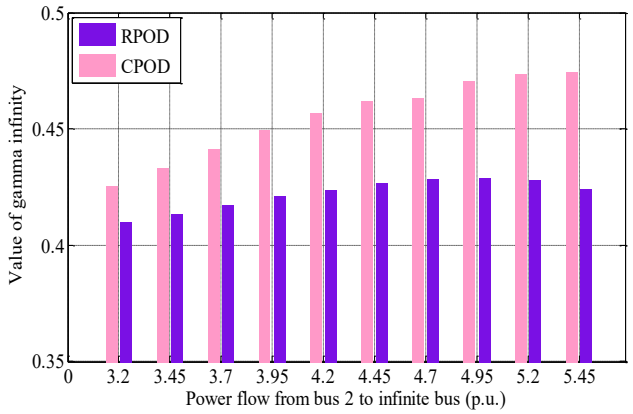

Fig. 11. Value of gamma infinity ($\|T_{Z\infty wI}\|_\infty$).

V. CONCLUSION

This paper presents a new POD parameters tuning technique based on a mixed H_2/H_∞ method. Since the POD structure is the 2nd-order lead/lag compensator with local input signal, it is easy to realize in real power system. The optimization of POD is conducted so that the desired system damping and robustness can be guaranteed The POD parameters are automatically tuned by backtracking search algorithm. Eigenvalue analysis results and nonlinear simulation clearly confirm the superior robustness and damping performance of the proposed POD over the conventional POD under various power flow levels and severe faults.

ACKNOWLEDGMENT

This research work was supported by ASEAN University Network /Southeast Asia Engineering Education Development Network (AUN/SEED-Net) and King Mongkut's Institute of Technology Ladkrabang (KMITL).

REFERENCES

[1] P. Kundur, Power System Stability and Control, New York, McGraw Hill, 1994.

[2] F. M. Hughes, O. A-Lara, N. Jenkins, and G. Strbac, "A power system stabilizes for DFIG-based wind generation," IEEE Trans. Power Systems, vol. 21, no.8, pp. 763-772, May 2006.

[3] M. de Industria Turismo y Comercio, " Secretaria de Estado de Energia. Instalaciones conectadas a la Red de Transporte y equipo generador: requisites minimos de diseno, equipaminento, funcionamiento, puesta en servicio y seguridad," Technical Report, Red Electrica., 2008.

[4] A.H.M.A. Rahim, and I.O. Habiballah, "DFIG rotor voltage control for system dynamic performance enhancement," Electr. Power Syst., Res., vol.81, pp. 503-509, Feb. 2011.

[5] Y. Misha, S. Mishar, M. Triphathy, N. Senroy, and Z. Y. Dong, "Improving stability of a DFIG-based wind power system with tuned damping controller," IEEE Trans. on Energy Convers., no.3, vol.24, pp.650-60, Sept. 2009.

[6] L. Yang, G.Y. Yang, Z. Xu, Z.Y. Dong, K.P. Wong, and X. Ma "Optimal controller design of a doubly-fed induction generator with wind turbine system for small signal stability enhancement," IET Gener Trans. Distrb., no. 5, vol.4, pp.579-97, 2010.

[7] F. Wu, Z. Zhang, K. Godfrey, and P. Ju "Small signal stability analysis and optimal control of a wind turbine with doubly fed induction generator", IET Gener. Trans. Distrib., no.5, vol. 1, pp.751-60, 2007.

[8] F. Milano, Power system analysis toolbox (PSAT), Documentation for PSAT version 2.1.6, Oct. 2011.

[9] S. Skoqestad, I. Postlethwaite, Multiple feedback control: analysis and design. Wiley, Sep. 2005.

[10] P. Civicioglu, "Backtracking search optimization algorithm," Appl. Math. Comput., vol. 219, no. 15, pp. 8121-8144, Apr. 2013.

Coordinated Control of DFIG Wind Turbine and SVC for Stabilization of Power System Oscillation

Sothy Uong
International College
King Mongkut's Institute of Technology Ladkrabang
Bangkok 10520, Thailand
uongsothy.itc@gmail.com

Issarachai Ngamroo
Electrical Engineering Department, Faculty of Engineering
King Mongkut's Institute of Technology Ladkrabang
Bangkok 10520, Thailand
knissara@kmitl.ac.th

***Abstract* — A coordinated control of doubly fed induction generator (DFIG) and static var compensator (SVC) facts device using power oscillation damper (POD) is a new control method that will be described in this paper. This coordinated control is studied with the two-area four machines system. The POD structure is a practical 2nd-order lead/lag compensator with single input, single output (SISO). The optimal tuning of POD parameters is automatically conducted by an improved backtracking search algorithm (BSA). Simulation results confirm the damping effect of the coordinated control.**

***Keywords* —Power Oscillation Damper, Coordinated Control, Doubly Fed Induction Generator Wind Turbine, Static Var Compensator, Backtracking Search Optimization Algorithm.**

I. INTRODUCTION

The interconnection among power systems not only improves the system reliability, but also gets more economic efficiency. On the other hand, it may cause the problem of power system oscillations with frequency between 0.2-1.0 Hz, i.e. local and inter-area oscillation modes [1]. With the poor damping of these oscillation modes, they may result in the loss of synchronism and wide area blackouts. To damp out the oscillation, the power system stabilizer (PSS) has been successfully used for a long time [2]. The conventional PSS generally is installed with the automatic voltage regulator (AVR) of the synchronous generator. The input signal of the PSS is the local signal such as the generator speed, the output power. As a result, the local oscillation problem can be effectively solved. However, since the lack of observability of the inter-area oscillation mode, the PSS using the local signal may not be able to damp out the inter-area oscillations. On the other hand, the static var compensator (SVC) which is one of flexible AC transmission systems (FACTS) devices, can be applied. In [3, 4], the SVC which is installed with the power oscillation damper (POD), has been successfully applied to stabilize the inter-area oscillation.

Currently, the wind farms have been widely installed in power systems. Especially the doubly fed induction generator (DFIG) wind turbine which is a variable speed type wind turbine, has been extensively paid attentions. The practical merits of DFIG wind turbines are low installation cost and controllability of active and reactive power outputs [5]. However, because the output power of the wind power generation is intermittent in nature, it may cause the negative impact on the power oscillations [6]. Under this condition, the stabilizing effect of SVC may be deteriorated. To enhance the control effect of SVC, the DFIG wind turbine which is equipped with a power oscillation damper (POD), can be employed [7]. In previous works, the DFIG with POD has been applied to handle the local oscillation problem [8, 9]. In previous works, there are no research works that presents the coordinated control of SVC and DFIG. To handle both local and inter-area oscillations, the coordinated control of the DFIG with POD and the SVC is expected. In this paper, the coordinated controller using DFIG wind turbine and SVC for stabilization of power system oscillation is presented. The POD with 2nd-order lead/lag compensator is equipped with the SVC and the DFIG. The optimal tuning of POD parameters is automatically conducted by an improved backtracking search algorithm (BSA) so that the stabilization and damping performance are satisfied. The stabilizing effect of the coordinated DFIG and SVC are evaluated in the two-area four-machine power system. Simulation study is used to elucidate the control effect of the proposed coordinated control.

II. STUDY SYSTEM AND MODELLING

A. Study System

Fig. 1 illustrates the two-area four machines system. The rating power and voltage of the synchronous generator are 900MVA and 20kV, respectively. The DFIG wind turbine with 50MVA/20kV is connected to bus 6. The SVC with 100 MVA/230kV is connected at bus 8. The synchronous generators are presented by a six-order model. The total power flows from bus 7 to bus 8 ($P_{7\text{-}8}$) is chosen as the heavy power condition in this study.

B. DFIG Model

Fig. 2 delineates the structure of DFIG wind turbine and control system [10], where v_a, v_b, v_c are voltages of phases *a, b, c*, respectively, i^*_a, i^*_b, i^*_c are reference currents of phases *a, b, c*, respectively, v_{dr} and v_{qr} are direct (*d*) and quadrature (*q*) axis voltages of the rotor side converter, respectively, i^*_{dr} and i^*_{qr} are reference *d* and *q* axis currents of the rotor side converter, respectively, i_{dr} and i_{qr} are *d* and *q* axis currents of the rotor side converter, M is a modulation ratio, and β is a phase angle.

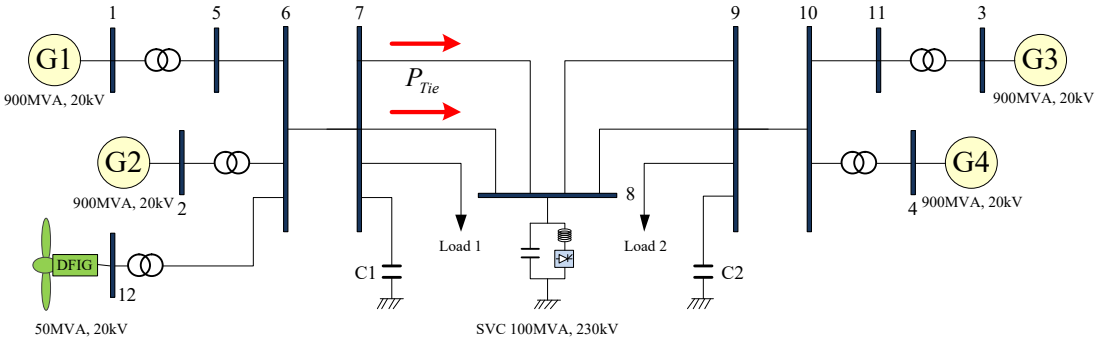

Fig. 1. Two-area four machines system.

As mentioned in [7], the control by rotor side converter provides better damping effect than that by grid side converter. In this study, the POD is additionally equipped with the controller of rotor side converter. By vector control technique in the rotor side converter, the independent control of active and reactive power outputs can be acquired. The converter is modeled by an ideal current source. As depicted in Figs. 3 (a) and 3 (b), i_{qr} and i_{dr} are used for rotor speed control and voltage control, respectively. The active and reactive power outputs of DFIG can be expressed in terms of i_{qr} and i_{dr} as:

$$p_e = \frac{x_s}{x_s + x_u} v i_{qr} \tag{1}$$

$$q_e = -\frac{x_u v i_{dr}}{x_s + x_u} - \frac{v^2}{x_u} \tag{2}$$

where p_e and q_e are active and reactive power outputs, respectively, ω_m is a rotor speed of DFIG, p^*_w is the power speed characteristic which roughly optimizes the wind energy capture, x_s is the stator self-reactance, x_u is the magnetizing reactance, T_e is the time constant of power control, v_{DFIG} is the magnitude of DFIG terminal voltage, v_0^{ref} is an actual reference voltage, v_{SI} is the input signal of POD, v_s^{POD} is an additional signal of POD, K_v is the voltage controller gain, and $i_{dr}^{\min}$, $i_{dr}^{\max}$, $i_{qr}^{\min}$, $i_{qr}^{\max}$ are d and q axis minimum and maximum rotor currents, respectively. Here, reactive power output which can be controlled by i_{dr}, is used to damp out the power oscillation by the stabilizing signal v_s^{POD} from POD.

C. SVC Model

The structure of SVC type 2 regulator is illustrated in Fig. 4 where v_{SVC}, v_0^{ref} ,*and* v_s^{POD} are the terminal voltage of SVC, initial reference voltage, and additional signal control of POD, respectively. The maximum and minimum phases of anti-wind up limiters are defined as α^{max} and α^{min}, respectively, and the signal output of SVC regulator is the firing angle α. There are many other parameters of this regulator such as K_M is the measure gain, T_M is the measure time delay, K is the regulator gain, t_1 and t_2 are transient regulator time constant and regulator time constant, respectively. The concept control of the SVC is to control the bus voltage of the system by using the reactive power (q_{SVC}). The control signal of the regulator

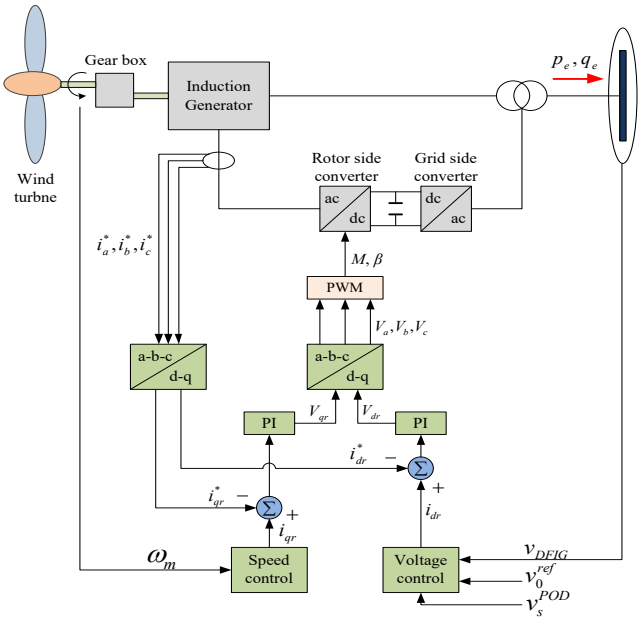

Fig. 2. DFIG model.

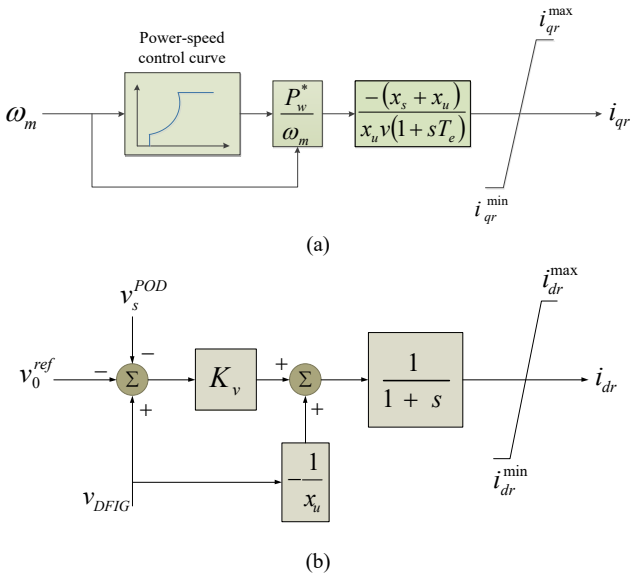

Fig. 3. (a) Voltage control scheme of DFIG. (b) Rotor speed control scheme of DFIG.

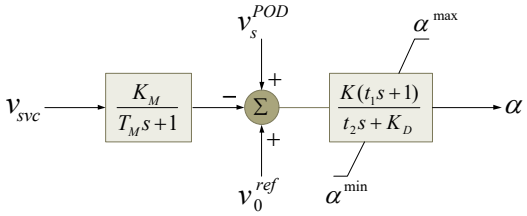

Fig. 4. SVC type 2 regulator.

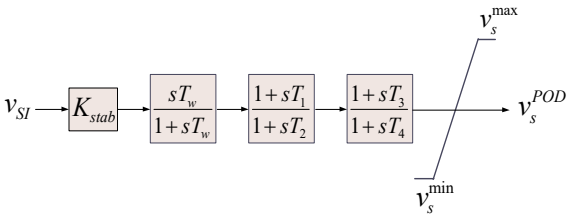

Fig. 5. POD model.

(α) is supplied into the thyristor electronic device of SVC so that q_{SVC} can be controlled. The relation between the q_{SVC} and α is described by

$$q_{svc} = \frac{2\alpha - \sin 2\alpha - \pi(2 - x_L / x_C)}{\pi x_L} v^2 \tag{3}$$

where v is the voltage of bus connected by SVC, x_L and x_C are the inductive and capacitive reactance of SVC, respectively.

D. POD Model

Fig. 5 shows the POD structure which is a 2nd-order lead-lag compensator. The POD is equipped with the DFIG and the SVC. The POD parameters are a stabilizer gain K_{stab}, a washout filter with time constant T_w =10 s, and two phase compensator blocks with time constants T_1, T_2, T_3 and T_4. The washout signal ensures that the POD output is zero in the steady state. The signal power flow of transmission lines from bus 6 to 7 and from bus 7 to 8 are the input signals (v_{SI}) of POD of DFIG and SVC, respectively. An anti-windup limiter is equipped at the output of the POD so that the output signal v_s^{POD} is between the minimum value (v_s^{min}) and the maximum value (v_s^{max}). To obtain the satisfactory damping and the phase lead compensator, K_{stab} and T_1, T_2, T_3 and T_4 are optimally tuned by the proposed optimization.

III. Proposed Optimization

A. Optimization Problem

Fig. 6 shows the proposed coordinated control of DFIG and SVC. The POD is individually equipped with DFIG and SVC. The input signals of both PODs are the local active power flow. The pole assignment method is applied to formulate the optimization problem of PODs. The objective of this method is illustrated in Fig. 7, and its objective function is defined as follows.

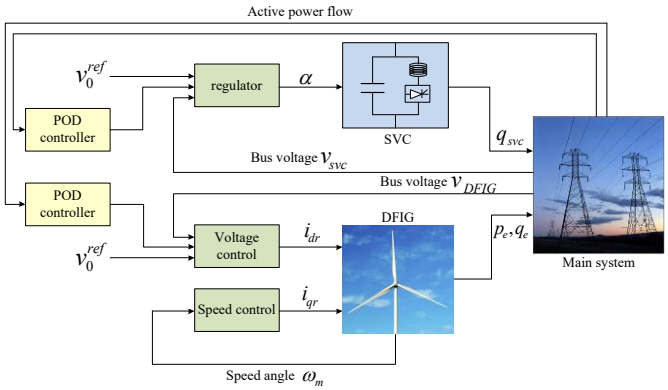

Fig. 6. Diagram of coordinated control processing.

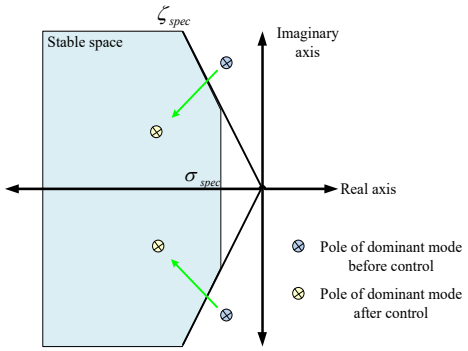

Fig. 7. Pole assignment in a specific damping region.

$$\text{Minimize} \sum_{i=1}^{mn} \left(\left| \zeta_i - \zeta_{spec} \right| + \left| \sigma_i - \sigma_{spec} \right| \right) \tag{4}$$

$$\text{Subject to} \begin{cases} \zeta_i \geq \zeta_{spec} \\ \sigma_i \leq \sigma_{spec} \\ 0.001 \leq K_{stab} \leq 4 \\ 0.001 \leq T_{1,4} \leq 1 \\ 0.001 \leq T_{2,3} \leq 2 \end{cases}$$

where mn is the mode number, specific damping ratio ζ_{spec}=5%, and specific real part of eigenvalue σ_{spec}= -0.1.

B. Backtracking Search Algorithm

The backtracking search algorithm (BSA) is a new evolutionary algorithm for solving real-valued numerical optimization problems. The BSA's unique mechanism for generating a trial individual enables it to solve numerical optimization problems successfully and rapidly. The BSA uses three basic genetic operators such as selection, mutation and crossover to generate trial individuals [11]. BSA has a random mutation strategy that uses only one direction individual for each target individual, in contrast with many genetic algorithms. Fig. 8 shows the flow chat of BSA which can be described step by step as follows:

- Step 1: this is the initial step that generates the initial

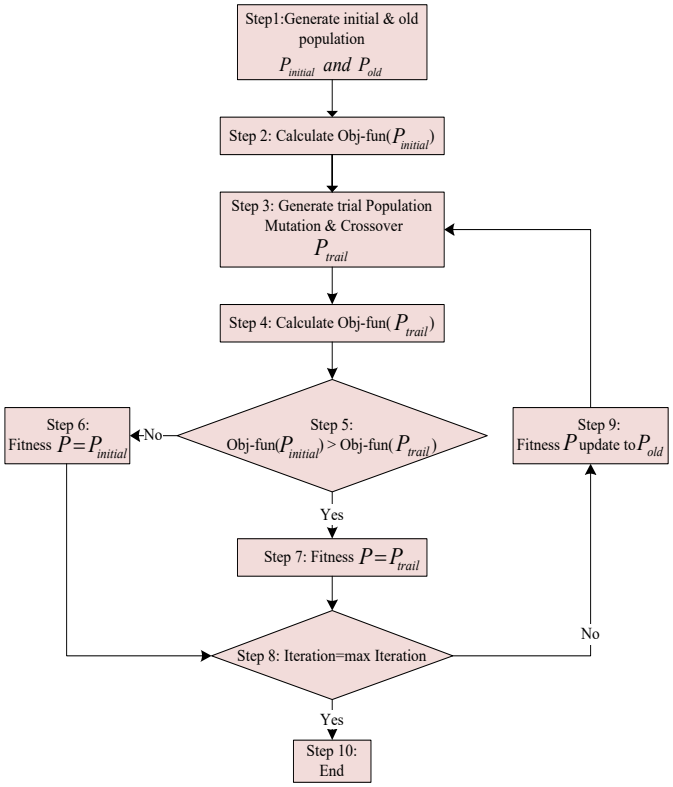

Fig. 8. Flow chat of BSA.

and old population, and it is described by formula as follow:

$$P_{initial} = rnd(up - low) + low$$
$$P_{old} = rnd(up - low) + low \quad (5)$$

where $P_{initial}$ and P_{old} are the initial and old population respectively. *Up* and *low* are the limit range of dimensions of population, and *rnd* is the uniformly distributed pseudorandom numbers.

- Step 2: The objective function of initial population (Obj-fun ($P_{initial}$)) is calculated.
- Step 3: The new populations which are called as trail population, are generated by using mixed method between mutation and crossover described by

$$P_{trail} = P + (map.F).(P_{old} - P) \quad (6)$$

where P_{trial} is the trail population, and P is population that obtains from selection randomly between old and initial population. *map* is a binary integer-valued matrix calculated for crossover term [11] . $F=3\times rndn$ is the get-scale-factor and *rndn* is the normally distributed pseudorandom numbers.

- Step 4: the objective function of trial population (Obj-fun (P_{trial})) is calculated.
- Step 5: this is the selection step. The objective function between initial and trial population are compared.
- Step 6: this is negative comment step "No". The fitness population (fitness P) is equal to the initial population ($P_{initail}$), and then it continues to step 8.
- Step 7: this is the positive comment step "Yes". The fitness population (fitness P) is equal to the trial population (P_{trail}), and then it will continue to step 8.
- Step 8: Check the maximum iteration. If "Yes", the process of minimization will stop and continue to step 10 "End", if No, it will continue to step 9.
- Step 9: In this step, the fitness population will update to old population, and the process of minimization will do again.
- Step 10: The end of the process.

IV. Simulation Results

The POD design is developed by MATLAB, Simulink and power system analysis toolbox (PSAT) [10]. The BSA parameters are set as follows; population = 25, maximum iteration = 200. The POD is designed under case 1 as shown in TABLE I. After the optimization, Fig. 9 demonstrates the convergence curve of objective function value of the proposed control method. The optimized parameters of POD are provided in TABLE II. The eigenvalue analysis results in case 1 are shown in TABLE III. Without POD, the damping ratio of the oscillation mode is very poor. On the other hand, the damping ratio of the oscillation mode is improved as expected by both coordinated controllers and individual controller.

Next, nonlinear simulations of case studies 1 to 3 in TABLE I are carried out. Figs. 11 (a)-(d) show the rotor speed of each generator from 1 to 4 in case of controlling by no POD, DFIG-POD, SVC-POD and DFIG-POD with SVC-POD, respectively. In case 1, the DFIG and SVC without POD cannot damp out the power oscillation. On the contrary, both PODs coordinated control and POD individual controls are

TABLE I. Case Studies (Base=100 MVA, 60 Hz)

Case	Condition study	P_{Tie} (p.u.)	Wind pattern (m/s)
1.	The 3 phase fault occurs on bus 9 at time 1s, naturally cleared at time 1.05s.	4.20	Fig. 10 (a)
2.	The 3 phase fault occurs on bus 7 at time 1s, naturally cleared at time 1.066s.	4.50	Fig. 10 (b)
3.	The 3 phase fault occurs on bus 6 at time 1s, naturally cleared at time 1.083s.	5.00	Fig. 10 (c)

TABLE II. OPTIMAL PARAMTERS OF PODS

Devices	K_{stab}	T_1	T_2	T_3	T_4
Coordinated control					
POD-DFIG	2.9703	0.1178	1.8243	0.0978	0.7267
POD-SVC	1.5935	0.0139	1.0835	1.6780	0.7375
Individual control					
POD-DFIG	3.6643	0.0981	1.4768	0.0191	0.4536
POD-SVC	3.2894	0.0926	0.7507	1.2945	0.6150

TABLE III. EIGENVALUE ANALYSIS RESULTS

Control device		Eigenvalue	Damping ratio	Frequency (Hz)
Coordinated control				
No POD	Local 1	-0.534 ± *j*6.84	7.78%	1.08
	Local 2	-0.524 ± *j*6.64	7.86%	1.05
	Inter-area	**-0.045 ± *j*3.56**	**1.28%**	**0.56**
With POD	Local 1	-0.535 ± *j*6.84	7.79%	1.08
	Local 2	-0.526 ± *j*6.64	7.90%	1.05
	Inter-area	**-0.393 ± *j*3.71**	**10.54%**	**0.59**
Individual control				
DFIG-POD	Local 1	-0.523 ± *j*6.64	7.85%	1.05
	Local 2	-0.530 ± *j*6.85	7.71%	1.09
	Inter-area	**-0.439 ± *j*4.00**	**10.90%**	**0.63**
SVC-POD	Local 1	-0.537 ± *j*6.84	7.82%	1.08
	Local 2	-0.528 ± *j*6.65	7.92%	1.05
	Inter-area	**-0.404 ± *j*3.70**	**10.87%**	**0.58**

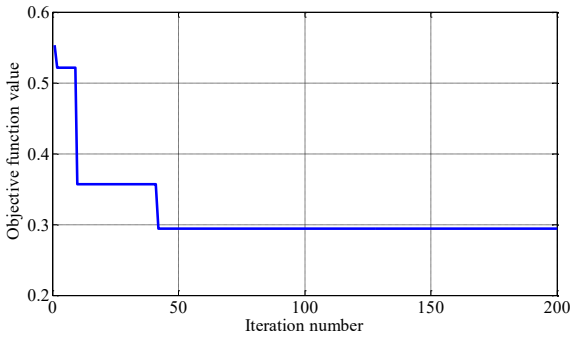

Fig. 9. Convergence curve of Objective function.

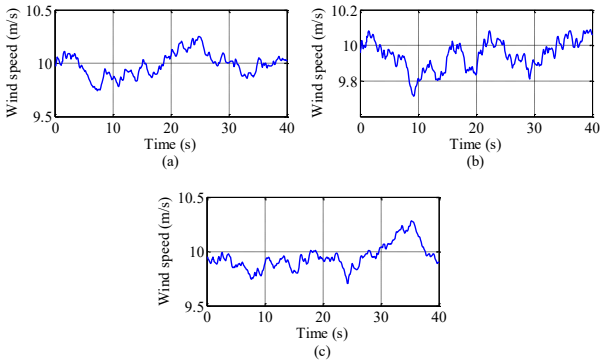

Fig. 10. Wind speed patterns of (a) case 1, (b) case 2, and (c) case 3.

able to suppress the rotor speed oscillations. In cases 2 and 3 showed in Figs. 12 and 13, the POD of individual control loses damping effect and has the oscillations much more than POD of coordinated control.

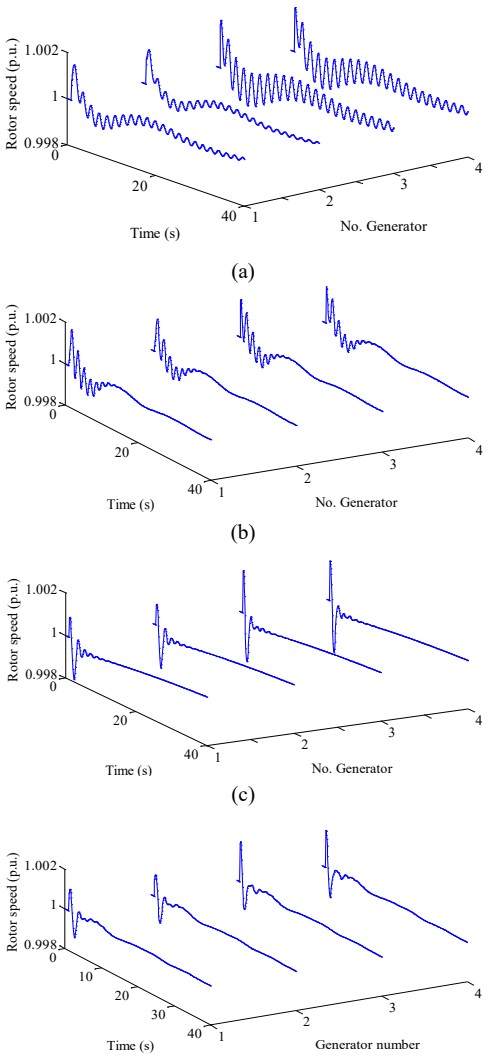

Fig. 11. Rotor speed of each generator in case 1 (a) No POD, (b) DFIG-POD, (c) SVC-POD and (d) DFIG-POD with SVC-POD.

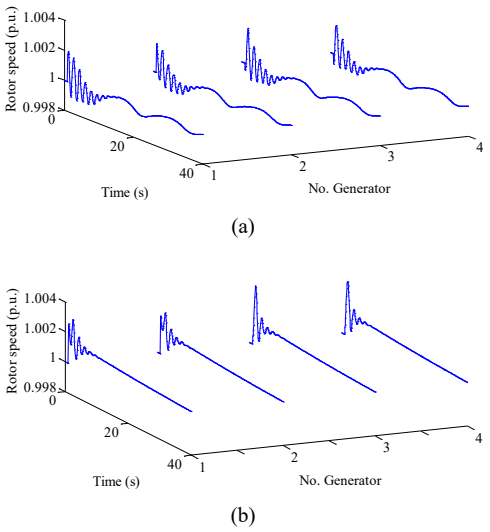

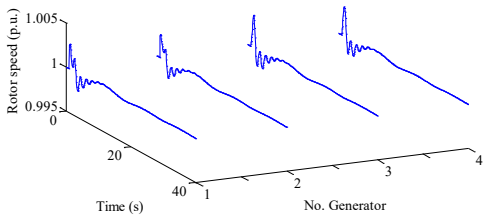

(c)

Fig. 12. Rotor speed of each generator in case 2 (a) DFIG-POD, (b) SVC-POD and (c) DFIG-POD with SVC-POD.

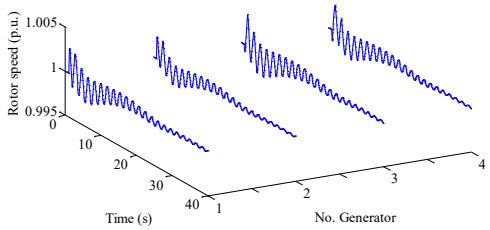

(a)

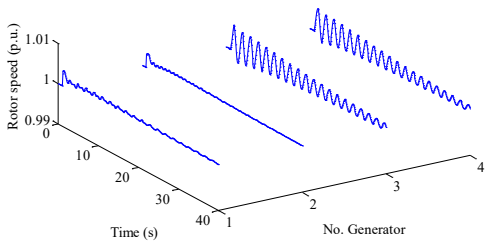

(b)

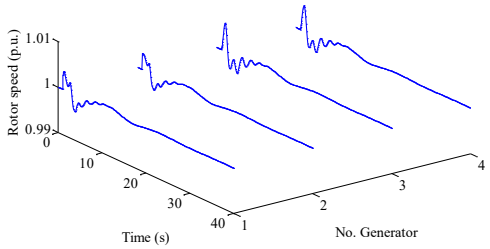

(c)

Fig. 13. Rotor speed of each generator in case 3 (a) DFIG-POD, (b) SVC-POD and (c) DFIG-POD with SVC-POD.

V. CONCLUSION

This paper deals with the new coordinated control using POD with DFIG wind turbine and SVC. The POD with the practical 2nd-order lead/lag structure with local input signal is installed with the DFIG and SVC. The parameters tuning of POD is conducted so that the desired damping ratios of oscillation modes can be obtained. The optimal parameters of PODs are automatically obtained by the backtracking search algorithm. Eigenvalue analysis results and nonlinear simulation clearly confirm the superior damping performance of the proposed coordinated control using DFIG-POD with SVC-POD the individual control under heavy power flow levels and faults.

ACKNOWLEDGMENT

This research work was supported by King Mongkut's Institute of Technology Ladkrabang (KMITL) and ASEAN University Network /Southeast Asia Engineering Education Development Network (AUN/SEED-Net).

REFERENCES

[1] P. Kundur, Power System Stability and Control. New York, NY, USA: McGraw-Hill, 1994.

[2] A.H. Ahmad, A.A. Abdelqader, "Power system stabilizer design using real-coded genetic algorithm," Con. Inst. Auto., Inter. Conf., pp. 25-31, 2011.

[3] M.W. Mustafa, N. Magaji, "Design of power oscillation damping controller for SVC device," IEEE Power Eng. Conf., pp. 1329-1332, 2008.

[4] N.N. Islam, M.A. Hannan, H. Shareef, A. Mohamed, "SVC damping controller design based on firefly optimization algorithm in multi machine power system," IEEE Conf. Clean Eng. Tech., pp. 66-70, 2013.

[5] L. Fan, H. Yin, and Z. Miao, "On active/reactive power modulation of DFIG-based wind generation for interarea oscillation damping," IEEE Trans. Energy Convers., vol. 26, no. 2, pp. 513–521, Jun. 2011.

[6] H. Yu, C. Y. Chung, K. P. Wong, and J. H. Zhang, "A chance constrained transmission network expansion planning method with consideration of load and wind farm uncertainties," IEEE Trans. Power Syst., vol. 24, no. 3, pp. 1568–1576, Aug. 2009.

[7] A.H.M.A. Rahim, and I.O. Habiballah, "DFIG rotor voltage control for system dynamic performance enhancement," Electr. Power Syst., Res., vol.81, pp. 503-509, Feb. 2011.

[8] H. Huang, C.Y. Chung, "Design of a Power Oscillation Damper for DFIG-based Wind Energy Conversion System Using Modified Particle Swarm optimizer," IEEE Trans. power syst., pp. 161-166, 2012.

[9] D.P. Ke, C.Y. Chung, X. Yusheng, "Controller design for DFIG-based wind power generation to damp interarea oscillation," Inter. Conf., pp. 1-6, 2010.

[10] F. Milano, Power system analysis toolbox (PSAT), Documentation for PSAT version 2.1.6, Oct. 2011.

[11] P. Civicioglu, "Backtracking search optimization algorithm," Appl. Math. Comput., vol. 219, no. 15, pp. 8121-8144, Apr. 2013.

ECTI-CON 2015

June 24 - 27, 2015

2015 12 International Conference on Electrical Engineering/Electronics, Computer, Telecommunications and Information Technology

Coordinated Control of DFIG Wind Turbine and SVC for Robust Power System Stabilization

Sothy Uong
International College
King Mongkut's Institute of Technology Ladkrabang
Bangkok 10520, Thailand
uongsothy.itc@gmail.com

Issarachai Ngamroo
Electrical Engineering Department, Faculty of Engineering
King Mongkut's Institute of Technology Ladkrabang
Bangkok 10520, Thailand
knissara@kmitl.ac.th

***Abstract*—In this paper, a coordinated control of doubly fed induction generator (DFIG) wind turbine and static var compensator (SVC) is proposed for the robust stabilization of interconnected power system. By modulating the reactive power output of DFIG and SVC, the power oscillation can be damped. To implement this control, the power oscillation damper (POD) with the 2nd-order lead-lag compensator is added to the voltage controller of DFIG and SVC. The mixed H_2/H_∞ control method is adopted to formulate the parameters optimization problem of POD. Solving the problem by an improved backtracking search algorithm (BSA), the optimal parameters of POD can be achieved. Simulation results in the two-area four-machine power system confirm the robustness and damping effect of the proposed coordinated control.**

Keywords—power oscillation damper; coordinated control; doubly fed induction generator wind turbine; static var compensator; backtracking search optimization algorithm.

I. INTRODUCTION

Recently, the interconnection among power systems has been increased considerably. The system interconnection does not merely augment the system reliability, but also increases more economic efficiency. However, the power system oscillation with frequency between 0.2 to 1 Hz such as local and inter-area oscillation mode [1] tends to occurs in interconnected power systems. Without effective countermeasures, the undamped power oscillation may cause the system to be unstable. To damp out the power oscillation, the conventional power system stabilizer (PSS) has been used for a long time [2]. The local signals such as the generator speed and the output power have been used as an input signal of the PSS. However, due to the lack of observability of the inter-area oscillation modes, the PSS using the local signal may fail to handle the inter-area oscillations. Besides, the static var compensator (SVC), which is one of the flexible AC transmission system (FACTS) devices, has been employed to deal with the inter-area oscillations. By installing the power oscillation damper (POD) with the SVC, the inter-area oscillations can be damped [3, 4].

On the other hand, the wind generators have been increasingly installed in power systems. Especially, the doubly fed induction generator (DFIG) wind turbine has been extensively paid attentions due to the controllability of active and reactive power output [5] and low installation cost. With the ability of power output control, the DFIG wind turbine equipped with a POD can be applied to stabilize the power oscillations [6-8]. To achieve the high stabilizing effect on the power oscillations, the coordinated control of PODs of SVC and DFIG can be anticipated.

This paper focuses on the coordinated controller using DFIG wind turbine and SVC for robust stabilization of power system oscillation. By appropriate control of the reactive power output of DFIG and SVC, the power oscillation can be suppressed. The POD with 2nd-order lead/lag compensator is equipped with the SVC and DFIG. To ensure the damping performance and robustness of POD, the mixed H_2/H_∞ control method is used to set the problem of POD parameters tuning. The POD parameters are automatically optimized by an improved backtracking search algorithm (BSA). The stabilizing effect of the robust coordinated control of DFIG and SVC is evaluated in the two-area four-machine system. Simulation results indicate the superior robustness and stabilizing effect of proposed robust coordinated control of DFIG and SVC over the conventional coordinated control.

II. STUDY SYSTEM AND MODELLING

A. Study System

The two area four machine system [1] which is used as the study system, is illustrated in Fig. 1. The rate power and voltage of each synchronous generator are 900 MVA and 20 kV, respectively. The DFIG wind farm with 50 MVA, 20 kV is installed at bus 6. To regulate the voltage at bus 8, the SVC with 100 MVA, 230 kV is connected. To stabilize the power oscillation in this system, the POD is added to the voltage control loops of both DFIG and SVC. Fig. 2 shows the concept of the proposed coordinated DFIG and SVC control.

B. DFIG Model

The structure of DFIG wind turbine and control system [9] is delineated in Fig. 3, where v_a, v_b, v_c are voltages of phases *a, b, c*, respectively, i^*_a, i^*_b, i^*_c are reference currents of phases *a, b, c*, respectively, v_{dr} and v_{qr} are direct (*d*) and quadrature (*q*) axis voltages of the rotor side converter, respectively, i^*_{dr} and i^*_{qr} are reference *d* and *q* axis currents of the rotor side converter, respectively, i_{dr} and i_{qr} are *d* and *q* axis currents of the rotor side converter, M is a modulation ratio, and is a phase angle, p_e and q_e are active power and reactive power

978-1-4799-7961-5/15/$31.00 ©2015 IEEE

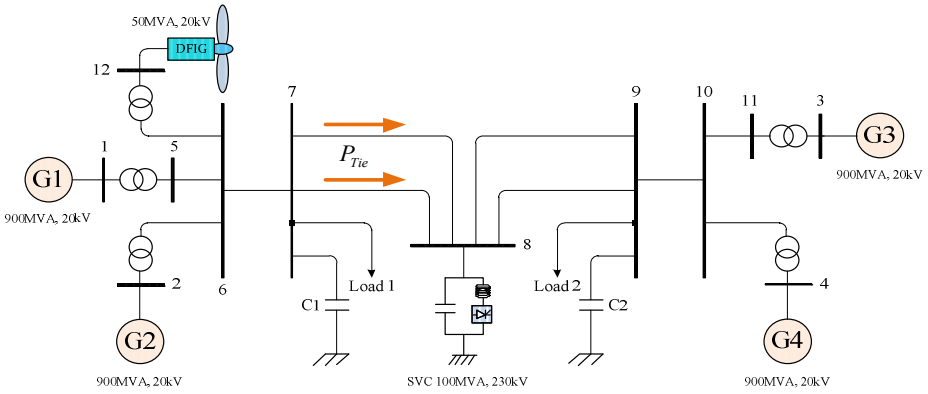

Fig. 1. Two-area four machine system.

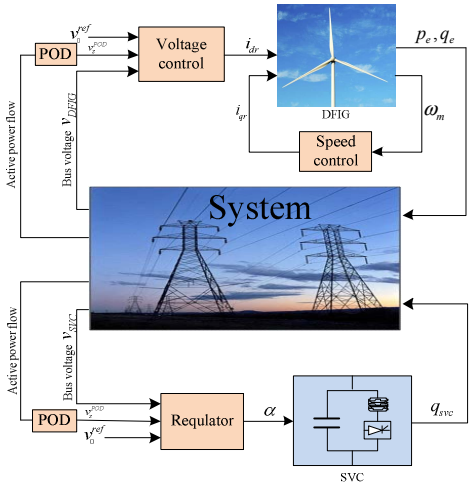

Fig. 2. Proposed coordinated control.

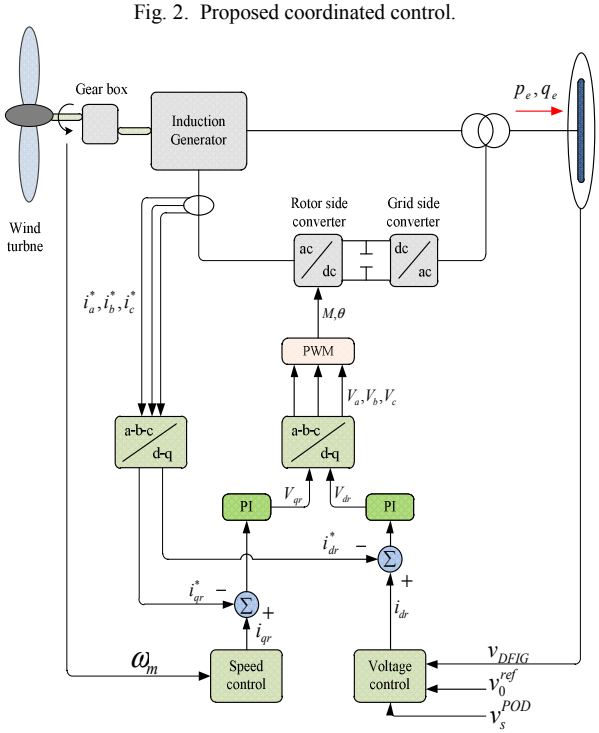

Fig. 3. DFIG model.

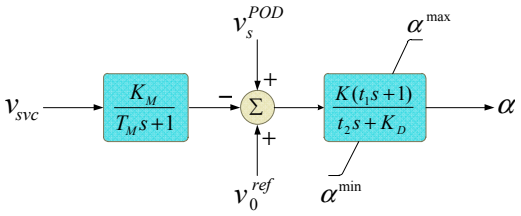

Fig. 4. SVC type 2 regulator.

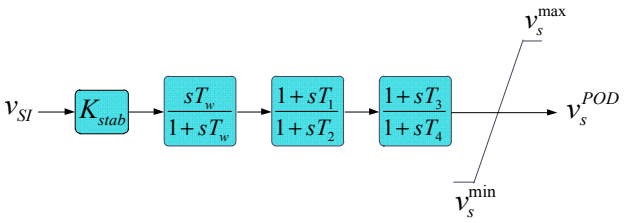

Fig. 5. POD model.

outputs of DFIG. Based on the study results in [6], the control using the rotor side converter gives more damping effect than using the grid side converter. In this work, the POD is equipped with the voltage controller of rotor side converter.

C. SVC Model

The structure of the SVC type 2 regulator [9] is illustrated in Fig. 4, where v_{SVC}, v_0^{ref}, and v_s^{POD} are the terminal voltage of SVC, the initial reference voltage, and the additional signal control of POD, respectively. The output signal of the SVC regulator is the firing angle α. The maximum and minimum firing angle of the anti-wind up limiter are defined as α^{max} and α^{min}, respectively, For other parameters, K_M is the measure gain, T_M is the measure time delay, K is the regulator gain, t_1 and t_2 are transient regulator time constant and regulator time constant, respectively. The SVC is used to maintain the bus voltage by the control of reactive power output. By equipping the POD with SVC, the reactive power output of SVC can be controlled to suppress the power oscillation.

D. POD Model

In Fig. 5, the POD with 2nd-order lead-lag compensator is illustrated. The POD is equipped with DFIG and SVC. For the

POD parameters, K_{stab} is the stabilizer gain, T_w =10 s is a washout filter with time constant, and T_1, T_2, T_3, T_4 are time constants of two phase compensator blocks. The washout signal ensures that the POD output is zero in the steady state. The active power flow in the transmission lines from bus 5 to 6 and from bus 7 to 8 are the input signals (v_{SI}) of POD of DFIG and SVC, respectively. $v_s^{\max}$ and $v_s^{\min}$ are the maximum and minimum values of an anti-windup limiter, respectively. To obtain the satisfactory damping, K_{stab} and T_1, T_2, T_3 and T_4 are optimally tuned by the proposed optimization.

III. PROPOSED OPTIMIZATION

A. Mixed H_2/H_∞ Control

Generally, the robust control is used to capture a set of special specifications. For instance, the H_∞ control is more used to maintain the close loop stability in the presence of model uncertainties, but the H_2 tracking design is used to deal with the transient performance [10]. To achieve both objectives, the mixed H_2/H_∞ control which is the powerful multi-objective control design [11], can be adopted. In Fig. 6 the closed loop system with a mixed H_2/H_∞ control is illustrated, where $G(s)$ is a nominal plant, Δ_M is the model of system uncertainties, $K(s)$ is a controller, w_1 and w_2 are disturbance and external input vector, respectively, y is a measured output vector, u is an input vector from controller, z_2 is an output channel associated with the Linear Quadratic Gaussian (LQG) aspects (H_2 performance), and z_∞ is an output channel associated with the H_∞ performance. $T_{z\infty w1}(s)$ is defined as the closed-loop transfer function from w_1 to z_∞.

Thus, by minimizing the infinite norm of $T_{z\infty w1}(s)$, i.e. $\|T_{z\infty w1}(s)\|_\infty$ and the two-norm of $T_{z2w2}(s)$, i.e. $\|T_{z2w2}(s)\|_2$, the robust stability of the system against uncertainties and the disturbance attenuation can be obtained as

$$\gamma\left\|T_{z\infty w1}(s)\right\|_\infty^2+\beta\left\|T_{z2w2}(s)\right\|_2^2,\gamma\geq 0,\beta\geq 0 \qquad (1)$$

In addition, by placing the dominant oscillation modes in the stability region with the specific damping ratio ζ_{spec} and specific real part σ_{spec} as shown in Fig. 7, the desired D-stability region can be guaranteed. Accordingly, the optimization problem can be formulated by

$$\text{Minimize}\quad \gamma\left\|T_{z\infty w1}\right\|_\infty^{\ 2}+\beta\left\|T_{z2w2}\right\|_2^{\ 2} \qquad (2)$$

$$\text{Subject to}\begin{cases}\zeta_{\mathrm{i}}\geq\zeta_{spec}\\ \sigma_{\mathrm{i}}\leq\sigma_{spec}\\ 0.001\leq K_{stab}\leq 5\\ 0.001\leq T_1,T_2,T_3,T_4\leq 5\end{cases}$$

where γ=0.1 and β=1, are the weights. The specific damping ratio of oscillation modes are set as ζ_{spec}=5%. Also the specific real part of the eigenvalue of oscillation modes are set as σ_{spec} = -0.1. ζ_i and σ_i are defined as the damping ratio and real part of eigenvalue of oscillation modes, respectively.

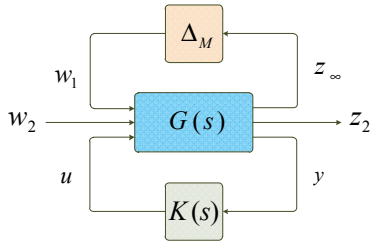

Fig. 6. Closed loop system with mixed H_2/H_∞ control.

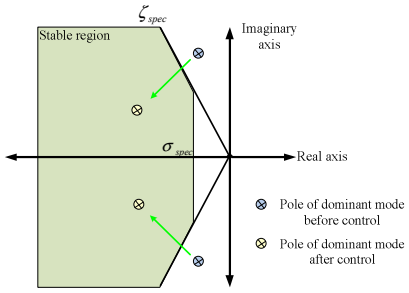

Fig. 7. D-stability region.

B. Conventional Optimization Method

Here, the pole assignment method was applied to formulate the optimization problem of conventional POD (CPOD). The objective function is defined as follows:

$$\text{Minimize}\ \sum_{i=1}^{3}\left(\left|\zeta_i-\zeta_{spec}\right|+\left|\sigma_i-\sigma_{spec}\right|\right) \qquad (3)$$

$$\text{Subject to}\begin{cases}\zeta_{\mathrm{i}}\geq\zeta_{spec}\\ \sigma_{\mathrm{i}}\leq\sigma_{spec}\\ 0.001\leq K_{stab}\leq 5\\ 0.001\leq T_1,T_2,T_3,T_4\leq 5\end{cases}$$

The optimization problems (2) and (3) are solved by the BSA.

C. Backtracking Search Algorithm

Backtracking search algorithm (BSA), which is a population-based iterative evolutionary algorithm (EA), is used for solving real-valued numerical optimization problems [12]. The BSA can be explained by dividing its functions into five processes as is done in other EAs: initialization, selection-I, mutation, crossover and selection-II. Fig. 8 shows the flow chat of BSA which can be described step by step as follows:

1) Initialization: This part is decribed by step 1 and step 2.

a) Step 1: this is the initial step that generates the initial and old populations, and it is described by

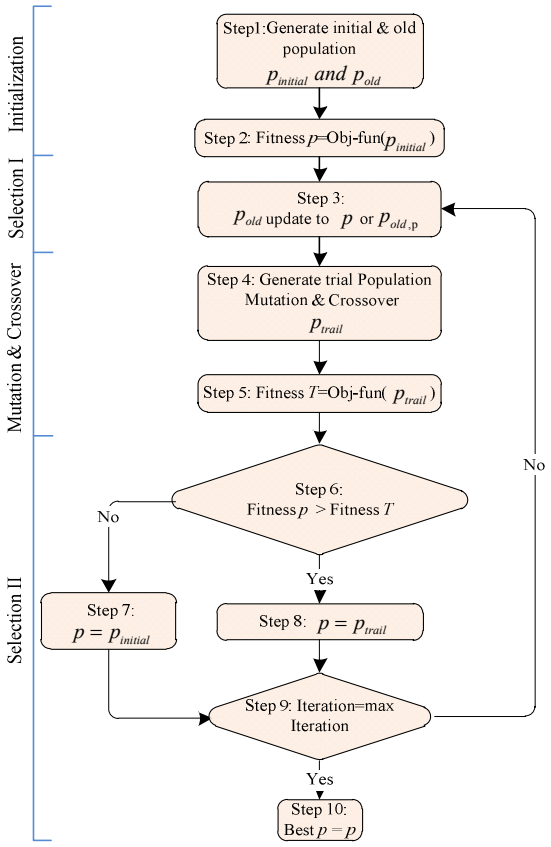

Fig. 8. Flow chat of BSA.

$$p_{initial} = rnd(up - low) + low$$
$$p_{old} = rnd(up - low) + low \quad (4)$$

where $p_{initial}$ and p_{old} are the initial and old populations, respectively, *up* and *low* are the limit range of dimensions of population, and *rnd* is the uniformly distributed pseudo-random numbers.

b) Step 2: The fitness value of initial population (Fitness p = Obj-fun ($p_{initial}$)) is calculated.

2) Selection-I: this part is used to determine the historical population p_{old} and to be used for calculating the search direction. This part is decribed by step 3. BSA has the option of redefining p_{old} at the beginning of each iteration through the 'if-then' rule in (5):

$$\text{If } i < j \text{ then } p_{old} \text{ update to } p$$
$$\text{else } p_{old} = p_{old,p} = \text{permuting}(p_{old}) \quad (5)$$

where p is the population that obtains from the selection randomly between old and initial population.

3) Mutation and Crossover: BSA's mutation and crossover process generates the form of the trial population using (6).

a) Step 4: The new populations which are called as trail population, are generated by using mixed method between mutation and crossover, described by

$$p_{trail} = p + (map.F).(p_{old} - p) \quad (6)$$

where p_{trial} is the trail population , and *map* is a binary integer-valued matrix calculated for crossover term [12] . $F=3\times rndn$ is the get-scale-factor and *rndn* is the normally distributed pseudo-random numbers.

b) Step 5: the fitness of trial population (Fitness T = Obj-fun (p_{trial})) is calculated.

4) Sellection-II : this part selects the best population by comparison method, and it is described in detail by steps 6, 7, 8, 9 and 10.

a) Step 6: this is the selection step. The fitness population (Fitness p) and fitness of trial population (Fitness T) are compared.

b) Step 7: this is the negative comment step "No". The best population (p) is equal to the initial population ($p_{initail}$), and then it continues to step 9.

c) Step 8: this is the positive comment step "Yes". The best population (p) is equal to the trial population (p_{trail}), and then it will continue to step 9.

d) Step 9: Check the maximum iteration. If "Yes", the process of minimization will stop and continue to step 10 "End", if No, it will return to step 3.

e) Step 10: The best population will be obtained.

IV. Simulation Results

The POD design is developed by MATLAB, Simulink and power system analysis toolbox (PSAT) [9]. The BSA parameters were set as follows; population = 25, maximum iteration = 200. The POD is designed under case 1 as shown in TABLE I. After the optimization, Fig. 9 demonstrates the convergence curve of the objective function value in (2). The optimized parameters of POD are provided in TABLE II. The eigenvalue analysis results in case 1 are shown in TABLE III. Without POD, the damping ratio of the inter-area mode is very poor. On the other hand, the damping ratio of the inter-area mode is improved by both robust and conventional coordinated control.

The locus of the eigenvalue corresponding to the inter-area mode under the variation of P_{Tie} from 4.0 to 6.0 p.u. is delineated in Fig. 10. At heavy P_{Tie}, the locus of the inter-area mode in case of without POD and CPOD coordinated control moves to the unstable region. On the other hand, the locus in case of RPOD coordinated control is still in the D-stability region. This result indicates that the robustness of RPOD coordinated control against heavy power flow is superior to that of CPOD coordinated control.

Next, nonlinear simulations of case studies 1 to 3 in TABLE I are conducted. Figs. 12, 13 and 14 show the comparison of the voltage at the faulted bus between CPOD and RPOD coordinated controls of case 1 to case3, respectively. Figs. 15, 16 and 17 demonstrate P_{Tie} of case 1 to case 3, respectively. In the first case, both RPOD coordinated control and CPOD coordinated control are able to damp out the oscillation. In case 2, the damping effect of the RPOD coordinated control is more than that of the CPOD coordinated

TABLE I. CASE STUDIES (BASE=100 MVA, 60 HZ)

Case	Condition study	P_{Tie} (p.u.)	Wind pattern (m/s)
1.	The 3 phase fault occurs on bus 9 at time 1 s, naturally cleared at time 1.05 s.	4.0	Fig. 11 (a)
2.	The 3 phase fault occurs on bus 8 at time 1 s, naturally cleared at time 1.06 s.	5.5	Fig. 11 (b)
3.	The 3 phase fault occurs on bus 8 at time 1 s, naturally cleared at time 1.08 s.	6.0	Fig. 11 (c)

TABLE II. OPTIMAL PARAMETERS OF PODS

Devices	K_{stab}	T_1	T_2	T_3	T_4
Robust coordinated control					
RPOD-DFIG	3.8820	0.8982	4.5501	0.0171	0.5068
RPOD-SVC	4.7952	4.6985	4.6487	0.0577	1.4426
Conventional coordinated control					
CPOD-DFIG	3.3754	0.0048	1.6353	0.1806	1.6139
CPOD-SVC	2.9063	1.0043	3.2355	4.5274	1.9796

TABLE III. EIGENVALUE ANALYSIS RESULTS

Control device		Eigenvalue	Damping ratio	Frequency (Hz)
Without POD	Local 1	-0.534 ± *j*6.84	7.78%	1.08
	Local 2	-0.524 ± *j*6.64	7.86%	1.05
	Inter-area	**-0.045 ± *j*3.56**	**1.28%**	**0.56**
Robust coordinated control	Local 1	-0.528 ± *j*6.84	7.69%	1.08
	Local 2	-0.529 ± *j*6.67	7.90%	1.06
	Inter-area	**-0.354 ± *j*3.49**	**10.10%**	**0.55**
Conventional coordinated control	Local 1	-0.538 ± *j*6.84	7.83%	1.08
	Local 2	-0.524 ± *j*6.64	7.86%	1.05
	Inter-area	**-0.397 ± *j*3.42**	**11.50%**	**0.54**

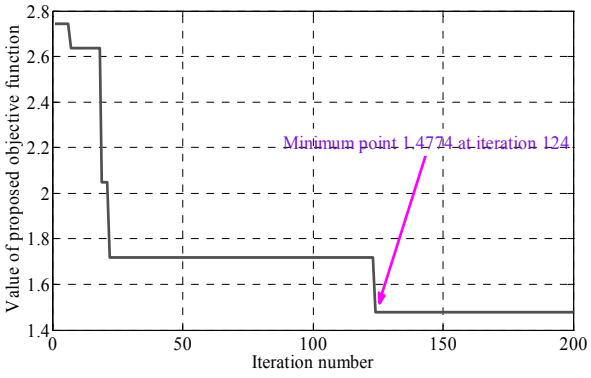

Fig. 9. Convergence curve of objective function.

control. Absolutely, the last case shows that the RPOD coordinated control can damp out the oscillation while the CPOD coordinated control fails to eliminate the oscillation. According to the simulation results, the superior robustness and stabilizing effect of the proposed RPOD coordinated control is obviously superior to the CPOD coordinated control.

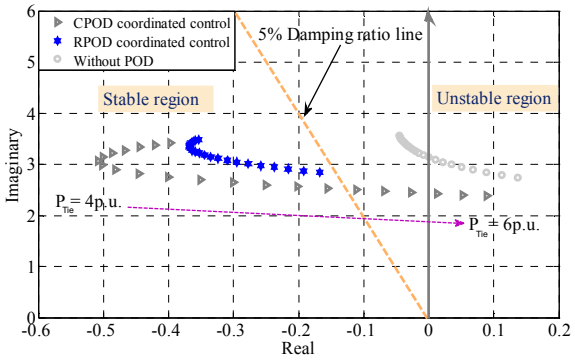

Fig. 10. Locus of inter-area mode.

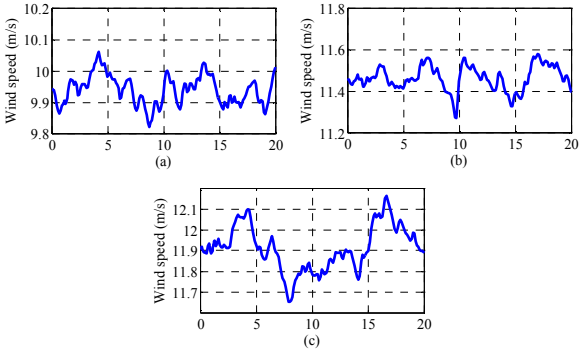

Fig. 11. Wind speed patterns of (a) case 1, (b) case 2, (c) case 3.

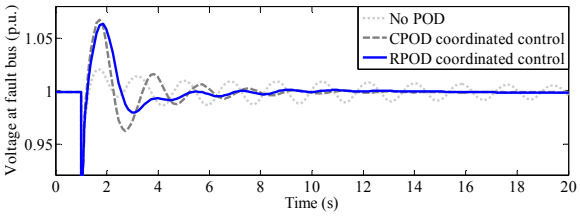

Fig. 12. Voltage at fault bus of case 1.

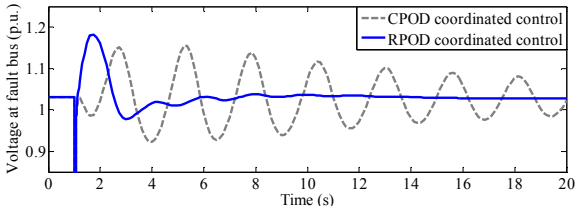

Fig. 13. Voltage at fault bus of case 2.

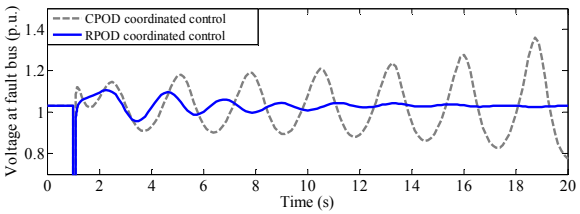

Fig. 14. Voltage at fault bus of case 3.

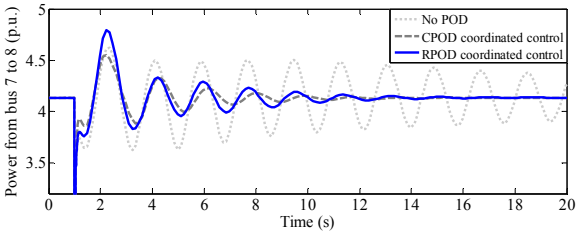

Fig. 15. P_{Tie} of case 1.

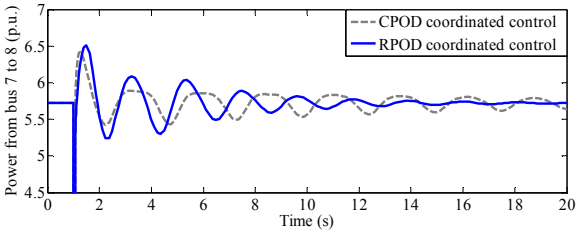

Fig. 16. P_{Tie} of case 2.

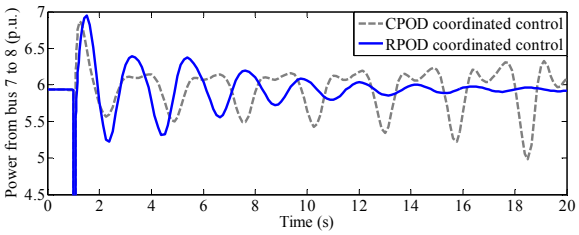

Fig. 17. P_{Tie} of case 3.

V. CONCLUSION

This paper deals with the new robust coordinated control of DFIG wind turbine and SVC. The POD with the practical 2nd-order lead/lag structure with local input signal is installed with the DFIG and SVC. The mixed H_2/H_∞ control method was employed to set the optimization problem of the POD parameters. The optimal parameters of PODs are automatically tuned by the backtracking search algorithm. Eigenvalue analysis results and nonlinear simulation show the higher robustness and damping effect of the proposed robust coordinated control under heavy power flow levels and various fault locations.

ACKNOWLEDGMENT

This research work was supported by King Mongkut's Institute of Technology Ladkrabang Research Fund and ASEAN University Network /Southeast Asia Engineering Education Development Network (AUN/SEED-Net).

REFERENCES

[1] P. Kundur, Power System Stability and Control. New York, NY, USA: McGraw-Hill, 1994.

[2] A.H. Ahmad, A.A. Abdelqader, "Power system stabilizer design using real-coded genetic algorithm," Con. Inst. Auto., Inter. Conf., pp. 25-31, 2011.

[3] M.W. Mustafa, N. Magaji, "Design of power oscillation damping controller for SVC device," IEEE Power Eng. Conf., pp. 1329-1332, 2008.

[4] N.N. Islam, M.A. Hannan, H. Shareef, A. Mohamed, "SVC damping controller design based on firefly optimization algorithm in multi machine power system," IEEE Conf. Clean Eng. Tech., pp. 66-70, 2013.

[5] L. Fan, H. Yin, and Z. Miao, "On active/reactive power modulation of DFIG-based wind generation for interarea oscillation damping," IEEE Trans. Energy Convers., vol. 26, no. 2, pp. 513–521, Jun. 2011.

[6] A.H.M.A. Rahim, and I.O. Habiballah, "DFIG rotor voltage control for system dynamic performance enhancement," Electr. Power Syst., Res., vol.81, pp. 503-509, Feb. 2011.

[7] H. Huang, C.Y. Chung, "Design of a Power Oscillation Damper for DFIG-based Wind Energy Conversion System Using Modified Particle Swarm optimizer," IEEE Trans. power syst., pp. 161-166, 2012.

[8] D.P. Ke, C.Y. Chung, X. Yusheng, "Controller design for DFIG-based wind power generation to damp interarea oscillation," Inter. Conf., pp. 1-6, 2010.

[9] F. Milano, Power system analysis toolbox (PSAT), Documentation for PSAT version 2.1.6, Oct. 2011.

[10] P. Khargonekar, and Mario A. Rotea, "Mixed H_2/H_∞ control: a convex optimization approach", IEEE Trans. Automatic Control, vol.36, no.7, pp. 824-837, July 1991.

[11] S. Skoqestad, I. Postlethwaite, Multiple feedback control: analysis and design. Wiley, Sep. 2005.

[12] P. Civicioglu, "Backtracking search optimization algorithm," Appl. Math. Comput., vol. 219, no. 15, pp. 8121-8144, Apr. 2013.

Author Biography

Personal Information

Name	SOTHY UONG
Nationality	Cambodian
Date of birth	July 20, 1989
Place of birth	Sro Ngae Commune, Prey Chhor District, Kampong Cham Province, Cambodia

Education

Bachelor degree

Field	Electrical and Energy Engineering
Duration	2008-2013
Department	Department of Electrical and Energy Engineering
University	Institute of Technology of Cambodia

Master degree

Field	Electrical Power System
Duration	2013-2015
Department	Electrical Engineering
Faculty	International College
University	King Mongkut's Institute of Technology Ladkrabang (KMITL), Thailand

Research Interests

Power system stability which focuses on the control design, application of control device for smart grid.